


5-2018

EPITHELIAL TO MESENCHYMAL TRANSITION AS A PREDICTOR OF RESPONSE TO POLO-LIKE KINASE 1 INHIBITION-INDUCED APOPTOSIS IN NON-SMALL CELL LUNG CARCINOMA

Pavitra Viswanath

Follow this and additional works at: https://digitalcommons.library.tmc.edu/utgsbs_dissertations

 Part of the [Cancer Biology Commons](#), and the [Medicine and Health Sciences Commons](#)

Recommended Citation

Viswanath, Pavitra, "EPITHELIAL TO MESENCHYMAL TRANSITION AS A PREDICTOR OF RESPONSE TO POLO-LIKE KINASE 1 INHIBITION-INDUCED APOPTOSIS IN NON-SMALL CELL LUNG CARCINOMA" (2018). *UT GSBS Dissertations and Theses (Open Access)*. 856.

https://digitalcommons.library.tmc.edu/utgsbs_dissertations/856

This Thesis (MS) is brought to you for free and open access by the Graduate School of Biomedical Sciences at DigitalCommons@TMC. It has been accepted for inclusion in UT GSBS Dissertations and Theses (Open Access) by an authorized administrator of DigitalCommons@TMC. For more information, please contact laurel.sanders@library.tmc.edu.

**EPITHELIAL TO MESENCHYMAL TRANSITION AS A PREDICTOR OF
RESPONSE TO POLO-LIKE KINASE 1 INHIBITION-INDUCED APOPTOSIS IN
NON-SMALL CELL LUNG CARCINOMA**

By

Pavitra Viswanath, B.E

APPROVED:

Faye M. Johnson, M.D., Ph.D.
Advisory Professor

Don L. Gibbons, M.D., Ph.D.

Joya Chandra, Ph.D.

Subrata Sen, Ph.D.

Pierre D. McCrea, Ph.D.

APPROVED:

Dean, The University of Texas
MD Anderson Cancer Center UTHealth Graduate School of Biomedical Sciences

**EPITHELIAL TO MESENCHYMAL TRANSITION AS A PREDICTOR OF
RESPONSE TO POLO-LIKE KINASE 1 INHIBITION-INDUCED APOPTOSIS IN
NON-SMALL CELL LUNG CARCINOMA**

A

THESIS

Presented to the Faculty of

The University of Texas

MD Anderson Cancer Center

UTHealth Graduate School of Biomedical Sciences

in Partial Fulfillment

of the Requirements

of the Degree of

MASTER OF SCIENCE

By

Pavitra Viswanath, B.E

Houston, Texas

May 2018

Dedicated to my family

Acknowledgements

I would like to thank my supervisor, Dr. Faye M. Johnson, for giving me the opportunity to undertake this project, who guided, taught and encouraged me throughout and for that I will be eternally grateful. Thank you for being a fantastic mentor and for helping me in developing the skillsets of a scientist. I would also like to acknowledge and thank the current and former members of my lab for all their help and making my lab experience wonderful: Drs. Tuhina Mazumdar, Shaohua Peng, Ratnakar Singh, Vaishnavi Sambandam, Kyriante Henry, Nene Kalu and Hongyun “Jane” Zhao. A huge thank you to Dr. Shaohua Peng for teaching me to work with mice and helping with the PDX studies and orthotopic lung injections. I am going to miss tag teaming with you in the animal facility. Thank you Drs. Ratnakar Singh and Vaishnavi Sambandam for being there to answer all my questions and help in troubleshooting experiments. I would also like to extend my gratitude to Xin “Cindy” Lieu from Dr. Jonathan Kurie’s lab for teaching me orthotopic lung injections. Thank you Dr. Peter Balter, for helping me in Raystation issues and brainstorming possible CT analysis techniques, one of which is leading to a publication. Thank you Charles Kingsley, Vivien Tran, Kiersten Maldonado and Houra Taghavi at SAIF for the CT imaging and teaching me how to intubate mice and operate the XRad.

Additionally, I would like to thank my advisory committee members (Drs. Don Gibbons, Joya Chandra, Subrata Sen and Pierre McCrea) for their guidance and support in helping me to cultivate and complete a thesis project that would improve our efforts in developing targeted therapies to treat various cancer types. Lastly, thank you to Dr. Lindsey Minter and my friends for creating a safe-haven where I could brainstorm and go to vent and attain peace without being judged. Thank you all for being there to advise and guide me during my academic tenure at GSBS.

Epithelial to Mesenchymal Transition as a Predictor of Response to Polo-Like Kinase 1 Inhibition-Induced Apoptosis in Non-Small Cell Lung Carcinoma

Pavitra Viswanath, B.E

Faye M. Johnson, MD, PhD

Non-small cell lung cancer (NSCLC) is the leading cause of cancer-related death worldwide. Outcomes are poor for patients with recurrent, advanced or metastatic NSCLC. Polo-like kinase 1 (PLK1), involved in the regulation of mitotic processes and the response to DNA damage, is overexpressed in NSCLC. Inhibiting PLK1 may be an effective treatment for NSCLC patients as it is involved in the mechanisms of resistance to several chemotherapy drugs. PLK1 inhibition or knock-down has various effects in cancer cells, including mitotic arrest, apoptosis, and senescence. Predictive biomarkers have not been identified to select those patients who are likely to respond to PLK1 inhibitors although a small subset of NSCLC patients respond well to single agent therapy.

Our lab found that mesenchymal NSCLC cell lines were more sensitive to PLK1 inhibitors than the epithelial cell lines *in vitro*. The induction of an epithelial phenotype using miR-200 expression increased resistance to PLK1 inhibition, whereas the induction of a mesenchymal phenotype using ZEB1 expression or TGF- β increased PLK1 inhibition-induced apoptosis. To elucidate the mechanisms of resistance to PLK1 inhibition, our lab compared gene and protein expression in sensitive and resistant NSCLC cell lines and we identified β -Catenin, SMAD4 and PDK1 to be differentially regulated between epithelial and mesenchymal NSCLC cell lines after PLK1 inhibition. We tested the role of β -Catenin, SMAD4 and PDK1 in PLK1 inhibition induced apoptosis in NSCLC.

Here, we demonstrate that mesenchymal NSCLC tumors are more sensitive to PLK1 inhibition compared to epithelial NSCLC *in vivo* in patient derived-xenograft (PDX) models as well as orthotopic mouse models in which the EMT properties are manipulable by modulating the miR200/ZEB1 axis. To facilitate analysis of these *in vivo* studies, we developed a novel semi-automated method of metastatic lung tumor burden calculation from computed tomography images by the calculation of the mass of the thoracic cavity. This method takes into account the aggregate tumor metastases in the thoracic cavity which significantly accounts for tumor burden in lung adenocarcinoma and provides details about the dynamic processes that occur *in vivo* over time.

Table of Contents

Dedication.....	iii
Acknowledgement.....	iv
Abstract.....	v
Table of Contents.....	vi
List of Figures.....	ix
List of Tables.....	xi
Chapter 1: Introduction.....	1
1. Non-Small Cell Lung Cancer.....	2
2. Known Genetic Alteration in Non-Small Cell Lung Cancer.....	2
3. Current Systemic Treatments Available to NSCLC Patients.....	4
3.1 Molecularly targeted Therapies.....	4
3.2 Cytotoxic Chemotherapy.....	4
3.3 Immunotherapy.....	5
4. Animal Models of NSCLC.....	5
5. PLK Family.....	6
6. PLK1 Regulation.....	9
7. Role of PLK1 in Cell Cycle Regulation.....	10
8. Role of PLK1 in DNA Damage Response.....	10
9. Effect of PLK1 Inhibition in cancer.....	11
10. Effect of PLK1 Inhibition in NSCLC.....	12
11. PLK1 Inhibitors in Clinical Development.....	13
12. Epithelial-to-Mesenchymal Transition (EMT) and Cancer.....	15
13. Hypothesis and Specific Aims.....	17

Chapter 2: Materials and Methods	20
1. Reagents and Antibodies.....	21
2. Cell Culture.....	24
3. Cell Viability Assay.....	24
4. Apoptosis Assay.....	24
5. Western Blot.....	24
6. Transfection.....	25
7. Subcutaneous Tumor Implantation for PDX Models.....	26
8. Orthotopic Lung Injection in immunocompetent mouse models.....	26
9. CT Imaging.....	27
10. CT Image Analysis.....	28
11. Statistical Analysis.....	30
Chapter 3: Results	31
1. EMT markers correlate with PLK1 inhibition in NSCLC cell lines in an independent dataset.....	32
2. Mesenchymal NSCLC tumors are more sensitive in comparison to epithelial NSCLC tumors to PLK1 inhibition induced apoptosis in patient-derived xenograft (PDX) mouse models.....	35
3. Mesenchymal PDX models demonstrate improved survival and sustained tumor growth inhibition after cessation of PLK1 inhibition treatment.....	45
4. Expression of EMT markers are heterogeneous in PDX tumors.....	47
5. Epithelial-to-mesenchymal transition by expression of ZEB1 leads to increase in sensitivity to PLK1 inhibition induced apoptosis in an orthotopic, syngeneic NSCLC mouse model.....	51

6. Tumor mass calculated from the Mass of Thoracic Cavity (MTC) of mice with metastatic lung adenocarcinoma gives an accurate quantification of metastatic tumor burden.....	57
7. Lung tumor burden quantification of MTC method as well as existing methods significantly correlated with lung weight.....	61
8. Validation study for MTC method shows that Volasertib treatment reduced tumor mass in a mesenchymal metastatic, orthotopic mouse model.....	67
9. β -Catenin knock-down (KD) did not reverse resistance to PLK1 inhibition induced apoptosis in epithelial NSCLC cell lines that express high levels of β -Catenin.....	72
10. SMAD4 knock-down (KD) did not change sensitivity to PLK1 inhibition induced apoptosis in NSCLC cell lines.....	76
11. PDK1 overexpression in a sensitive mesenchymal NSCLC cell line leads to resistance to PLK1 inhibition induced apoptosis.....	81
Chapter 4: Discussion.....	87
Chapter 5: Bibliography.....	94
Vita.....	113

List of Figures

Figure 1: Frequency of molecular aberrations in various driver oncogenes in lung adenocarcinomas and current available drugs against these oncogenic proteins.....	3
Figure 2: Structure of PLK family proteins.....	8
Figure 3: EMT markers correlate with PLK1 inhibition in a panel of NSCLC cell lines in an independent dataset.....	33
Figure 4: PDX tumors have diverse EMT phenotypes.....	38
Figure 5: Mesenchymal NSCLC PDX tumors are more sensitive to PLK1 inhibition induced apoptosis in comparison to epithelial NSCLC PDX tumors.....	39
Figure 6: Western blot analysis of PDX tumors for markers of apoptosis, proliferation and target inhibition.....	42
Figure 7: Sustained tumor growth inhibition is observed in TC424 and TC370 Mesenchymal PDX models after cessation of Volasertib treatment.....	46
Figure 8: Expression of EMT markers are heterogeneous in PDX tumors.....	48
Figure 9: Disease progression in 393P Vector and 393P ZEB1 orthotopic mouse model treated with vehicle control or Volasertib.....	53
Figure 10: The Mas of Thoracic Cavity does not change over time.....	59
Figure 11: Tumor mass calculated from the Mass of Thoracic Cavity of mice with metastatic lung adenocarcinoma gives an accurate quantification of metastatic tumor burden.....	60
Figure 12: Lung tumor burden quantification of existing methods besides the MTC method significantly correlated with lung weight.....	63
Figure 13: Correlation of tumor mass with tumor burden from SCP method, ellipsoid tumor volume, tumor + vessel volume and end point lung volume.....	65

Figure 14: Validation study for MTC method shows that Volasertib treatment reduced tumor mass in a mesenchymal metastatic, orthotopic mouse model.....69

Figure 15: β -Catenin knock-down (KD) did not reverse resistance to PLK1 inhibition induced apoptosis in epithelial NSCLC cell lines that express high levels of β -Catenin.....74

Figure 16: SMAD4 knock-down (KD) did not change sensitivity to PLK1 inhibition induced apoptosis in NSCLC cell lines.....78

Figure 17: PDK1 protein expression is altered after PLK1 inhibition in mesenchymal but not epithelial NSCLC cell lines.....82

Figure 18: PDK1 overexpression in a sensitive mesenchymal NSCLC cell line leads to resistance to PLK1 inhibition induced apoptosis.....85

List of Tables

Table 1: PLK1 inhibitors in clinical development.....	14
Table 2: List of siRNA used in the study.....	21
Table 3: Description of antibodies used in the study.....	22
Table 4: Tukey’s multiple comparison results for changes in MTC.....	58
Table 5: Summary of MTC and other CT analysis methods.....	66

Chapter 1: Introduction

1. Non-Small Cell Lung Cancer

Lung cancer is one of the deadliest cancers in the world. It is estimated that there will be 154,050 deaths and 234,030 new cases of lung cancer in the United States (US) in 2018 alone (1). The 5-year relative survival rate for lung cancer is 18% (15% for men and 21% for women) (1). Non-small cell lung cancer (NSCLC) accounts for about 80-85% of lung cancers. NSCLCs are classified into three main subtypes by the World Health Organization based on histopathology: adenocarcinoma (40% of lung cancers), squamous cell carcinoma (25% lung cancers) and large cell carcinoma (10% of lung cancers) (2). Some of the rarer types of NSCLC include adenosquamous carcinoma, spindle cell carcinoma, giant cell carcinoma, carcinosarcoma, pulmonary blastoma, carcinoid tumors, mucoepidermoid carcinoma, adenoid cystic carcinoma and other unclassified carcinoma (2). Smoking is the biggest cause and risk factor for lung cancer and is responsible for around 80% of lung cancer deaths in the US (1). Some of the other risk factors include radon gas exposure, exposure to second-hand smoke, air pollution, asbestos, radiation, chromium and cadmium exposure as well as diesel exhaust (1).

2. Known Genetic Alteration in Non-Small Cell Lung Cancer

In the recent years, genotyping studies in addition to histology have been carried out to identify genetic or molecular abnormalities in the various subtypes of NSCLC (3, 4). Some of the main driver mutations that have been identified include mutations or alterations in the epidermal growth factor receptor (EGFR), anaplastic lymphoma kinase (ALK), KRAS, HER2, BRAF, PIK3CA, and ROS1 (5, 6). These genetic alterations cause an increase in tumor cell proliferation, angiogenesis, metastasis as well as decreased apoptosis. Many targeted therapies have been developed, targeting these genetic

alterations and are outlined in Figure 1. Many of the kinase inhibitors targeting each of these oncogenes are either the standard of care or undergoing active development in the clinic, providing a fertile ground for investigations of drug resistance.

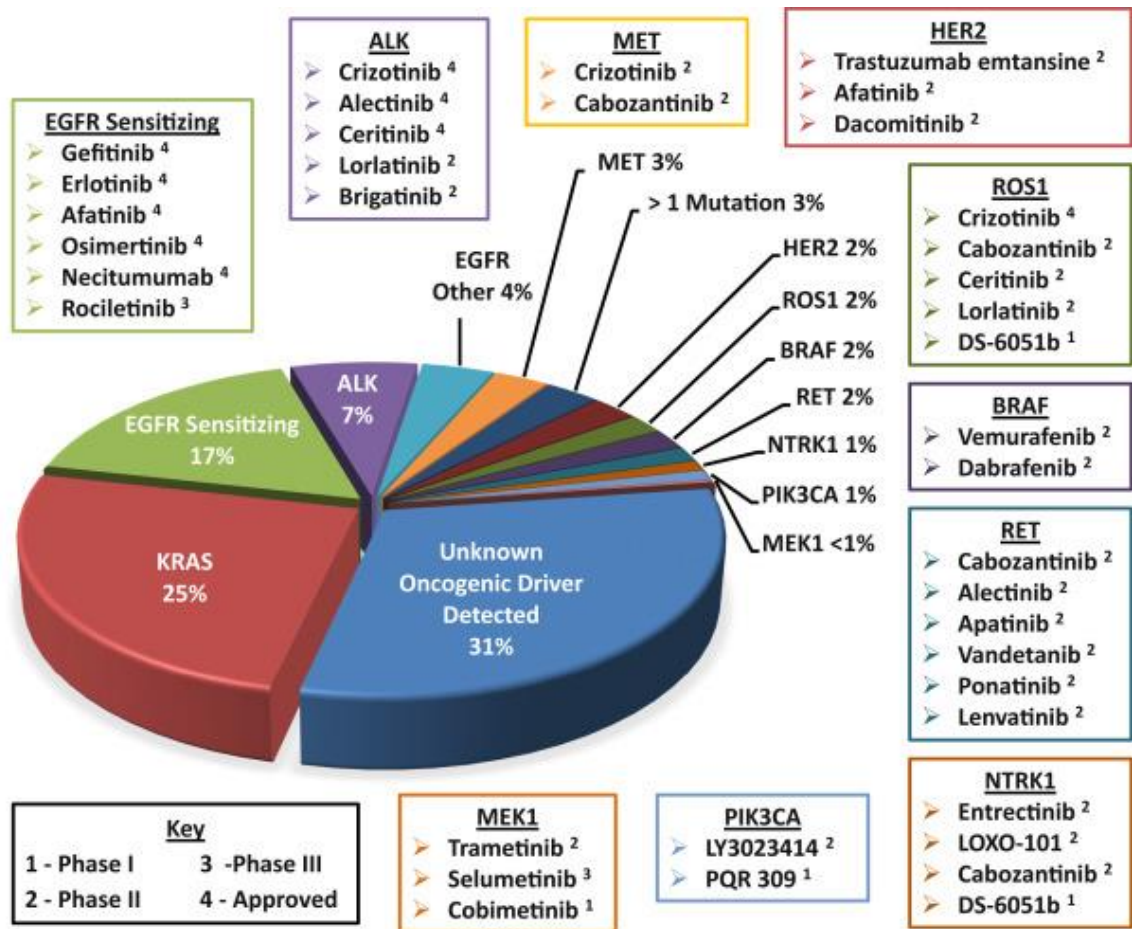


Figure 1: Frequency of molecular aberrations in various driver oncogenes in lung adenocarcinomas and current available drugs against these oncogenic proteins.

Reprinted with permission from Journal of Thoracic Oncology. Tsao AS, Scagliotti GV, Bunn PA, Jr., Carbone DP, Warren GW, Bai C, et al. Scientific Advances in Lung Cancer 2015. J Thorac Oncol. 2016;11(5):613-38. (6)

3. Current Systemic Treatments Available to NSCLC Patients

3.1 Molecularly targeted Therapies

One of the first driver mutations to be clinically targeted in NSCLC was the activating mutations in EGFR. Activating mutations in EGFR most commonly occur as either in-frame amino acid deletions in exon 19 or L858R substitutions in exon 21 (7). These EGFR mutations tend to make the cancer cells rely on EGFR for survival and this is known as oncogene addiction (8). This phenomenon allows the tumors to respond to EGFR-specific tyrosine kinase inhibitors (TKIs), such as Erlotinib, Gefitinib, Afatinib and Osimertinib. Additionally, the US Food and Drug Administration (FDA) approved kinase inhibitors that target ALK-fusion and these include Crizotinib, Ceritinib, and Alectinib. Other potential targeted therapies are listed in Figure 1. One of the main barriers that limits the effectiveness of kinase inhibitor therapy is the issue of resistance which develops in nearly all patients despite robust and durable responses in many (9). Therapy resistance is categorized as primary or intrinsic resistance and secondary or acquired resistance. In primary resistance, patients lack response to the targeted therapy. In secondary resistance, patients initially respond and achieve some benefit after which disease progression is observed (9).

3.2 Cytotoxic Chemotherapy

Cytotoxic chemotherapy is used as an anticancer treatment for the vast majority of NSCLC patients, especially those who do not have any targetable genetic alterations. The response to cytotoxic combination chemotherapy is influenced by histology, age, comorbidity and performance status (PS) (10). Based on American Society of Clinical Oncology (ASCO) standards, the treatment for a patient with PS 0 or 1 is a regimen of a

platinum (cisplatin or carboplatin) plus paclitaxel, gemcitabine, docetaxel, vinorelbine, irinotecan, or pemetrexed (11). Other chemotherapeutic agents such as paclitaxel, docetaxel, vinorelbine, gemcitabine, and irinotecan have shown significant single-agent activity in advanced NSCLC(12). As with targeted therapy resistance develops in nearly all NSCLC patients.

3.3 Immunotherapy

One of the latest breakthroughs in cancer treatment has been immunotherapy, which includes targeting the immune-modulating mechanisms that help cancer cells defend themselves against the immune system. This approach targets immune checkpoint pathways which include the blockade of cytotoxic T-lymphocyte-associated antigen 4 (CTLA4), programmed cell death-1 (PD-1) and its ligand PD-L1, and others (13). Ipilimumab is a CTLA4 human IgG1 monoclonal antibody that targets the inhibitory interaction between CTLA4 and CD80 or CD86. It is said to deplete tumor-infiltrating regulatory T-cells through antibody-dependent cell-mediated cytotoxicity, producing elevated levels of cell surface CTLA4 (14). Pembrolizumab and nivolumab are FDA approved for the treatment of metastatic NSCLC. Both are humanized monoclonal antibodies that inhibit the interaction between the PD-1 coinhibitory immune checkpoint expressed on tumor cells and infiltrating immune cells and its ligands, PD-L1 and PD-L2 (15).

4. Animal Models of NSCLC

Many genetically engineered mouse models (GEMMS) have been generated that encompass a number of mutations found in NSCLC. These include KRAS, BRAF, EGFR, LKB1, p53, NFκB (16). Most mouse models for NSCLC are focused on adenocarcinoma

where studies have been performed using a Lox-Stop-Lox conditional KRASG12D mutation engineered in the endogenous KRAS locus (17, 18). Combining KRASG12D activation along with the concomitant inactivation of p53 results in more aggressive tumors that also metastasize. The relationship between primary tumor nodules and individual metastases could be established in studies in which activation of KRASG12D and inactivation of p53 was achieved by infection of mouse lung with lentiviral Cre (19).

The other type of mouse models that have been used and play a very important role in preclinical studies are human xenografts. These include cell line and patient-derived xenografts (PDXs). In PDX models, direct implantation of small patient tumor fragments in immunocompromised mice leads to the development of tumors that may accurately represent the heterogeneity of the patient population. These models can be serially propagated in mice by subsequent passaging as explants (20). PDX models are generated in immunodeficient mice by engrafting patients' cancerous tissues or cells (21-26). PDX models are extensively used in preclinical screening and evaluation of drugs for various cancers as they accurately depict the patient's tumors with respect to genetic mutations, response to systemic therapy, gene expression and histopathology.

5. PLK Family

Polo-like kinases (PLKs) are a family of serine-threonine kinases that regulate multiple processes such as mitosis, cytokinesis and DNA damage response. PLKs regulate the molecular signals that are integrated to initiate and maintain checkpoints that halt the progression of cell growth and allow time for DNA repair (27). There are five members of the PLK family, named PLK1 to PLK5. The proteins PLK1, PLK2, PLK3 and PLK4 have similar structures: they have a conserved serine-threonine kinase domain the amino-

terminal end. PLK1, PLK2 and PLK3 have two regulatory polo-box domains (PBDs) at the carboxy-terminal end while PLK4 has one PBD (28). PLK5 is different from the other family members as it is a protein that has a PBD but lacks the serine-threonine kinase domain (29). The PBD of PLK1 is critical for PLK1 function. Studies have shown that that a PBD-dependent protein-protein interaction is critically required for proper M-phase progression (30). The PBD functions as a molecular mediator by recognizing a p-Ser/p-Thr consensus motif (31) and brings the kinase domain of PLK1 in proximity to its substrates by interacting with a phosphorylated motif on the substrate itself or its associated proteins (32). The PBD-dependent interaction with a phosphorylated target occurs by the generation of a phosphorylated binding motif and the binding of PLK1 with the resulting target protein (32). This PBD-dependent protein-protein interaction is thereby central to various PLK1-mediated biological processes. The structure of PLK family proteins is depicted in Figure 2 below. PLK1 is the best characterized of all the family members, it is expressed in NSCLC, and it has a well-established role in cancer progression.

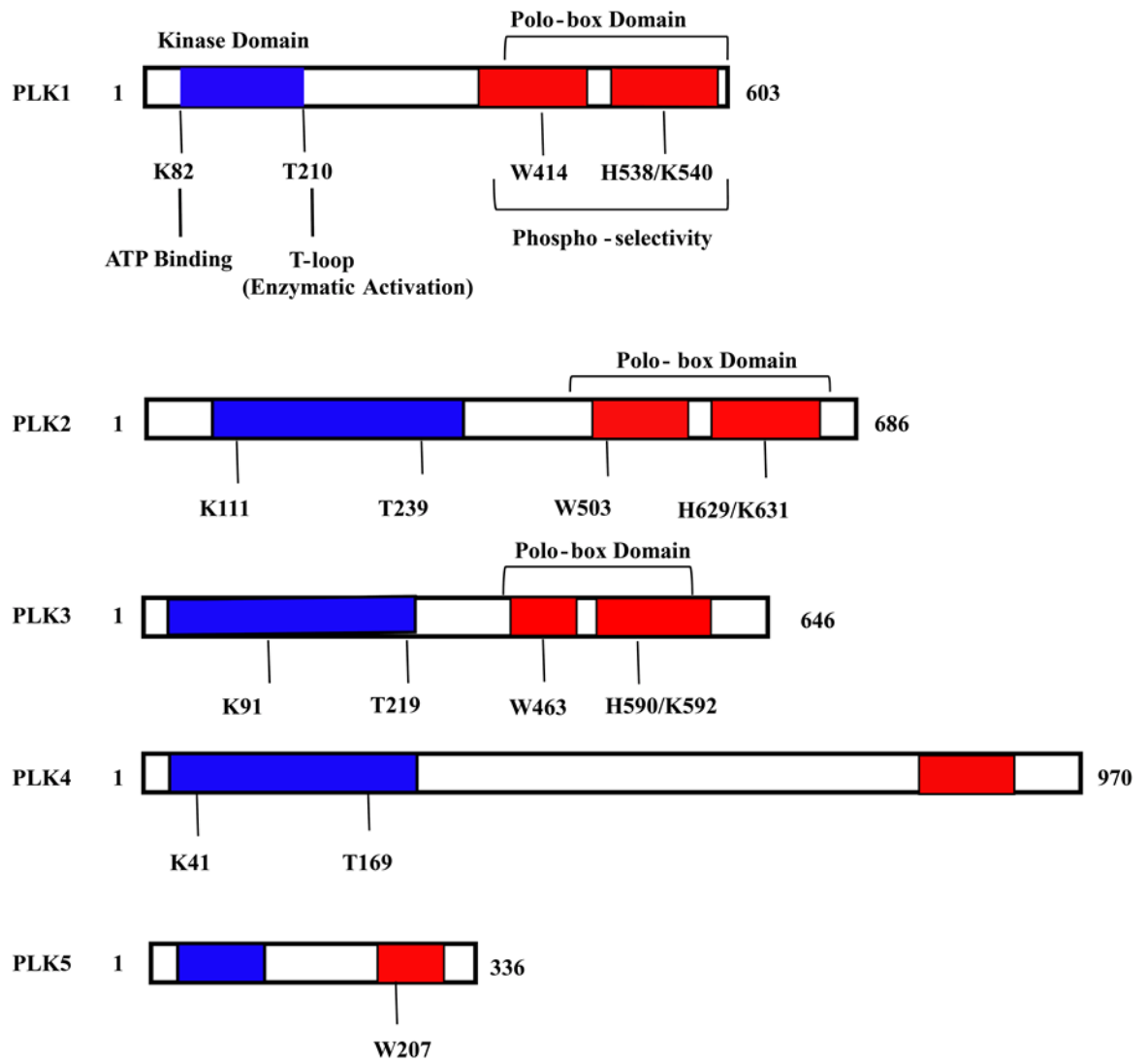


Figure 2: Structure of PLK family proteins

The open-reading frame amino-acid lengths are shown on the right. The kinase domain is depicted in blue while the polo-box domain is depicted in red. The residues that are critical for ATP-binding and enzymatic activation (T-loop) within the kinase domains and phospho-selectivity within the polo-boxes are indicated.

6. PLK1 Regulation

Many studies have shown that PLK1 expression as well as activity during the cell cycle is regulated at the transcriptional level (33). PLK1 transcription is regulated by several transcription factors such as FOXM1, p53 and the E2F family during various stages of the cell cycle (34, 35). PLK1 protein activity is regulated by phosphorylation on a conserved threonine residue (Thr210) in the kinase domain and this phosphorylation is mediated by Bora and Aurora A during normal mitotic entry and after DNA damage checkpoint recovery (36). Before entry into mitosis, PLK1 is phosphorylated by Aurora A kinase together with Bora, at the Thr210 site, activating it. Bora is able to open up the closed formation of PLK1 and Aurora A is able to phosphorylate PLK1 for activation during the mitotic entry (37). Other kinases such as PDK1 and phosphatases have also been identified to be involved in the regulation of PLK1 at this residue (34). PLK1 protein expression is cell cycle dependent. PLK1 expression is elevated in actively proliferating cells and is significantly different among different stages of the cell cycle (38). PLK1 usually gathers in the centrosome of the spindle poles during the early period of mitosis and then migrates gradually from spindle poles to the equatorial plate after entering into middle and late period of mitosis. At the end of mitosis, PLK1 gathers in the midbody. Therefore, PLK1 expression is barely detectable in G1 and S phase, gradually increases in G2 phase, and peaks in M phase (38). PLK1 regulation is also carried out by ubiquitination and proteosomal degradation by APC/C which is the ubiquitin ligase for PLK1 at mitotic exit (39).

7. Role of PLK1 in Cell Cycle Regulation

The PLK family of serine/threonine kinases are responsible for the control of mitotic regulatory networks (34, 38). Some of the cell cycle processes controlled by PLK1 include mitotic entry (40-42), centrosome maturation (43), chromosome segregation (42, 44, 45) and cytokinesis (46-48). At the time of cell division, PLK1 localizes to the cytoplasm and centrosomes in interphase and concentrates to the kinetochores and cytokinetic bridge (49). PLK1 when localized at the centromere contributes to ensure accurate chromosome alignment at metaphase and prevents lagging chromosomes at anaphase (49). At the time of mitotic entry, PLK1 regulates the activity of CDK1/Cyclin B complex and promotes G2/M cell cycle phase transition. The CDK1/Cyclin B complex is kept inactive by an inhibitory phosphorylation of CDK1 at Thr 14 and Tyr 15 by WEE1 and MYT1 kinases respectively, leading to the accumulation of Cyclin B1 during G2 phase of cell cycle. During the onset of mitosis, PLK1 activates the CDK1/Cyclin B complex by two means: by the activating phosphorylation of CDC25 phosphatase (50) which is a positive regulator and the inhibitory phosphorylation of MYT1 and WEE1 kinases which are the negative regulators (51). In late mitosis, PLK1 regulates the activity of APC/C which an E3 ubiquitin ligase responsible for the timely degradation of various mitotic regulators. This is also important for the regulation of chromosome segregation, mitotic exit and a subsequent stable G1 phase (52).

8. Role of PLK1 in DNA Damage Response

When DNA damage occurs, cells are unable to proceed into mitosis until the DNA is repaired— a process termed the G2 DNA damage checkpoint (53). Inactivation of PLK1 is a key mediator of this checkpoint. This checkpoint is particularly pertinent for double

stranded breaks as the duplicated DNA can be used as a template for homologous recombination; this opportunity is lost after mitosis. In response to the DNA damage, two kinases: ATM (ataxia telangectasia mutated) and ATR (ATM and RAD3-related) are activated. ATM and ATR phosphorylate Bora at Thr 501, causing it to be recognized by the E3 ubiquitin ligase for degradation (53). Once degraded, however, Bora cannot cooperate with Aurora A to facilitate the activation of PLK1 (53). The loss of PLK1 activity results in CDK1 inactivation, resulting in a G2 arrest. Following DNA repair, Bora expression is restored and PLK1 is again activated, allowing for the mitotic entry and recovery of cell division. The DNA damage response is distinct during mitosis. Phosphorylation of 53BP1 by CDK1 and PLK1 during mitosis impairs its function by inhibiting its ability to bind to ubiquitinated histone H2A (54). In this way, inhibition of PLK1 might enhance DNA repair by non-homologous end joining during mitosis (55).

9. Effect of PLK1 Inhibition in Cancer

PLK1 is overexpressed in many cancers such as lung, breast, kidney, head and neck carcinoma to name a few (56). PLK1 is implicated the development of genomic instability and aberrant cell proliferation and survival associated with tumorigenesis (57). PLK1 is a potential therapeutic target for cancer. PLK1 knockdown decreases cancer cell survival, induces apoptosis, and increases sensitivity a number of drugs and has a little effect in normal cells (58-60). PLK1 inhibition by RNA interference in cancer cells *in vitro* resulted in mitotic arrest and subsequent apoptosis (61). Some studies have shown that tumors with p53 deficiency and/or RAS mutations as well as PLK1 overexpression are sensitive to PLK1 inhibitors (62, 63). PLK1 has also been shown to facilitate survival

in PTEN depleted prostate cancer cells as PLK1 overexpression is required for PTEN-depleted cells to adapt to mitotic stress for survival (64).

10. Effect of PLK1 Inhibition in NSCLC

The 5-year survival rate of the patients with tumors with moderate expression of PLK1 was higher (52%) than those with a high level of PLK1 transcript (24%) in the tumors (65), thereby making PLK1 a potential target for NSCLC therapy. Also, activating mutations in KRAS are common in NSCLC (66) and previous studies have shown that RAS mutant cancer cells are sensitive to PLK1 inhibitors (62, 63). Based on a study published by our lab, we did not observe a robust, consistent correlation between KRAS mutation and PLK1 inhibitor sensitivity *in vitro* (67).

A study showed that short hairpin RNAs (shRNAs) against PLK1 reduced the growth of A549 NSCLC cells in mouse tumor xenografts and suppressed tumor PLK1 expression (68). Another study showed that PLK1 inhibition using systemic treatment with siRNA inhibited the growth of A549 cells in the mouse liver, thereby showing a role for PLK1 in lung cancer liver metastasis (69). Previous studies in our lab showed that mesenchymal NSCLC cells were more sensitive to PLK1 inhibition in comparison to epithelial NSCLC cells based on differential E-Cadherin mRNA and protein expression as well as the 76-gene EMT score developed by the department (67, 70).

Studies have also shown that PLK1 inhibition is effective in NSCLC with acquired EGFR-TKI resistance (71) as well as NSCLC with acquired EGFR-TKI resistance that had undergone EMT (72).

11. PLK1 Inhibitors in Clinical Development

Two main types of PLK1 inhibitors have been developed: ATP-competitive kinase inhibitors and PBD inhibitors. The ATP-competitive inhibitors target the deep groove in the ATP binding serine-threonine kinase domain (73). One of the main drawbacks of the ATP-competitive inhibitors is the development of resistance due to high conservation of ATP binding domains of different kinases and frequent mutations in the ATP binding sites (74). Also, one of the major problems associated with the currently available ATP-competitive inhibitors is their low degree of selectivity against other kinases, and their toxicity could be partly due to their interference with other kinases (75). In order to develop more specific inhibitors against PLK1, anti-PLK1 agents that target the PBD domain are currently being tested pre-clinically and have demonstrated improved specificity towards PLK1 (76). The PBD inhibitors are unique to polo-like kinases and are therefore much more specific than inhibitors that target the ATP-binding domain (77).

The drug used in this study is Volasertib or BI6727, an ATP-competitive PLK1 inhibitor derived from a dihydropteridinone lead structure (78). Volasertib potently inhibits PLK1 and PLK2 with IC₅₀ values of 0.87 and 5 nM, respectively, and shows relatively lower potency on PLK3 (56 nM) but does not inhibit PLK4 (>20 μ M) (78). Volasertib inhibits PLK1 which leads to a disruption of the mitotic spindle assembly resulting in a distinct mitotic arrest phenotype (known as ‘Polo arrest’) in prometaphase, accumulation of phospho-histone H3 and formation of aberrant monopolar mitotic spindles followed by apoptosis (78-80). All the PLK1 inhibitors in clinical development have been summarized in the table below.

Table 1: PLK1 inhibitors in clinical development

Inhibitor	Status	Company or Lab	Class
BI2536	Experimental	Boehringer Ingelheim	ATP-competitive
GSK461364	Experimental	GlaxoSmithKline	ATP-competitive
Volasertib (BI6727)	Experimental	Boehringer Ingelheim	ATP-competitive
ZK-thiazolidinone	Experimental	Bayer Schering Pharmacy	ATP-competitive
Rigosertib (ON01910)	Experimental	Onconova Therapeutics Inc.	ATP-competitive
Cyclapolin 9	Experimental	Cyclacel	ATP-competitive
GW 843682X	Experimental	GlaxoSmithKline	ATP-competitive
NMS-937	Experimental	Nerviano Medical Sciences	ATP-competitive
SBE 13 hydrochloride	Experimental	Institute of Organic Chemistry & Chemical Biology, Goethe-University	ATP-competitive

TAK960 hydrochloride	Experimental	Takeda Pharmaceutical Company	ATP-competitive
Poloxin	Experimental	Max Planck Institute of Biochemistry and Munich Center for Integrated Protein Science	Non-ATP-competitive
Poloxin-2	Experimental	Institute of Organic Chemistry, University of Leipzig	Non-ATP-competitive
RO3280	Experimental	Hoffmann-La Roche	Non-ATP-competitive

12. Epithelial-to-Mesenchymal Transition (EMT) and Cancer

Epithelial-to-mesenchymal transition (EMT) is a process that involves the transdifferentiation of epithelial cells into motile mesenchymal cells (81). The EMT phenomenon plays a very important role in tumor progression and metastasis (82). EMT results in the loss of cell-cell contacts and the reorganization of the intracellular cytoskeleton thereby leading to increased cell migration and invasion (83). EMT allows cancer cells to invade the stroma and vasculature, thereby leading to tumor dissemination and metastases (84). More importantly, EMT enables cancer cells to avoid apoptosis, anoikis, and oncogene addiction (85). EMT can be easily recognized in the molecular level by the reduced expression of epithelial markers such as E-Cadherin and β -Catenin, and the elevated expression of mesenchymal markers such as N-Cadherin and vimentin. One of the well studied proteins that induce EMT are the two-handed δ EF1 family transcription factors ZEB1 and ZEB2 (86-88). These transcription factors induce EMT by the

suppression of E-Cadherin and other epithelial differentiation genes by binding to the E-boxes of their promoters (89). MicroRNAs (miRs) are small non-coding RNAs that control development and maintenance by pleiotropic regulation of cellular functions (90). The microRNA-200 family are expressed in epithelial cells (91). In normal as well as cancer epithelial cells, the miR-200 family exists in a double negative feedback loop with the ZEB1 and ZEB2 transcriptional repressors (92-95). The ZEB/miR-200 balance is regulated by inducers of EMT such as TGF β , which leads to the loss of miR-200 expression and a shift to a mesenchymal phenotype (93).

A study carried in prostate cancer cells showed that forced overexpression of PLK1 in prostate epithelial cells led to the downregulation of epithelial markers E-cadherin and cytokeratin 19 and upregulation of mesenchymal markers N-cadherin, vimentin, fibronectin, and SM22 (96). The studies carried out in our lab showed that mesenchymal NSCLC cell lines were sensitive while epithelial NSCLC cell lines were resistant to PLK1-inhibition induced apoptosis (67). The cells were defined as epithelial or mesenchymal based on a 76-gene EMT score developed by the department (70).

13. Hypothesis and Specific Aims

NSCLC cell lines have diverse sensitivities to PLK1 inhibition, which is consistent with the results of clinical trials of PLK1 inhibitors. However, predictive biomarkers have not been used to select patients likely to respond to PLK1 inhibitors, and the mechanisms of sensitivity and resistance to PLK1 inhibitors have not been elucidated, making these unknowns a major gap in knowledge. The main goal of the project is to test the hypothesis that PLK1 inhibition will cause apoptosis in mesenchymal but not epithelial NSCLC *in vivo*. Furthermore, to identify the mechanisms of PLK1 inhibitor-induced sensitivity, we will test the role of molecules that are differentially expressed or modulated in sensitive and resistant NSCLC cell lines.

Aim 1: To test the hypothesis that PLK1 inhibition will cause apoptosis in mesenchymal NSCLC but not epithelial NSCLC *in vivo*.

1(a). To test the effects of PLK1 inhibition in epithelial and mesenchymal patient derived xenograft (PDX) models.

A minimum of 14 PDX models is required to have 80% power to detect a spearman correlation of 0.7 between the tumor size and E-cadherin score using a 2-sided test at a significance level of 0.05. For each model, tumors will be implanted in 25 mice and will be monitored daily. Once the tumor reaches a volume of ~150 mm³, the mice will be treated with 30 mg/kg of the PLK1 inhibitor Volasertib or vehicle. Tissue for RNA and protein analysis will be obtained from the PDX tumors to study gene and protein expression. The EMT score, protein and gene expression of E-Cadherin, E-Cadherin score, markers of apoptosis, proliferation and target inhibition will be measured.

1(b). To determine if manipulation of EMT will affect PLK1 inhibition-induced apoptosis in an orthotopic, immunocompetent NSCLC mouse model.

Cell lines derived from a $Kras^{LA1/+}p53^{R172H\Delta G/+}$ (KP) genetically engineered mouse model that develop advanced lung adenocarcinomas have EMT properties that are manipulable by ectopic expression of ZEB1 or miR-200a/b. The stable 393P cell lines that express ZEB1 or the 344SQ cell lines that express miR200 will be injected into syngeneic, immunocompetent mice (6-8 week old 129S/V male mice). The induction of miR200 or ZEB1 expression will be done through doxycycline dissolved in water. Following injection, mice will be randomized into two groups to receive vehicle (control) or 30 mg/kg Volasertib weekly for 4 weeks. The mice lungs will be imaged by micro-CT once a week to measure tumor volume. The lungs of the mice will be collected at the end of the experiment for analysis.

Aim 2: To develop a method for accurate metastatic lung tumor burden calculation from CT in an orthotopic mouse model.

To develop a novel method for accurate lung tumor burden calculation from CT in an orthotopic mouse model. The rationale for the development of this method is because there is no respiratory gating in the CT, no contrast agents are used to identify tumors thus making it difficult to distinguish between tumors and blood vessels and metastatic tumors (such as the tumors in the thoracic cavity) are not taken into consideration while calculating tumor burden.

Hypothesis: Mass of Thoracic Cavity does not change over time and observed changes are due to tumor burden.

Aim 3: To test the hypothesis that molecules that are differentially expressed at baseline or differentially modulated following PLK1 inhibition mediate PLK1 inhibitor-induced apoptosis.

Hypothesis: Higher β -Catenin expression in epithelial cells mediates PLK1 inhibition-induced apoptosis in NSCLC by EMT and interacting with PLK1 in the centrosome. SMAD4 mediates sensitivity of mesenchymal NSCLC to PLK1 inhibition-induced apoptosis by activation of TGF- β Pathway. Differential modulation of PDK1 following PLK1 inhibition mediates PLK1 inhibitor-induced apoptosis by regulating downstream survival signaling pathways.

Chapter 2: Materials & Methods

1. Reagents and Antibodies

The PLK1 inhibitor Volasertib was purchased from Selleck Chemicals (Houston, Texas) and a stock solution of 10mmol/L was prepared in DMSO. The non-targeting control, CTNNB1 and SMAD4 SMARTpool siRNAs were purchased from Dharmacon (GE Lifesciences) and the sequences are as outlined in Table 1 below:

Table 2: List of siRNA used in the study

GENE	TARGET SEQUENCE
Non-targeting Control	1. UGGUUUACAUGUCGACUAA 2. UGGUUUACAUGUUGUGUGA 3. UGGUUUACAUGUUUUCUGA 4. UGGUUUACAUGUUUCCUA
CTNNB1	1. GAUCCUAGCUAUCGUUCUU 2. UAAUGAGGACCUAUACUUA 3. GCGUUUGGCUGAACCAUCA 4. GGUACGAGCUGCUAUGUUC
SMAD4	1. GUGUGCAGUUGGAAUGUAA 2. GUACAGAGUUACUACUAG 3. GAGUAUUGGUGUCCAUG 4. GUAAUGCUCUCAAGUAU

PDK1-EGFP overexpression plasmid was kindly provided by Dr. Gordon Mills. The antibodies that were used in the study were diluted in 5% BSA in TBST with 0.05% NaN₃ and are outlined in the table below:

Table 3: Description of antibodies used in the study

ANTIBODY	COMPANY	HOST SPECIES	CATALOG NO.	DILUTION
PLK1	Cell Signaling Technologies	Rabbit	4513	1:1000
p-PLK1 T210	Cell Signaling Technologies	Rabbit	9062	1:1000
PARP	Cell Signaling Technologies	Rabbit	9532	1:1000
Cleaved PARP	Cell Signaling Technologies	Rabbit	5625	1:1000
Caspase 3	Cell Signaling Technologies	Rabbit	9665	1:1000
p-Histone H3 (S10)	Cell Signaling Technologies	Rabbit	3377	1:1000
TCTP	Cell Signaling Technologies	Rabbit	5128	1:1000
p-TCTP (S46)	Cell Signaling Technologies	Rabbit	5251	1:1000
NPM	Cell Signaling Technologies	Rabbit	3542	1:1000
p-NPM (S4)	Cell Signaling Technologies	Rabbit	3520	1:1000
γ -H2AX (S139)	Cell Signaling Technologies	Rabbit	9718	1:1000
E-Cadherin	Cell Signaling Technologies	Rabbit	3195	1:1000
Vimentin	Cell Signaling Technologies	Rabbit	5741	1:1000
β -Catenin	Cell Signaling Technologies	Rabbit	8480	1:1000

SMAD4	Cell Signaling Technologies	Rabbit	38454	1:1000
GAPDH	Cell Signaling Technologies	Rabbit	5174	1:10000
Wee1	Cell Signaling Technologies	Rabbit	13084	1:1000
p-Wee1 (S642)	Cell Signaling Technologies	Rabbit	4910	1:1000
PDK1	Cell Signaling Technologies	Rabbit	13037	1:1000
p-PDK1 (S241)	Cell Signaling Technologies	Rabbit	3438	1:1000
CMYC	Cell Signaling Technologies	Rabbit	5605	1:1000
p-CMYC (S62)	Cell Signaling Technologies	Rabbit	13748	1:1000
AKT	Cell Signaling Technologies	Rabbit	4691	1:1000
p-AKT (S473)	Cell Signaling Technologies	Rabbit	4060	1:1000
4E-BP1	Cell Signaling Technologies	Rabbit	9452	1:1000
p-4B-BP1 (S65)	Cell Signaling Technologies	Rabbit	13443	1:1000
ZEB1	Cell Signaling Technologies	Rabbit	3396	1:1000
PCNA	Cell Signaling Technologies	Mouse	2586	1:1500
β -Actin	Cell Signaling Technologies	Mouse	3700	1:10000

2. Cell Culture

Human NSCLC cell lines were obtained, maintained and genotyped by Short Tandem Repeat (STR) profiling as described previously (67). Murine 344SQ cell lines with an inducible miR200 expression was kindly provided by Dr. Don Gibbons' lab. Murine 393P cell line with constitutively active ZEB1 was kindly provided by Dr. Jonathan Kurie's lab. The cells were routinely tested for mycoplasma contamination using a Mycoplasma detection kit (Lonza). The cell lines were cultured in RPMI-1640 media containing 10% Fetal Bovine Serum (FBS) and 2% Penicillin/Streptomycin. The cells were maintained in a humidified atmosphere with 5% CO₂ at 37°C.

3. Cell Viability Assay

CellTiter Glo (Promega) luminescent assay was used as per the manufacturer's specifications to determine cell viability based on intracellular ATP levels. In brief, 800 cells were plated in each well in a 384-well plate. The cells were incubated with 7 different concentrations (half-fold serial dilution) of the PLK1 inhibitor Volasertib, the highest being 500nM for 72h. The luminescence measured is proportional to the amount of intracellular ATP and is an index of cell number.

4. Apoptosis Assay

TUNEL (terminal deoxynucleotidyl transferase dUTP nick end labeling) staining (APO-BrdU kit; BD Biosciences) was used to measure apoptosis. In general, DNA breaks and total cellular DNA is labelled to detect apoptotic cells based on the manufacturer's protocol and the data was generated using a flow cytometer (Gallios, Beckman Coulter). The data was analyzed using Kaluza (Beckman Coulter).

5. Western Blot

Sub-confluent NSCLC cell lines were lysed with 1X Cell Lysis Buffer containing 20mM Tris-HCl (pH 7.5), 150mM NaCl, 1mM Na₂EDTA, 1mM EGTA, 1% Triton, 2.5mM sodium pyrophosphate, 1mM β-glycerophosphate, 1mM Na₃VO₄ and 1 μg/ml

leupeptin (Cell Signaling Technology) on ice, The lysed cells were collected and centrifuged at 14,000 x g for 15 minutes and the supernatant lysate was collected. The protein concentration of the lysates was measured using the Pierce bicinchonic acid (BCA) protein assay kit (ThermoFisher Scientific). Lysates of 1 $\mu\text{g}/\mu\text{l}$ concentration was prepared by mixing with Laemmli Sample Buffer (Bio-Rad Laboratories) and water. Equal amounts of proteins from the NSCLC lysates were separated using 4-20% SDS-PAGE gels and were immunoblotted with primary antibodies overnight. The proteins were detected with horseradish peroxidase-conjugated secondary antibodies and enhanced chemiluminescent substrate (ThermoFisher Scientific). The densitometric quantification of the protein normalized to β -Actin was carried out using ImageJ (NIH, Bethesda).

6. Transfection

For knockdown assays, 1.5×10^6 NSCLC cells were plated in 10cm 24 hours prior to transfection. The following day, Lipofectamine RNAiMAX transfection reagent (Invitrogen) was mixed in 1X OPTI-MEM Media (Gibco). In a separate tube, the SMARTpool siRNA which comprises of a predesigned set of 4 siRNA for the respective targets was mixed in 1X OPTI-MEM Media. The siRNA mixture was added to the Lipofectamine RNAiMAX mixture and incubated in room temperature for 5 minutes. This siRNA-liposomal mixture was then added to the cells and were incubated at 37°C for 72 hours. Protein lysates were then collected at the aforementioned time point and analyzed via western blot.

For stable transfection of the PDK1-EGFP plasmid, 1.5×10^6 cells were plated 24 hours prior to transfection. 5 μg of plasmid was transfected with the help of Lipofectamine 3000 transfection reagent (Invitrogen) in OPTI-MEM Media (Gibco) and the cells were incubated at 37°C for 48 hours. Fresh RPMI1640 medium with 10% FBS was added to

the NSCLC cell culture plates, and the NSCLC cells were allowed to recover for 24 hours. Transfected NSCLC cells were selected using 700 μ g/ml Geneticin.

7. Subcutaneous Tumor Implantation for PDX Models

All animal research was conducted in accordance with The University of Texas MD Anderson Cancer Center's Institutional Animal Care and Use Committee. PDX tumors that were growing logarithmically were implanted into the right flank of female nude mice (Envigo Harlan Laboratories, Indianapolis). The tumors were measured twice a week with the help of Vernier calipers. Tumor volume was calculated by using the formula $(\text{length} \times \text{width}^2)/2$. Once the tumor volumes reached $\sim 150\text{mm}^3$, the mice were randomized into two groups, control and Volasertib. The mice were treated with 30mg/kg of vehicle control or Volasertib intravenously (IV tail vein injection) once a week up to 4 weeks. The mice were then euthanized and the tumors were excised. Protein was extracted from the tumor in order to check for target inhibition, apoptosis and proliferation. Multiple row t-tests was used in order to see the differences in tumor volume between the two groups over time.

8. Orthotopic Lung Injection in immunocompetent mouse models

All mice were manipulated and maintained conducted in accordance to UT MD Anderson's Office of Research Administration and IACUC committee guidelines. 129/sv male mice at 4-6 weeks of age were purchased from Charles River Laboratory (Massachusetts). The mice were of 8 weeks of age and at the start of the experiment. CT imaging of the lungs was carried out to serve as baseline study. The mice were fully anesthetized by 2-4% isofluorane inhalation throughout the entire procedure.

The mice were placed in a right lateral decubitus position. The lower edge of the right rib cage was identified by palpation and the area trimmed with a hair clipper. After cleaning with 70% ethanol solution, the area was shaved with a razor blade. Finally, the incision site was sterilized with Betadine solution. A 1-cm incision in the skin was made along the lower edge of the rib cage. The cephalic edge of the skin was retracted with forceps to reveal the underlying subcutaneous tissue and fat. A second incision was made through the fatty tissue to reveal the rib cage and the thoracic cavity. The respiring lung was identified as a pale structure under the rib cage, whereas the more caudal spleen was identified as a dark red organ.

Tumor cells (200,000 cells in 50 μ l) were injected into the lower third of the left lung using an insulin syringe. The left lung was checked for an absence of intra-thoracic hemorrhage or collapse prior to closing the incision. Using forceps, the opposing skin was held together and stapled with an Auto-clip stapler using two to three 9-mm staples.

The mice were given 0.05-0.10 mg/kg Buprenorphine analgesic following this procedure. The mice were kept warm under a heat lamp and monitored for recovery. The cage was returned to the rack when the mice were able to move on all four limbs.

9. Endotracheal Intubation and CT Imaging

The mice were placed in an inhalation anesthesia induction chamber (Isoflurane 5% for induction, and 1.5% to 3% for maintenance). When the mice were fully anesthetized, an endotracheal tube (22 gauge x 1 inch length) was placed using a BioLite mouse intubation system (Braintree Scientific). The mice were then placed onto a holder and moved to the CT system (Precision XRay Incorporated XRAD 225Cx). The CT parameters used were 60Kv 4mA and 3RPM. The mice were mechanically ventilated at 60BPM throughout the procedure and a 20 second breathe hold was applied during the

acquisition at 20cm/H₂O (97). The pressure was monitored through an inline manometer. After the acquisition was complete, the mice were extubated, and recovered in a clean, warm cage until sternal.

10. CT Image Analysis

Tumor Mass from Mass of Thoracic Cavity

The CT images were exported in Digital Imaging and Communications in Medicine (DICOM) format. The DICOM image sequence was uploaded in Raystation 5.0.2 Research (Raysearch, Sweden). The lung volume with a constant threshold of -800 to 0 was determined based on the lung region growing algorithm in order to remove bias. A Region of Interest (ROI) was drawn in the chest cavity from the base of the lung to the top of the trachea using the smart contour option of Raystation. Mass of the thoracic cavity (MTC) was calculated as a function of ROI Volume and CT Intensity. Tumor Mass was extrapolated by comparison with the MTC of the mice from the CT images at baseline.

Sum of Cross-Product (SCP) Method

The quantification of tumor burden by the manual cross-product analysis of micro CT images was carried out as previously described (98). The lung micro CT DICOM images were viewed in the coronal plane on Fiji (ImageJ) software (<http://fiji.sc/Fiji>). The tumors were visualized in the coronal plane and the largest cross-sectional plane of each tumor was identified. From this, the maximal tumor diameter (d_1) and the largest perpendicular diameter (d_2) was determined by placing a ruler on the screen. The total tumor burden was then calculated by the sum of cross products ($SCP = \sum (d_1 * d_2)$) of all tumors per animal. This method has been validated by *ex vivo* micro CT analysis (98).

Tumor & Vessel Volume (T&V) Method

Tumor and vessel volume was calculated as previously described (99). In brief, the functional lung volume was calculated based on a region growing algorithm with a threshold value set -800 to 0 voxels chosen empirically based on visual inspection of a few mice on Raystation 5.0.2. the total chest space volume excluding the heart was calculated using the region growing algorithm and semi-automated contouring. The combined tumor and vasculature volume (T&V) was determined by subtracting the functional lung volume from total chest space volume (99).

Ellipsoidal Tumor Volume Method

The images were viewed on MicroView analysis + version 2.2 software (GE Healthcare). One to five tumors were identified and selected in each mouse on the axial view. The three greatest diameters of each tumor were measured on the axial, coronal and sagittal views (referred to as x, y, and z). These values were then used to calculate the volume of the tumor using the formula of an ellipsoid ($[4\pi/3][x/2][y/2][z/2]$) (100, 101).

Aerated Lung Volume Method

Functional lung volume measurement is a fully automated method that utilized the gray-level, morphological and texture features to segment the aerated lung region using a region-growing algorithm (102). Measurement of the functional lung volume is an inverse surrogate measure of tumor burden (102). The measurement of aerated lung volume was done at the last time point of the studies due to lack of respiratory gating facilities.

11. Statistical Analysis

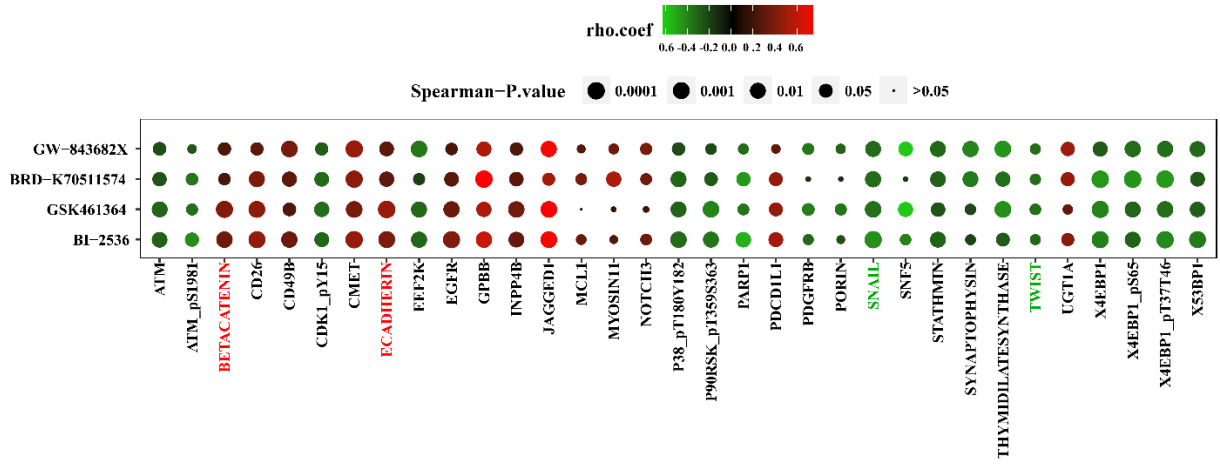
Statistical analysis was carried out using GraphPad Prism 7 software (GraphPad, USA). Multiple row t-tests was used to compare changes in tumor volume between control and Volasertib treated mice. One-way anova and Tukey's multiple comparison test was used to compare the changes in the mass of thoracic cavity of the disease-free mice. Pearson correlation and linear regression was carried out to compute R value for the correlation graphs. Unpaired t-tests was used to compare changes in protein expression between the NSCLC cell lines.

Chapter 3: Results

1. EMT markers correlate with PLK1 inhibition in NSCLC cell lines in an independent dataset

In order to identify novel biomarkers of response to PLK1 inhibition, reverse phase protein array (RPPA) protein expression data was downloaded from MD Anderson Cell Lines Project (MCLP) database (<http://tcpaportal.org/mclp/#/>) and PLK1 inhibitor sensitivity data for BI2536, GSK461364, BRD-K70511574 and GW-843682X were downloaded from The Cancer Therapeutics Response Portal V2 (Broad Institute, <https://portals.broadinstitute.org/ctrp/>) for 64-71 NSCLC cell lines (71 for BI2536, 69 for GSK461643, 68 for BRD-K70511574 and 64 for GW843682X). Spearman Correlation was applied to identify the correlation between drug sensitivity and protein expression using R package. Thirty three proteins correlated significantly with sensitivity to two or more PLK1 inhibitors (Figure 3). As seen in our previous study, E-cadherin ($p < 0.001$, $r > 0.3$), and β -Catenin ($p < 0.001$, $r > 0.3$) protein expression was higher and Snail ($p < 0.01$, $r > -0.3$) and Twist ($p > 0.05$, $r < -0.3$) protein expression was lower in the NSCLC cell lines resistant to the PLK1 inhibitors (103).

A



B

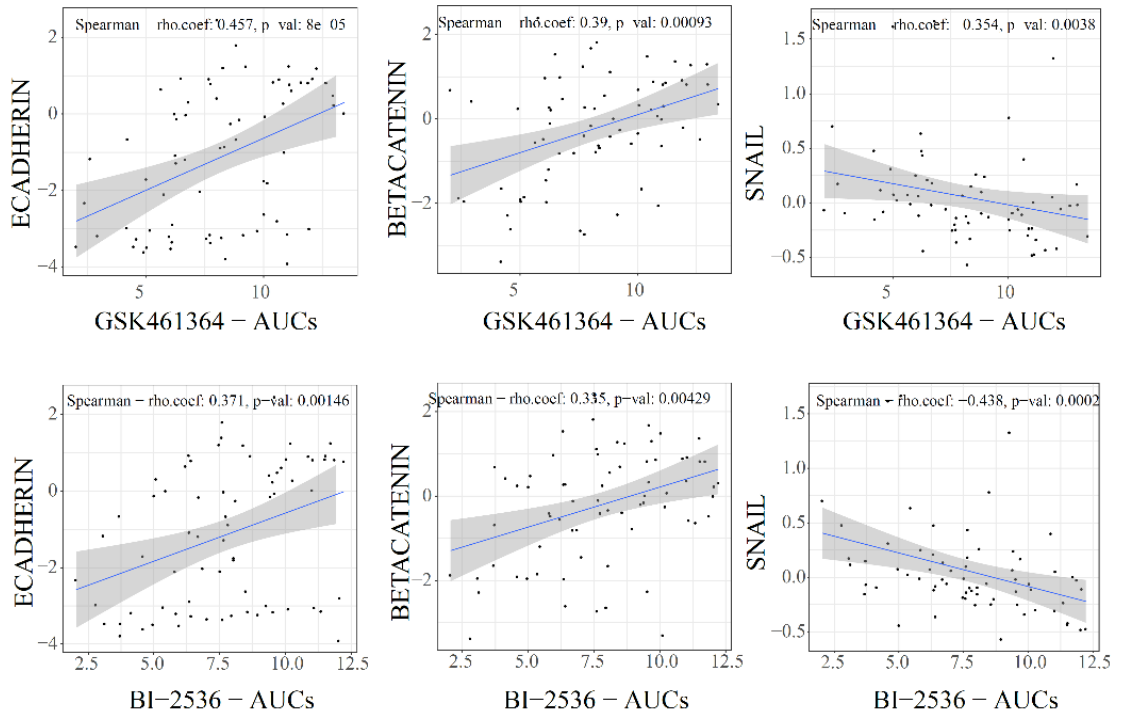


Figure 3: EMT markers correlate with PLK1 inhibition in a panel of NSCLC cell lines in an independent dataset.

A: Dot plot showing correlation between PLK1 inhibitors (BI2536, GSK461364, BRD-K70511574 and GW-843682X) sensitivity from CTRPv2 and RPPA data from MCLP (104).

B: Correlations of E-Cadherin, β -Catenin, and Snail with area under the curve (AUC) of GSK461364 and BI2536 respectively.

2. Mesenchymal NSCLC tumors are more sensitive in comparison to epithelial NSCLC tumors to PLK1 inhibition induced apoptosis in patient-derived xenograft (PDX) mouse models

In order to test the hypothesis that mesenchymal NSCLC tumors are more sensitive than epithelial NSCLC tumors to PLK1 inhibition induced apoptosis *in vivo*, 13, 29 or 84 PDX models are required to have 80% power to detect Spearman correlations of 0.7, 0.5 or 0.3 between the tumor size ratio and E-Cadherin score using a 2-sided t-test and a null hypothesis correlation of 0 at a significance level of 0.5. The PDX tumors were obtained from our lab and Dr. Bingliang Fang's lab (23) and their EMT status was determined by E-Cadherin and vimentin protein expression. The tumors with high E-Cadherin protein expression were considered epithelial and those with high vimentin expression were considered mesenchymal PDX models (Figure 4). We implanted tumors of four different PDX models HLC4, TC402, TC424 and TC370 that have diverse EMT status and the mice were randomized into two groups, vehicle control and Volasertib. The tumors were measured twice a week for 4 weeks after which the tumors were resected.

In HLC4 PDX model which has an intermediate EMT phenotype based on membrane E-Cadherin score which is calculated based on the intensity and completeness of membrane E-Cadherin immunostaining (105) (E-Cadherin score 67.4), there was no significant change in mean tumor volume at the end of the experiment between the vehicle and Volasertib treated mice ($p=0.0947$) based on Mann-Whitney t-test. Based on multiple row t-tests in order to compare tumor volumes between the groups over time, a significant decrease in tumor volume was observed from day 6 up to day 24 between vehicle and Volasertib treated mice ($p<0.05$) (Figure 5). Two out of 10 mice in the Volasertib treated group had tumor regression and 8/10 grew on therapy (Figure 5). There was no change in

the levels of apoptosis or proliferation based on cleaved PARP and PCNA protein expression in the tumor tissues as seen in immunoblotting (Figure 6). PLK1 inhibition was demonstrated by the increase in the levels of phosphorylated histone H3 (Ser 10).

In the epithelial TC402 PDX model, there was a significant decrease in tumor volume between the vehicle and Volasertib treated mice ($p=0.012$) at the end of the experiment based on Mann-Whitney t-test. Based on multiple row t-tests to compare tumor volumes between the groups over time, a significant difference in tumor volume was observed from day 6 until the end of experiment, i.e., day 34 ($p<0.05$) (Figure 5). Two out of 10 mice in the Volasertib treated group had tumor regression and 8/10 tumors grew on therapy (Figure 5). There was an increase in the level of phospho histone H3 (S10) in the Volasertib treated tumors. There was no significant difference in the levels of cleaved PARP or PCNA between the vehicle and Volasertib treated tumors (Figure 6).

In the mesenchymal TC424 PDX model, there was a significant decrease in tumor volume between the vehicle and Volasertib treated mice ($p<0.0001$) based on Mann-Whitney t-test. Based on multiple row t-tests to compare tumor volumes between the groups over time, a significant difference in tumor volume was observed from day 3 until the end of experiment, i.e., day 39 ($p<0.05$) (Figure 5). Eight out of 10 mice in the Volasertib treated group had tumor regression and 2/10 treated tumors grew on therapy (Figure 5). There was an increase in the level of phospho histone H3 (S10) in the Volasertib treated tumors. There was no significant difference in the levels of cleaved PARP or PCNA between the vehicle and Volasertib treated tumors (Figure 6).

In the mesenchymal TC370 PDX model, there was a significant decrease in tumor volume between the control and Volasertib treated mice ($p<0.0001$) based on Mann-Whitney t-test. Based on multiple row t-tests to compare tumor volumes between the

groups over time, a significant difference in tumor volume was observed from day 3 until the end of experiment, i.e. day 34 ($p < 0.05$) (Figure 5). Six out of 10 mice in the Volasertib treated group had tumor regression and 4/10 treated tumors grew on therapy (Figure 5). There was no change in the level of phospho histone H3 (S10) between the vehicle and Volasertib treated tumors. There was no significant difference in the levels of cleaved PARP or PCNA between the control and Volasertib treated tumors (Figure 6).

Together, these data demonstrate that tumor regression is observed in the mesenchymal TC424 and TC370 PDX models after PLK1 inhibition while slower tumor growth or growth arrest is observed in the intermediate HLC4 and epithelial TC402 PDX models (Figure 5). It also suggests that lung tumor heterogeneity might be playing a role in mediating response to PLK1 inhibitors.

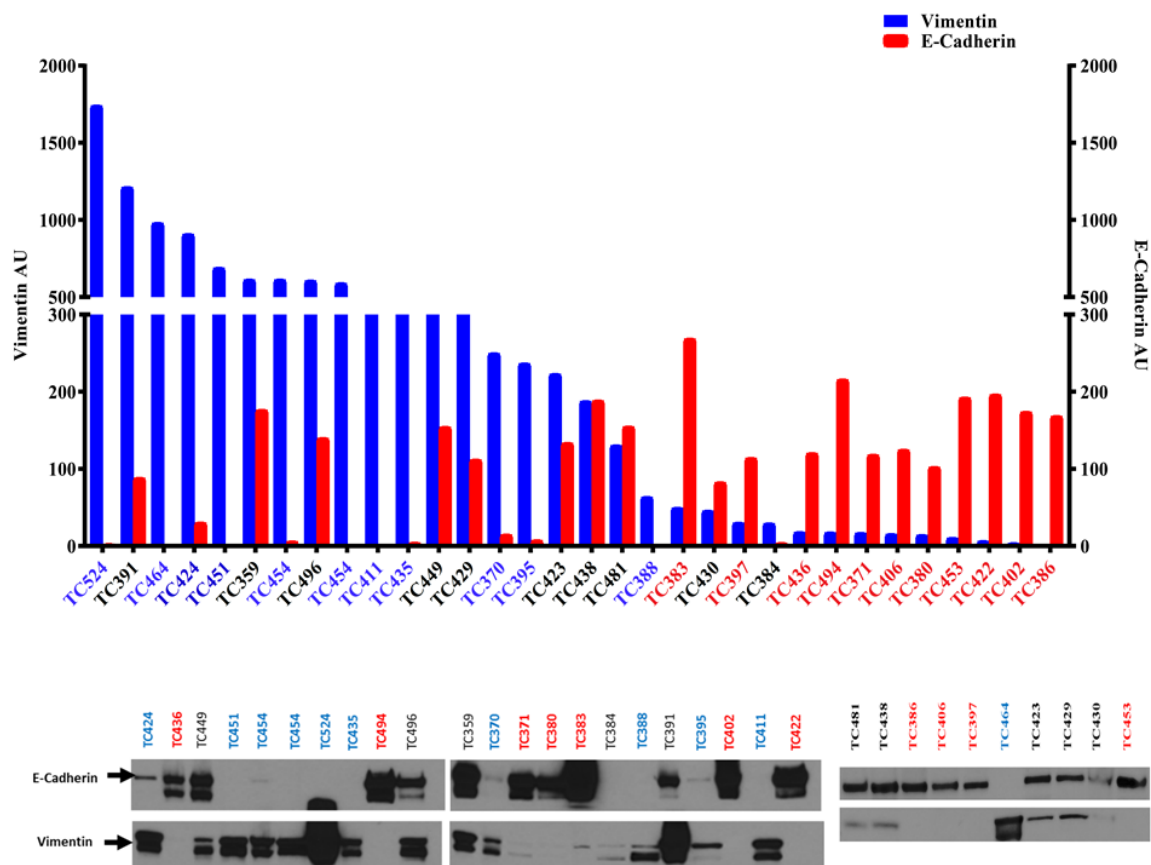
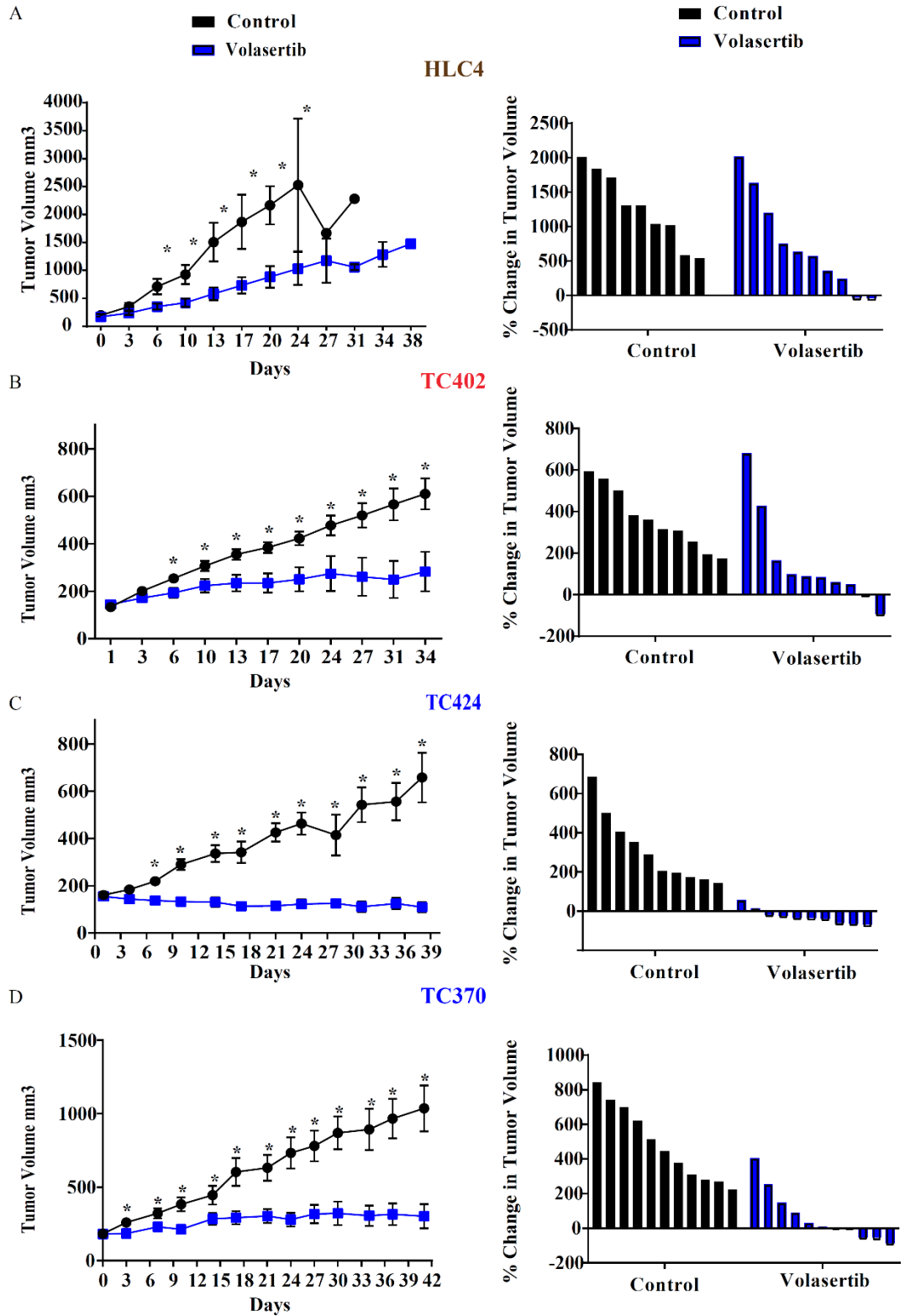


Figure 4: PDX tumors have diverse EMT phenotypes

The epithelial or mesenchymal phenotype of the PDX tumors were determined based on E-Cadherin and vimentin protein expression as seen in the immunoblot (lower). The bar plot is a quantification of the protein expression (upper). Those tumors with higher E-Cadherin expression are considered epithelial (as depicted in red text) while those that have higher vimentin expression are considered mesenchymal (as depicted in blue text). The PDX tumors that express both are considered intermediate (as depicted in black text).



E

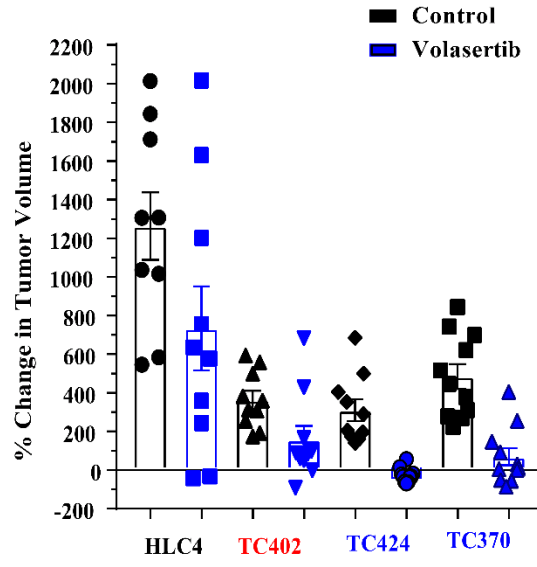


Figure 5: Mesenchymal NSCLC PDX tumors are more sensitive to PLK1 inhibition induced apoptosis in comparison to epithelial NSCLC PDX tumors

A: The HLC4 intermediate PDX tumor volumes of control and Volasertib treated mice over time are depicted in the left. A significant difference in tumor volume was observed from day 6 to day 24. The waterfall plot on the right depict the percentage change in tumor burden of each individual mouse at the end point.

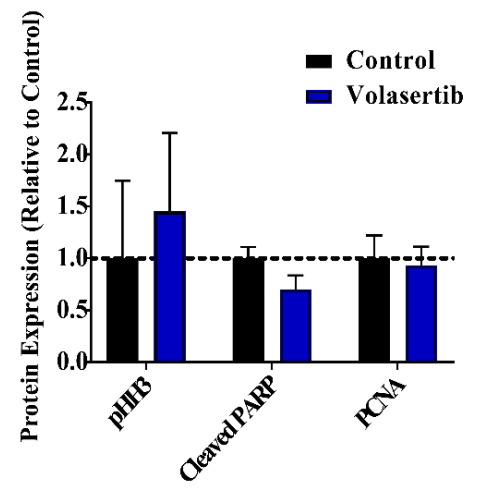
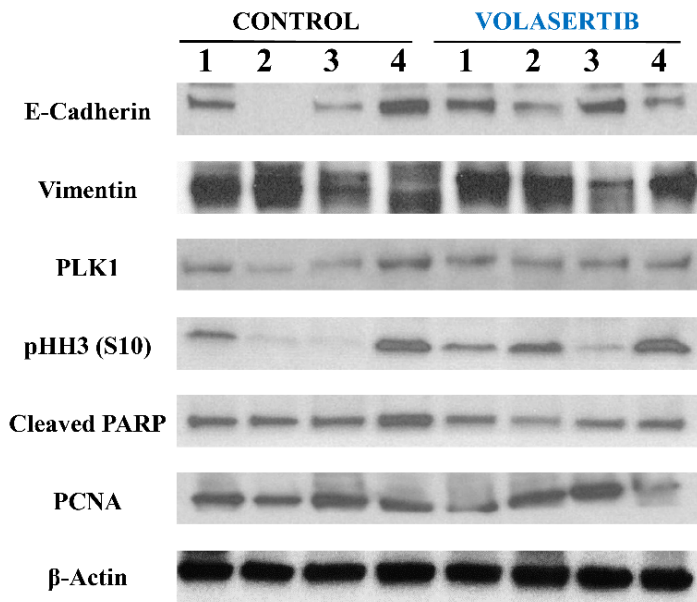
B: The TC402 epithelial PDX tumor volumes of control and Volasertib treated mice over time are depicted in the left. A significant difference in tumor volume was observed from day 6 to day 34. The waterfall plot on the right depict the percentage change in tumor burden of each individual mouse at the end point.

C: The TC424 mesenchymal PDX tumor volumes of control and Volasertib treated mice over time are depicted in the left. A significant difference in tumor volume was observed from day 6 to day 39. The waterfall plot on the right depict the percentage change in tumor burden of each individual mouse at the end point.

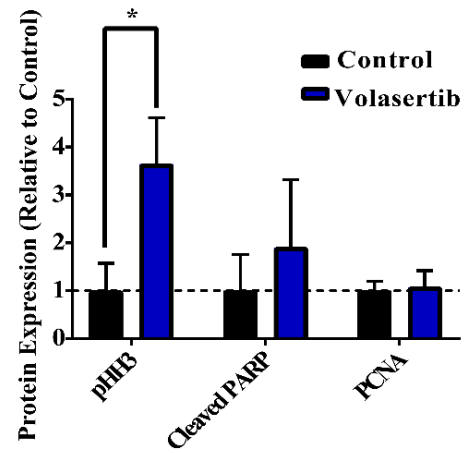
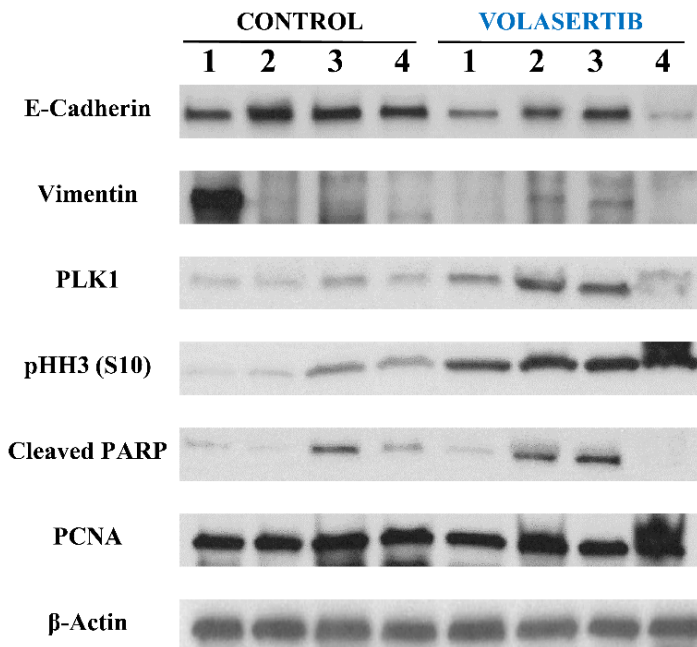
D: The TC370 mesenchymal PDX tumor volumes of control and Volasertib treated mice over time are depicted in the left. A significant difference in tumor volume was observed from day 6 to day 42. The waterfall plot on the right depict the percentage change in tumor burden of each individual mouse at the end point.

E: The overall percent change in tumor volume between the vehicle and Volasertib treated mice at the end of the experiment for all the PDX models is depicted. Each data point represents one mouse in the respective group.

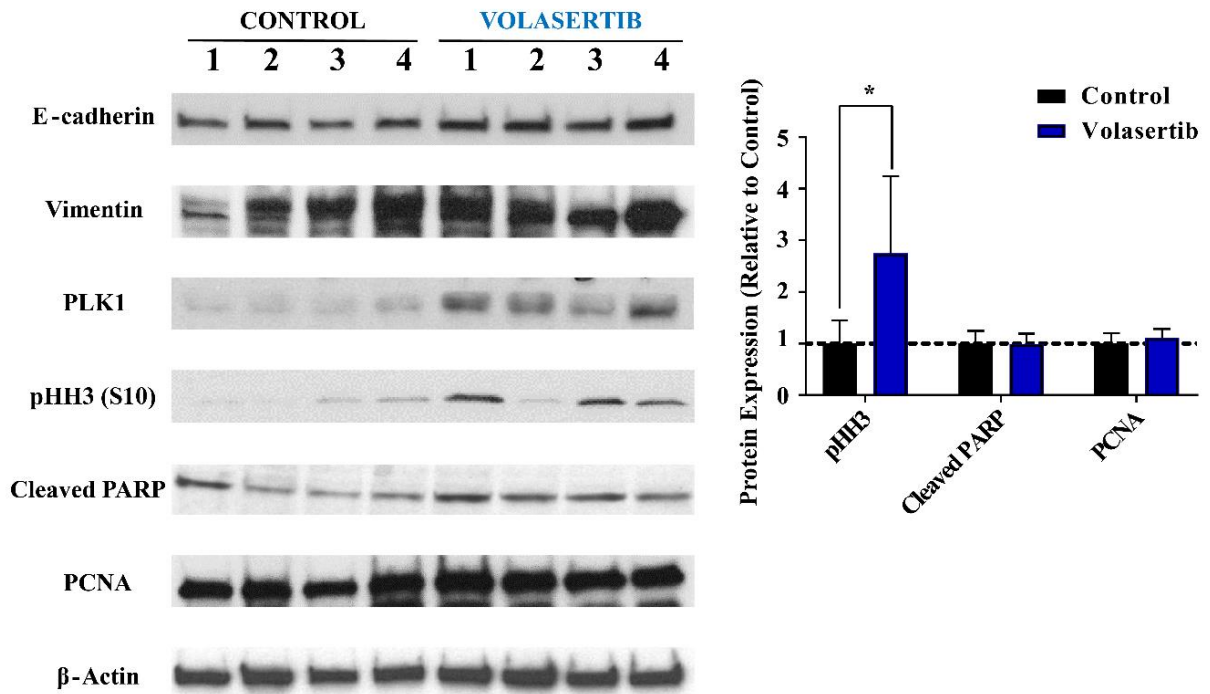
HLC4



TC402



TC424



TC370

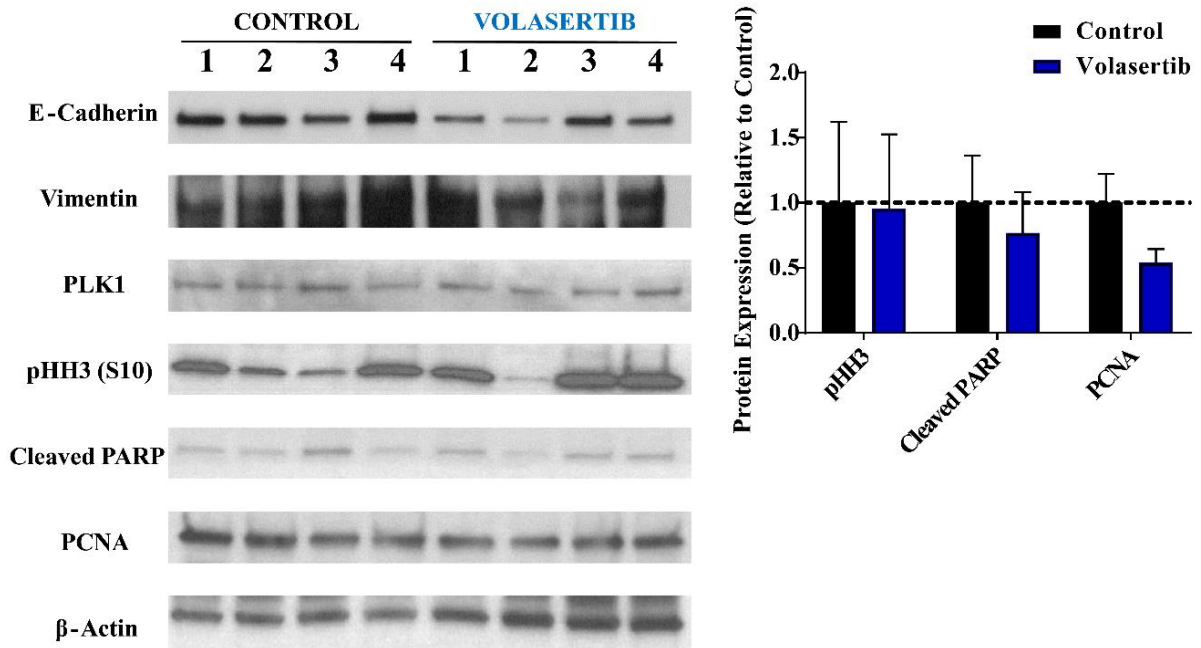


Figure 6: Western blot analysis of PDX tumors for markers of apoptosis, proliferation and target inhibition

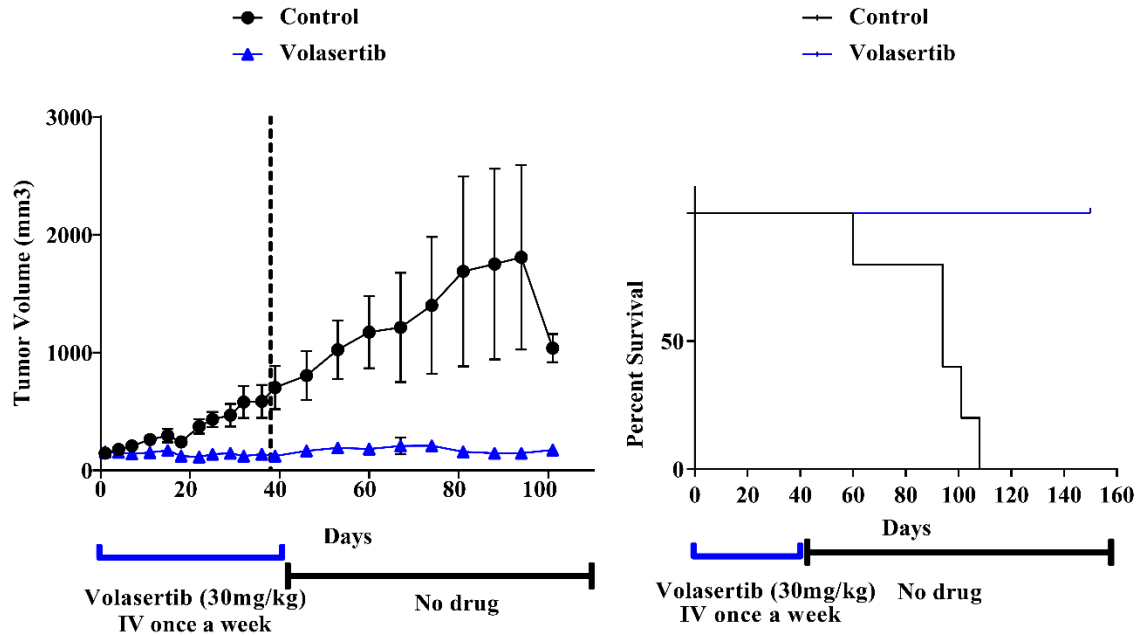
Western blot analysis of PDX tumors collected at the end of the experiment was carried out to measure protein expression for markers of apoptosis (cleaved PARP), proliferation (PCNA) and target inhibition (pHH3 (S10)). The graphs on the right are quantification of the markers relative to control.

3. Mesenchymal PDX models demonstrate improved survival and sustained tumor growth inhibition after cessation of PLK1 inhibition treatment

In order to assess the potential of PLK1 inhibition to result in sustained tumor suppression, 5 mice in both vehicle and Volasertib treated groups of TC424 and TC370 mesenchymal PDXs were monitored for up to 100 days after the 4-week Volasertib treatment ceased. Tumors were measured once a week up to day 100 after which the mice were monitored for survival analysis.

Volasertib treatment was stopped at day 41 after which tumors were measured once a week for 100-103 days. Sustained tumor growth inhibition was observed in the Volasertib treated mice while the tumors continued to grow in the vehicle-treated mice (Figure 7). A significant difference in survival was observed between the two groups in both TC424 ($p=0.004$) and TC370 ($p=0.012$). The control mice were euthanized within 108 (TC424) to 140 (TC370) days due to tumor burden while the Volasertib mice were alive up to day 150 (TC424) to 140 (TC370) (Figure 7).

TC424



TC370

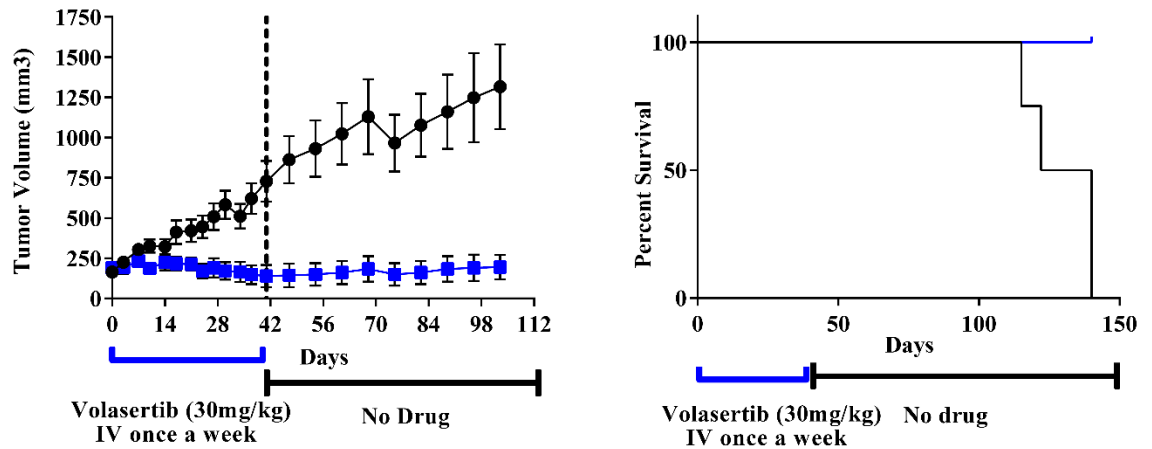


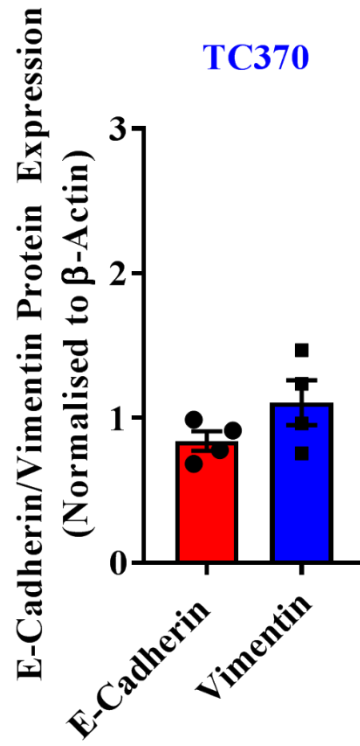
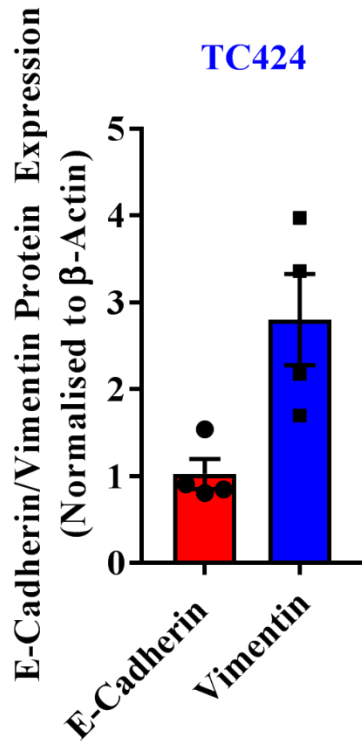
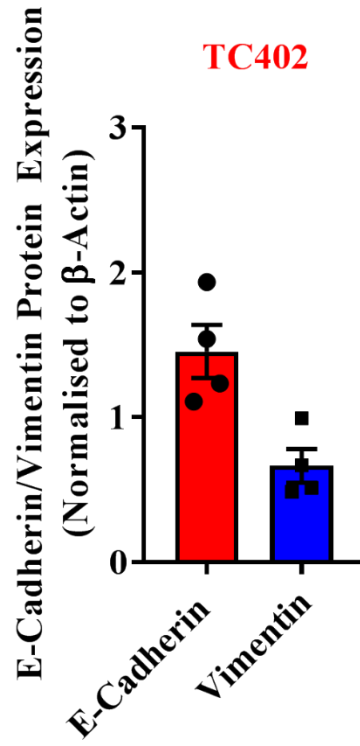
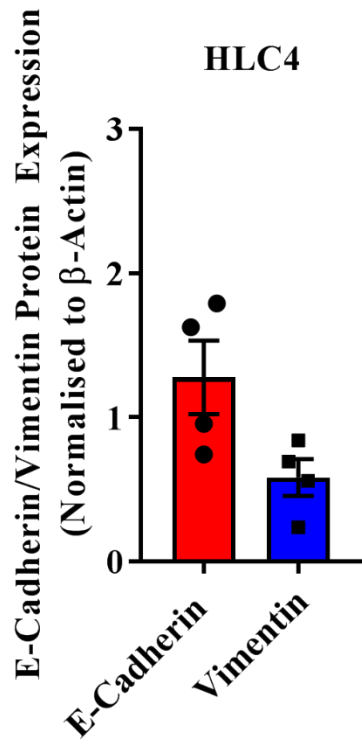
Figure 7: Sustained tumor growth inhibition is observed in TC424 and TC370 Mesenchymal PDX models after cessation of Volasertib treatment

The graphs on the left depict tumor volume over time (up to day 101 or 103) after cessation of Volasertib treatment. The mice were then monitored for survival. A significant difference in survival between vehicle and Volasertib treated mice was observed.

4. Expression of EMT markers are heterogeneous in PDX tumors

The PDX tumors have diverse EMT expression. The EMT status of the PDX tumors were validated at the end of the experiment. Two out of 4 mice in HLC4 PDX model have a high expression of E-cadherin in comparison to Vimentin (Figure 6). Based on the overall E-Cadherin and Vimentin expression, HLC4 has an intermediate phenotype. In TC402 PDX model, the 4 mice have high E-Cadherin expression in comparison to vimentin protein expression and thus has an epithelial phenotype. Overall, TC424 and TC370 have high vimentin expression in comparison to E-Cadherin and is considered to have a mesenchymal phenotype. Interestingly, there are some mice in each PDX model that have varying expressions of E-Cadherin and Vimentin (Figure 8). The quantification of E-Cadherin and vimentin protein in the different PDX models is depicted in Figure 8. The H&E stains of the PDX tumors also depicts heterogeneous populations of tumor cells (Figure 8).

A



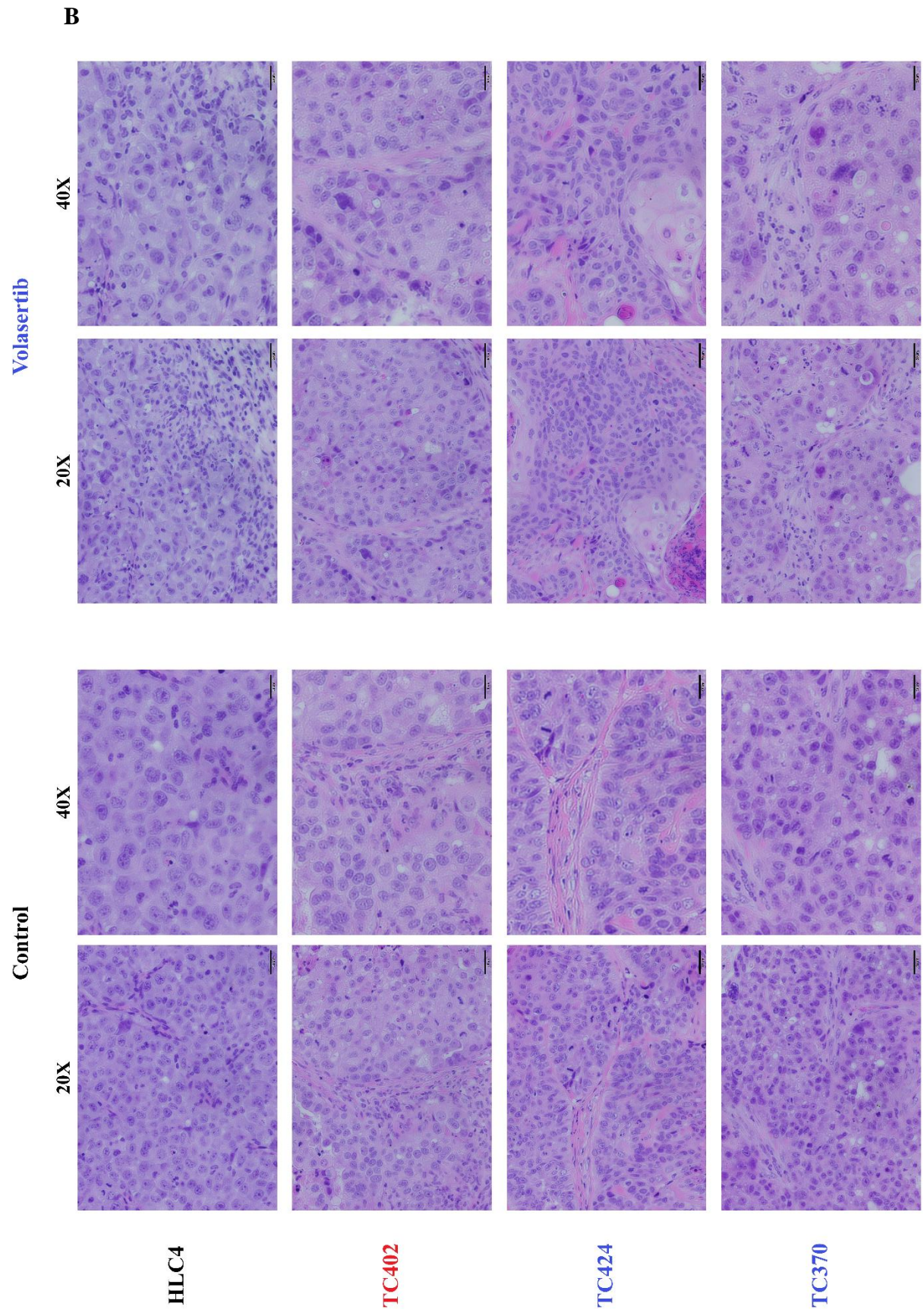


Figure 8: Expression of EMT markers are heterogeneous in PDX tumors

A: Quantification of E-Cadherin and vimentin expression in the PDX tumors shows that HLC4 and TC402 have a more epithelial phenotype with higher E-Cadherin expression in comparison to vimentin expression.

B: The H&E images of the PDX tumors in the vehicle and Volasertib-treated mice depict the heterogeneous population of cells present in the lung tumors.

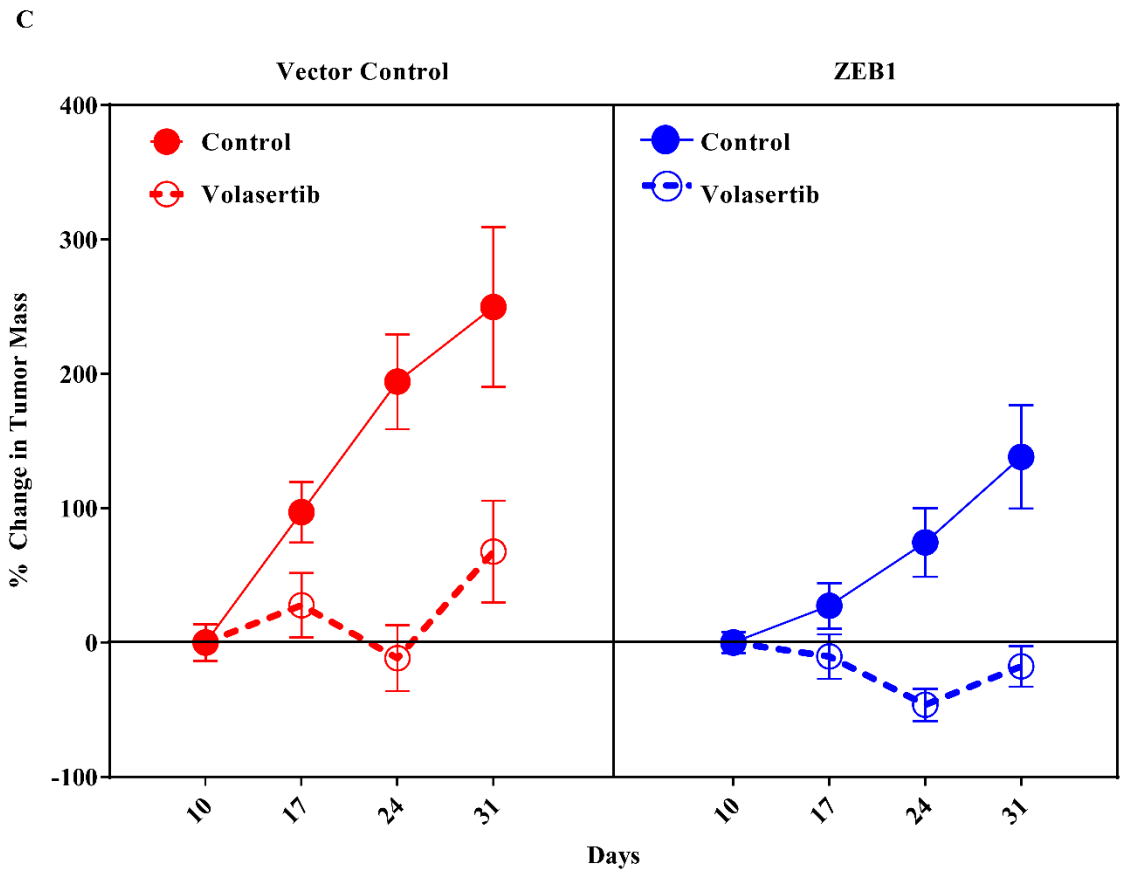
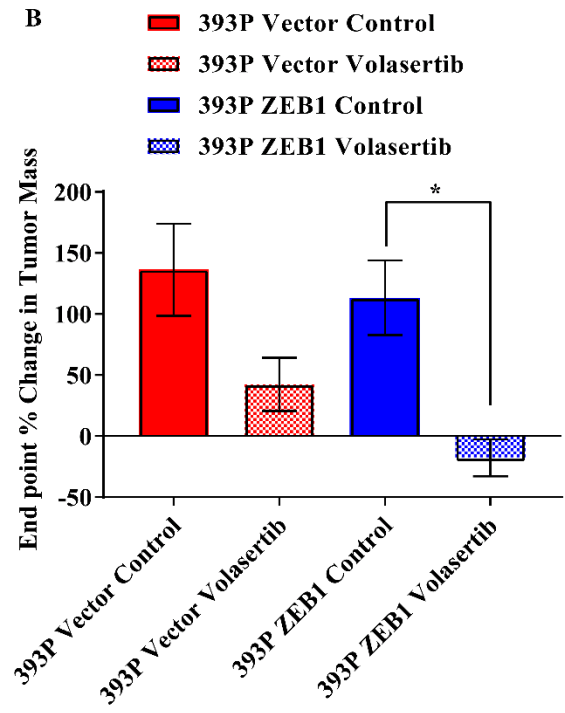
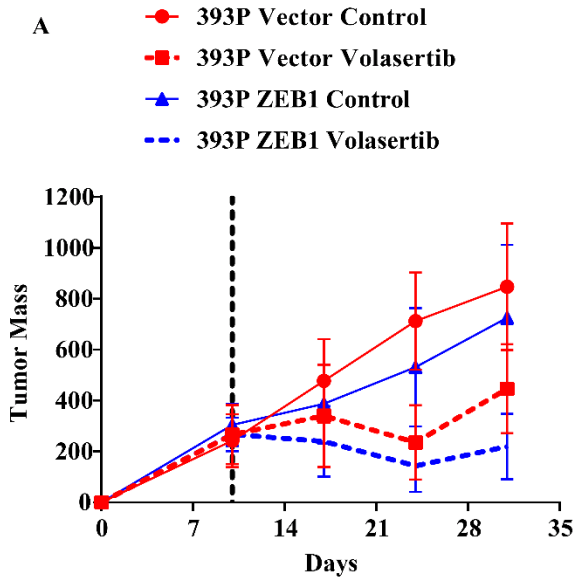
5. Epithelial-to-mesenchymal transition by expression of ZEB1 leads to increase in sensitivity to PLK1 inhibition induced apoptosis in an orthotopic, syngeneic NSCLC mouse model

To test the hypothesis that PLK1 inhibition will cause apoptosis in mesenchymal NSCLC but not epithelial NSCLC *in vivo*, we used syngeneic murine cell lines derived from a KP GEMM in which EMT properties are manipulable by the ectopic expression of miR200 a/b and ZEB1 (106).

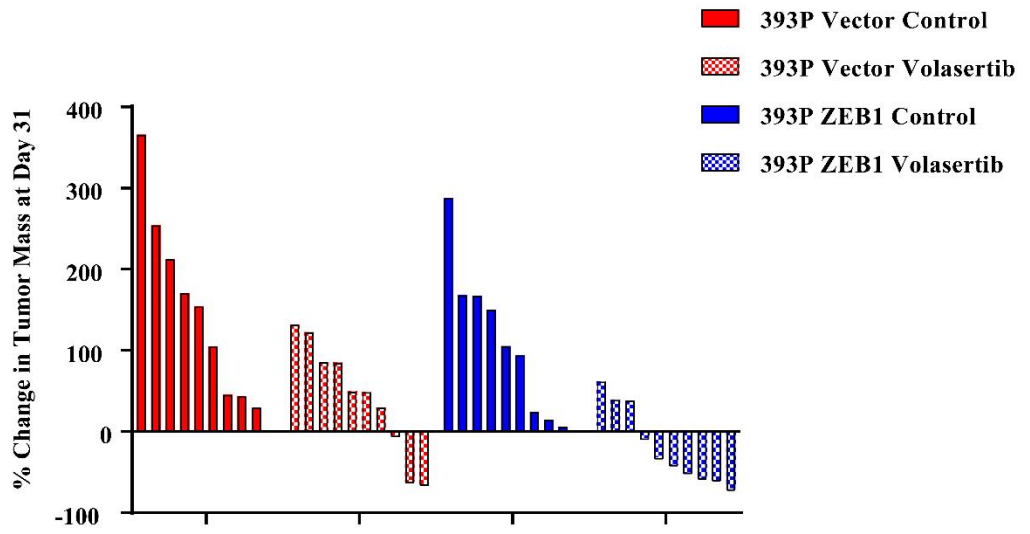
393P cells transfected with vector alone (epithelial) or ZEB1 (mesenchymal) were injected into 55 mice with 5 mice serving as negative control, i.e., mice with no cancer cells injected. CT imaging was carried out at baseline and once a week for 4 weeks. Pilot experiments demonstrated that mice developed tumors by day 10. The two groups of mice (vector, ZEB1) were each randomized into 2 groups at day 10 (Volasertib, vehicle). This design resulted in 4 groups: 393P vector + vehicle, 393P vector + Volasertib, 393P ZEB1 + vehicle and 393P ZEB1 + Volasertib. Each group consisted of 9-10 mice. The mice were treated with vehicle or 30mg/kg of Volasertib by IP injections once a week for 4 weeks. The mice were euthanized at the end of the experiment and the lungs were collected.

In the epithelial 393P vector model, Volasertib led to a decrease in tumor mass (method described in detail below) on day 31 but the change was not statistically significant ($p=0.08$) using Mann-Whitney t-test statistical method. The 393P cells with ZEB1 overexpression were slower growing *in vivo* in comparison to the 393P Vector cells. We observed a significant decrease in tumor mass in the 393P ZEB1 mice treated with Volasertib in comparison to the 393P ZEB1 vehicle control mice ($p=0.011$) as determined by one way anova (Figure 9A, C). In the 393P vector mice treated with Volasertib, 3/10 tumors regressed while 7/10 tumors grew on therapy. In the 393P ZEB1 mice treated with

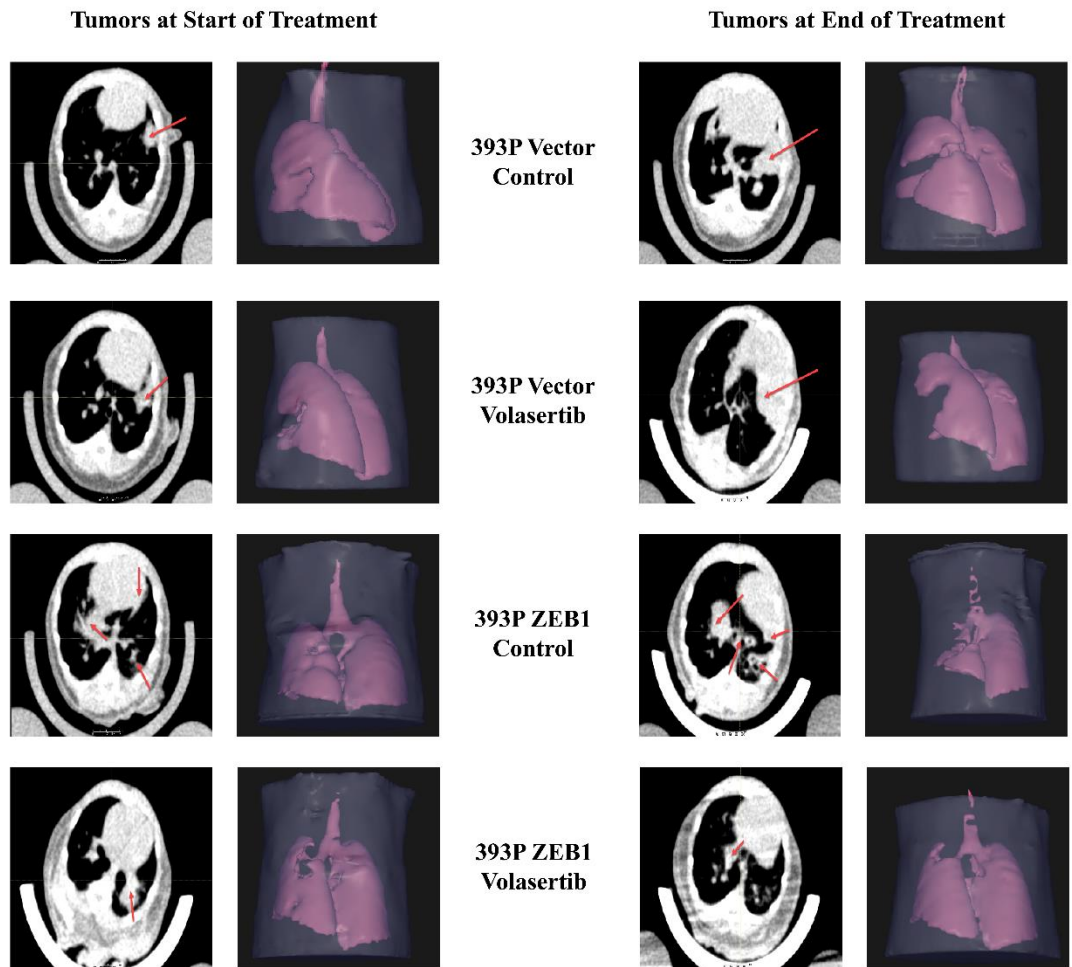
Volasertib, 7/10 tumors regressed and 3/10 tumors grew on therapy. The overall percent change in tumor mass at day 31 in the four groups is depicted in Figure 9B which demonstrates that tumor regression was observed in the mesenchymal 393P ZEB1 mice treated with Volasertib in comparison to the 393P Vector group where growth arrest of tumors was observed. Representative CT images as well as 3D representation of changes in tumor mass in all the four groups is also depicted (Figure 9E). The results are recapitulated in the H&E staining. It can be seen that the 393P vector mice treated with Volasertib still have tumor cells present in the lung while the 393P ZEB1 mice treated with Volasertib has very few or no cancer cells present (Figure 9F).



D



E

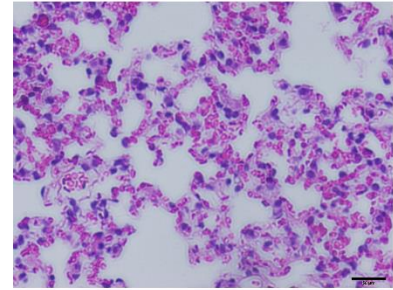
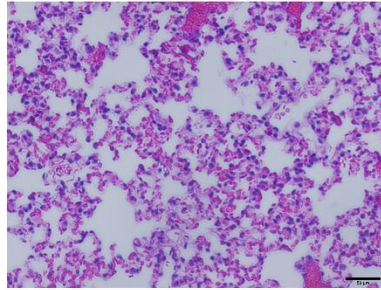


F

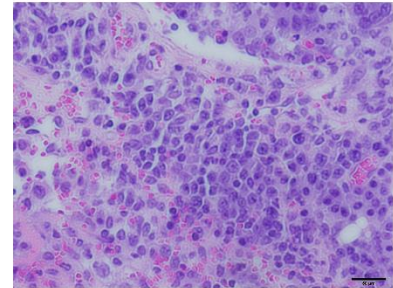
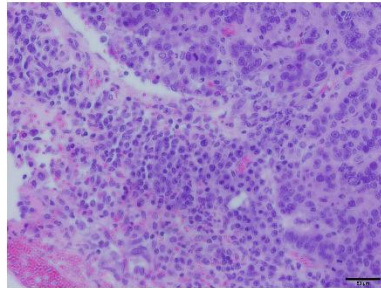
20X

40X

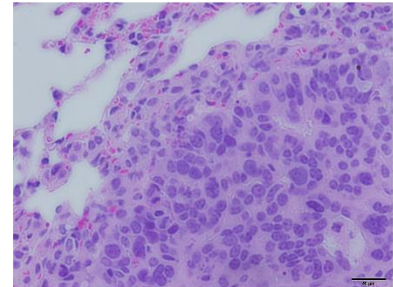
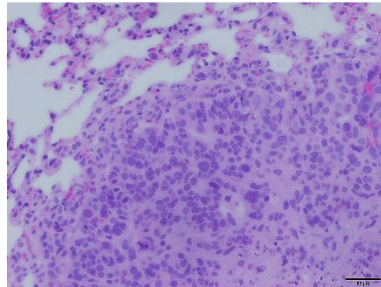
**Negative Control
(No Cancer Cells Injected)**



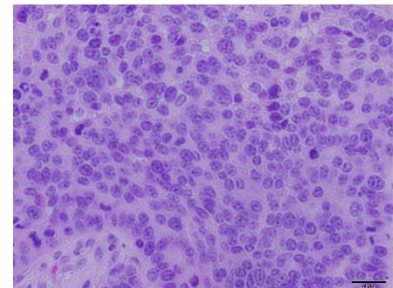
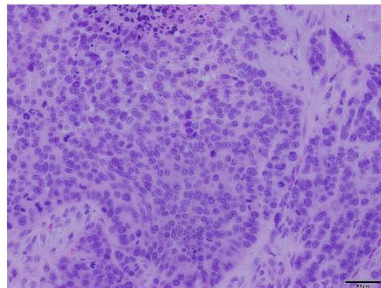
**393P Vector
Vehicle Control**



**393P Vector
Volasertib**



**393P ZEB1
Vehicle Control**



**393P ZEB1
Volasertib**

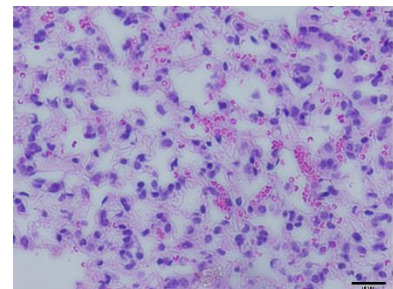
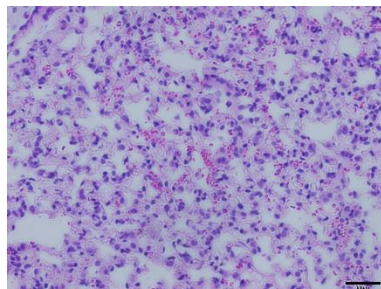


Figure 9: Disease progression in 393P Vector and 393P ZEB1 orthotopic mouse model treated with vehicle control or Volasertib

A: The figure represents the tumor mass of mice in the 4 over groups over time. The dotted line represents the start of Volasertib or vehicle control treatment, i.e. day 10.

B: The bar graph represents the percent change in tumor mass in the 4 groups at day 31. Tumor regression was observed in the 393P ZEB1 mice treated with Volasertib.

C: The graph depicts the percent change in tumor mass in the 393P vector group treated with vehicle control or Volasertib and the 393P ZEB1 group treated with vehicle control or Volasertib.

D: The waterfall plot depicts the percent change in tumor mass at day 31.

E: The figures on the left depict the CT images of the lung tumors in the four groups 393P Vector control, 393P Vector treated with Volasertib, 393P ZEB1 control and 393P ZEB1 treated with Volasertib. Also shown is the 3D representation of the MTC calculated to measure tumor mass.

F: The figure represents the H&E staining of lungs from negative control, 393P vector and 393P ZEB1 mice treated with either vehicle or Volasertib.

6. Tumor mass calculated from the Mass of Thoracic Cavity (MTC) of mice with metastatic lung adenocarcinoma gives an accurate quantification of metastatic tumor burden.

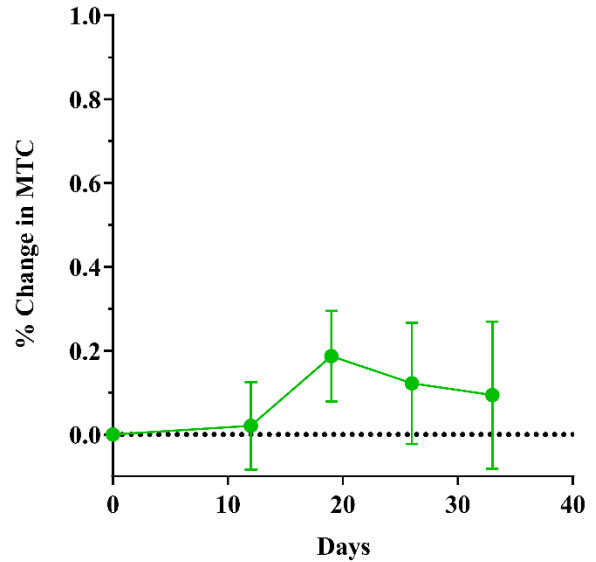
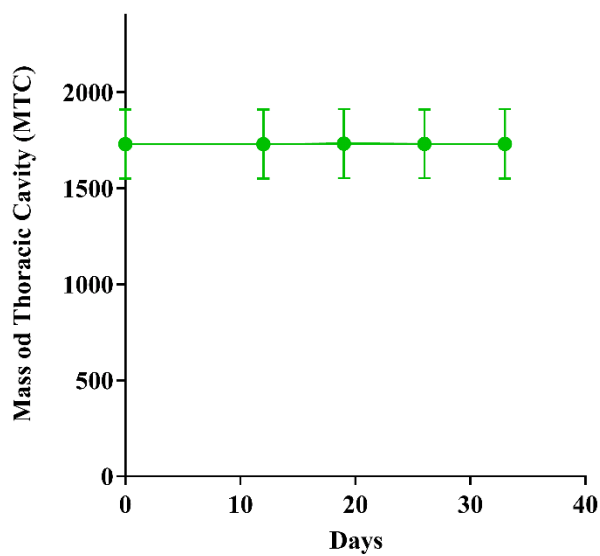
To address the need for a semi-automated, unbiased method for the *in vivo* quantitative assessment of lung tumor mass in mice, we used micro CT without respiratory gating to estimate the tumor mass. With a basic assumption that aerated MTC of the adult mice does not change over time unless due to disease progression, our imaging and analysis protocol permits comparison between different groups, enables evaluation over time in individual animals and provides specific information on the progress of metastases. Moreover, we confirm the validity and thereby extend the applicability of our lung tumor mass analysis in an orthotopic lung xenograft mouse model.

In order to test the assumption that the MTC does not change over time unless there is change in tumor burden, five healthy mice with no tumors were imaged periodically at the same time as the mice with the metastatic lung adenocarcinoma (details below) and the MTC was calculated over time by drawing the region of interest (ROI) from the base of the lungs to the top of the trachea. There was no change in the MTC over time, and the percent change in the mass of thoracic cavity was ± 0.2 , $p > 0.9999$ based on one-way anova and Tukey's multiple comparison analysis (Figure 10). No changes in MTC were observed despite breath hold stage of the mice. The summary of the anova results is outlined in Table 4.

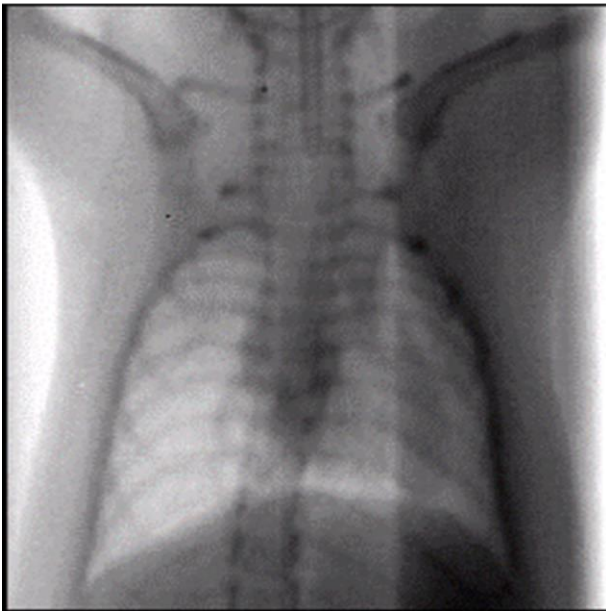
Table 4: Tukey's multiple comparison results for changes in MTC

Tukey's multiple comparisons test	Mean Diff.	95.00% CI of diff.	Significant?	Adjusted P Value
0 vs. 12	-0.5499	-763.4 to 762.3	No	>0.9999
0 vs. 19	-3.183	-766 to 759.6	No	>0.9999
0 vs. 26	-1.919	-764.7 to 760.9	No	>0.9999
0 vs. 33	-2.15	-765 to 760.7	No	>0.9999
12 vs. 19	-2.633	-765.4 to 760.2	No	>0.9999
12 vs. 26	-1.369	-764.2 to 761.4	No	>0.9999
12 vs. 33	-1.6	-764.4 to 761.2	No	>0.9999
19 vs. 26	1.264	-761.5 to 764.1	No	>0.9999
19 vs. 33	1.033	-761.8 to 763.8	No	>0.9999
26 vs. 33	-0.2314	-763 to 762.6	No	>0.9999

To test the proposed method we used the orthotopic KP GEMM model in which the mice were imaged at baseline and the MTC was calculated. The 344SQ mouse lung adenocarcinoma cells were then injected into the left lung of the mice via orthotopic injection. The mice were then serially imaged and the MTC was calculated on days 12, 19, 26 and 33 to study the course of tumor development. The tumor mass was then calculated by subtracting the MTC on the specific day from the MTC at baseline. The workflow is as depicted (Figure 11). The mice survived for an average of 3 weeks after the orthotopic injection of the metastatic mouse lung adenocarcinoma cells. The mice were euthanized when they were moribund or at the end of 4 weeks on day 33 immediately after the last micro-CT imaging session. The mice were necropsied, the number of primary and metastatic tumors were counted and the lungs were collected and weighed.



Breath Hold



No Breath Hold

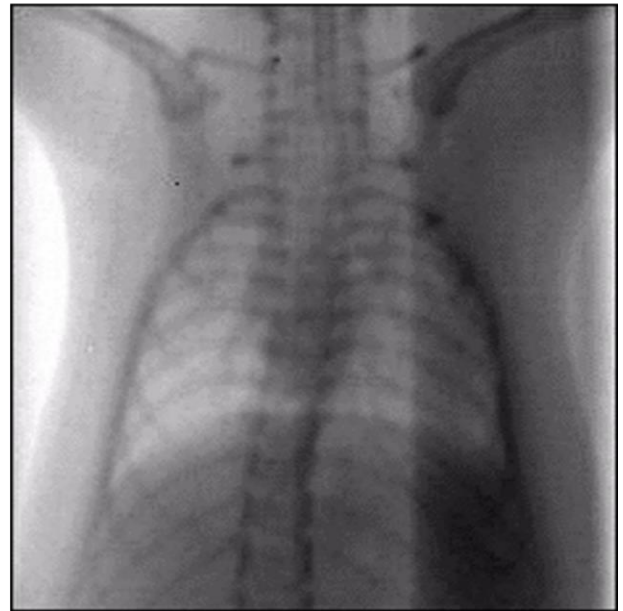


Figure 10: The Mas of Thoracic Cavity does not change over time

The graph on the left depicts that the MTC of adult mice does not change over time. The graph on the right depicts the percent change in the MTC of mice. No changes in MTC were observed irrespective of breath hold stage of mice.

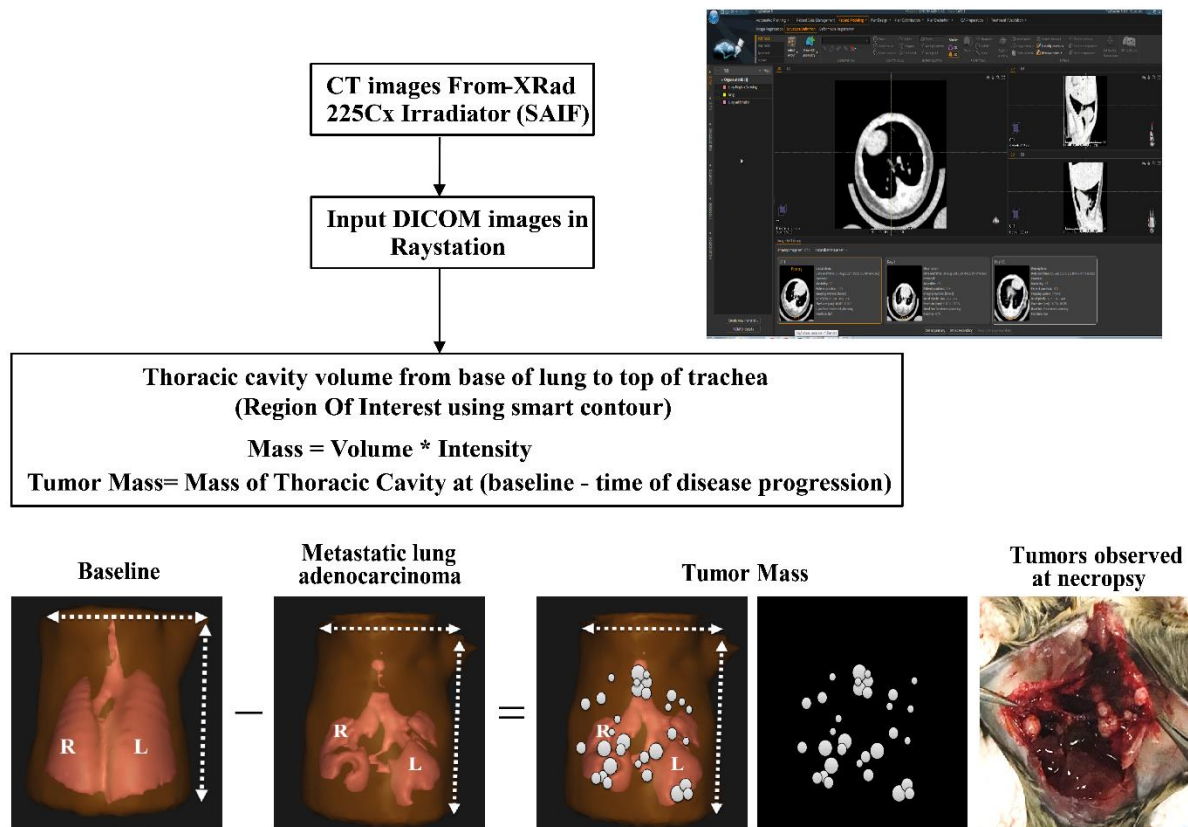


Figure 11: Tumor mass calculated from the Mass of Thoracic Cavity of mice with metastatic lung adenocarcinoma gives an accurate quantification of metastatic tumor burden

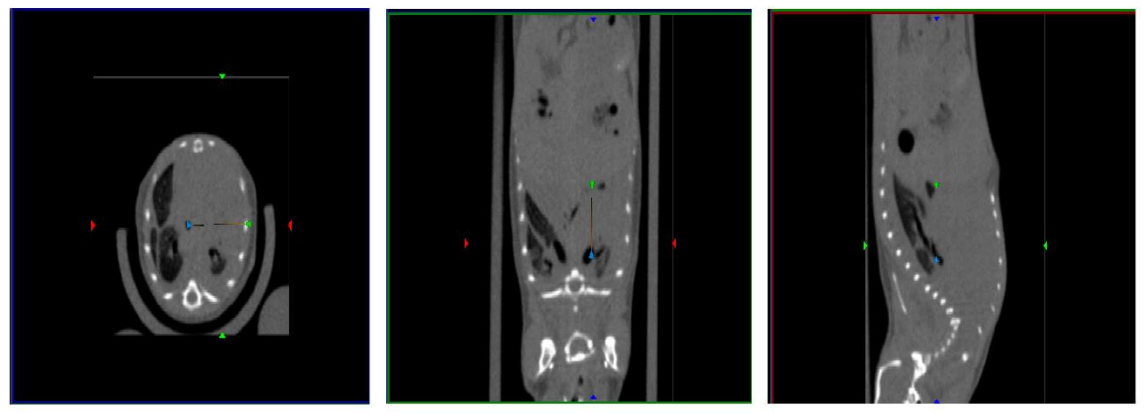
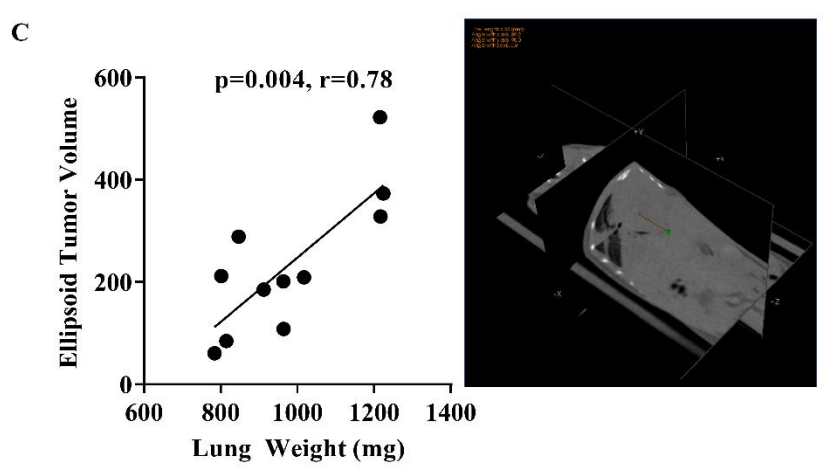
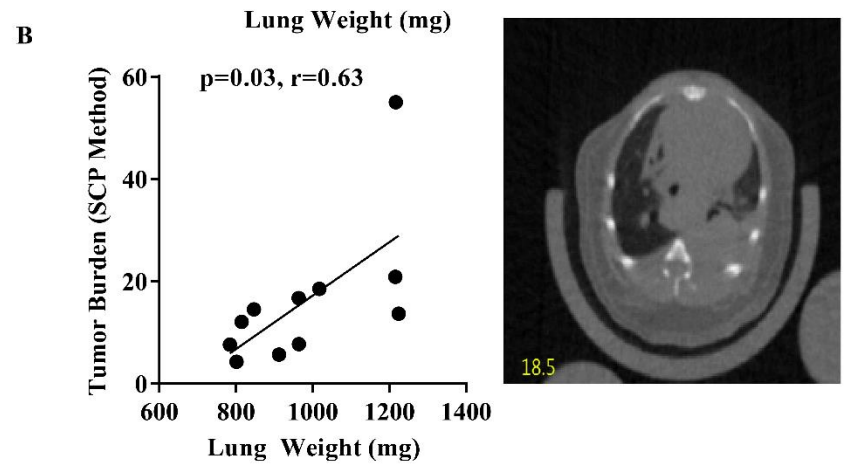
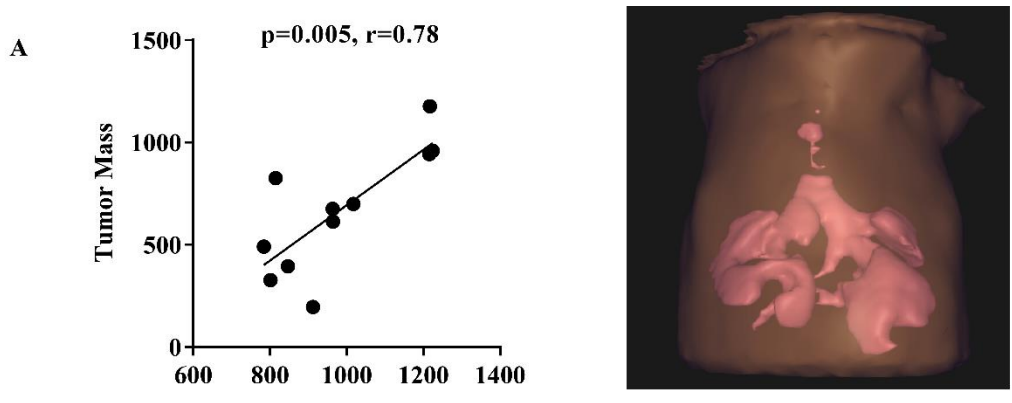
The flowchart depicts the workflow used to calculate MTC from CT Images and tumor mass calculation.

7. Lung tumor burden quantification of MTC method as well as existing methods significantly correlated with lung weight

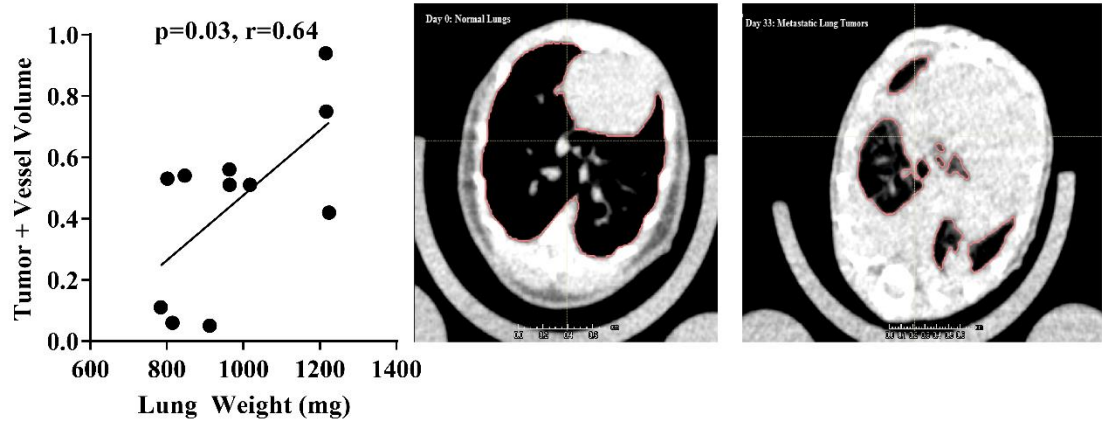
We compared multiple methods of lung tumor burden measurement: MTC method, the RECIST-like Sum of Cross-Products (SCP) method (98), segmentation of aerated lung volume (102) without respiratory gating, volumetric measurement of combined tumor and vasculature from a threshold-based region growing algorithm with manual and semi-automated segmentation (99) as well as ellipsoid tumor burden measurement (107). In order to determine the intrinsic accuracy of each method to measure tumor burden, the tumor burden of 10 mice with lung adenocarcinoma was calculated from each method was correlated with the gold standard, i.e., lung weight. The correlation values of lung weight with MTC ($r=0.78$, $p=0.005$), tumor burden from SCP ($r=0.63$, $p=0.03$), ellipsoid tumor volume ($r=0.78$, $p=0.004$), tumor and vessel volume ($r=0.65$, $p=0.02$) as well as aerated lung volume ($r=-0.69$, $p=0.01$) validated the ability of these methods to accurately determine tumor burden in mice with lung adenocarcinoma (Figure 12).

The tumor burden values from all these methods was plotted against tumor mass calculated by the proposed MTC method. Tumor burden calculation from the SCP method significantly correlated with tumor mass calculated from MTC method ($p=0.0085$, $r=0.74$) (Figure 13). The SCP method is very similar to the RECIST guideline which is a standardize measure of tumor response, especially in clinical trials (108). There was no significant correlation between ellipsoid tumor volume and tumor mass ($p=0.13$, $r=0.48$), tumor & vessel volume and tumor mass ($p=0.12$, $r=0.49$) and end point lung volume and tumor mass ($p=0.12$, $r=-0.48$). This may be due to the small sample size ($n=10$) (Figure

13). Table 5 outlines the various features of the MTC method as well as the other CT analysis methods that have been used for tumor burden measurement.



D



E

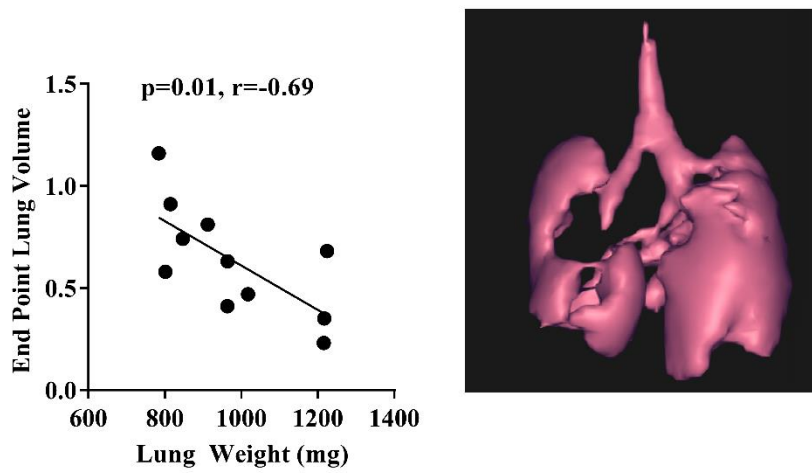


Figure 12: Lung tumor burden quantification of existing methods besides the MTC method significantly correlated with lung weight

A: Tumor mass calculated from MTC significantly correlated with lung weight.

B: Tumor burden calculated by SCP Method significantly correlated with lung weight.

C: Ellipsoid tumor volume significantly correlated with lung weight.

D: Tumor & Vessel volume significantly correlated with lung weight.

E: End point lung volume significantly correlated with lung weight.

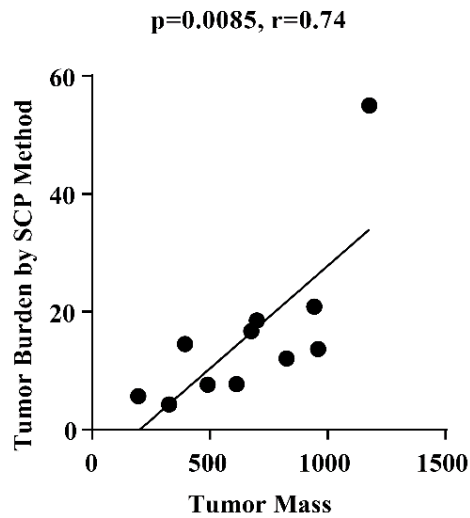
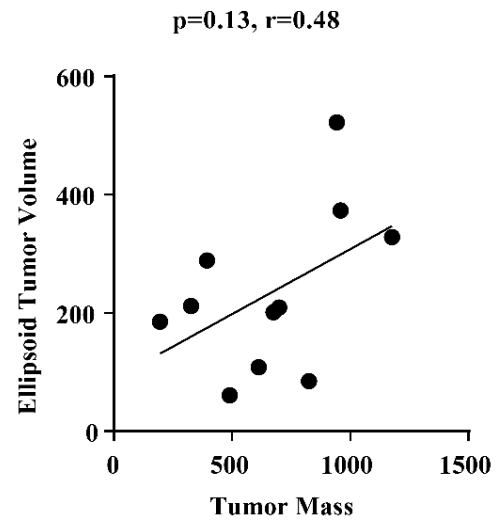
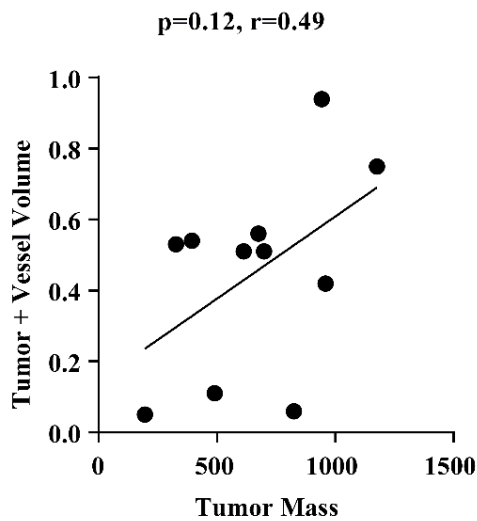
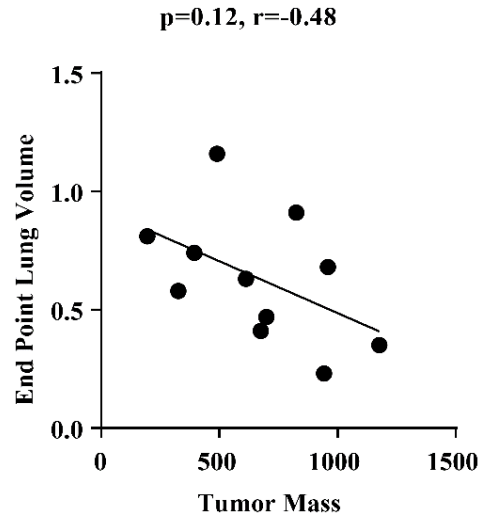
A**B****C****D**

Figure 13: Correlation of tumor mass with tumor burden from SCP method, ellipsoid tumor volume, tumor + vessel volume and end point lung volume

A: Tumor burden calculated from the RECIST-like MCP method significantly correlated with tumor mass calculated from MTC

B: Ellipsoid tumor burden correlated with tumor mass calculated from MTC

C: Tumor + Vessel volume correlated with tumor mass calculated from MTC

D: End point lung volume correlated with tumor mass calculated from MTC

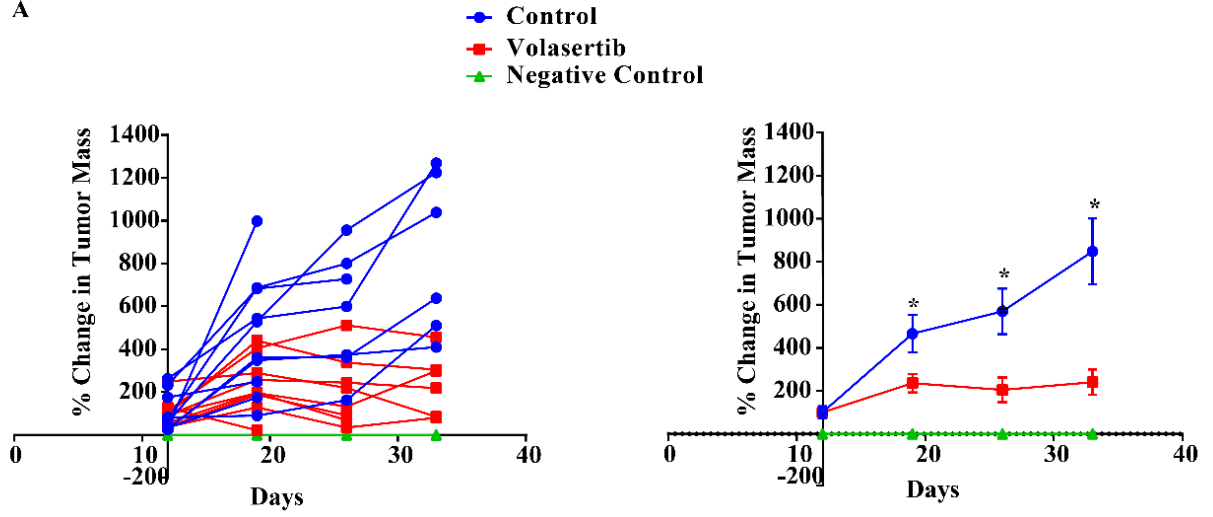
Table 5: Summary of MTC and other CT analysis methods

MTC Method (Study Method)	SCP (RECIST-Like) Method	Ellipsoidal Method	T&V Volume Method	End Point Lung Volume Method	Lung Weight (Reference Method)
Primary Tumor Measurement	YES	YES	YES	YES	YES
Metastatic Tumor Measurement	YES Measures all the metastatic tumors	YES Largest 5 tumors are measured	YES All tumors in lung are measured	YES All tumors in lung are measured	YES
Measurement of metastatic tumors in thoracic cavity	YES	NO	NO	NO	NO
Dynamic Changes in Tumor Volume or Mass	YES	YES	YES	NO	NO
Semi-Automated analysis	YES	NO	YES	YES	NO
Dimensional Measurement	3D	3D	3D	3D	
Time taken for analysis per mouse	5-8 min	15-20 min	10-15 min	3-5 min	2-5 min
Software/Tool Used	Raystation	Microview	ImageJ	Raystation	Surgical tools and Weighing Scale
Correlation with Reference method (R value/p Value)	0.78/0.005	0.78/0.004	0.65/0.02	-0.69/0.01	

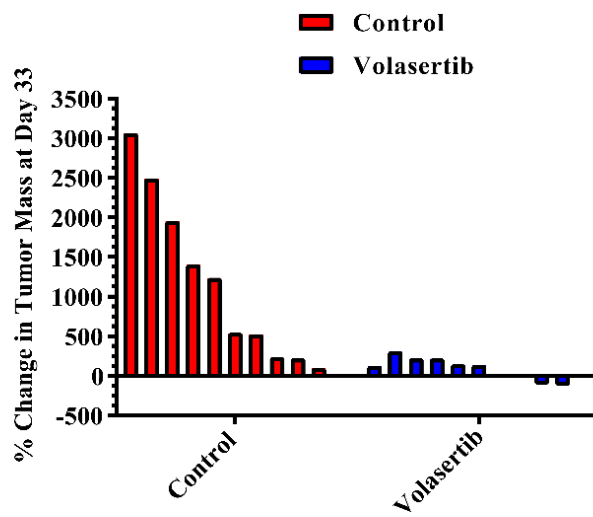
8. Validation study for MTC method shows that Volasertib treatment reduced tumor mass in a mesenchymal metastatic, orthotopic mouse model

In order to test the MTC method in an independent dataset, we tested the effect of the PLK1 inhibitor Volasertib in an orthotopic mouse model. 25 mice were imaged at baseline. We injected 344SQ cells which were derived from a KP mouse model into the left lung of 20 mice. 5 mice served as negative control, i.e., mice in which cancer cells were not injected. The mice were then serially imaged at days 12, 19, 26 and 33. At day 12, the mice had tumors of treatable size and were randomized into two groups, and treated with vehicle control or 30mg/kg of Volasertib intravenously for 4 weeks. The percent tumor mass increased more than 10 fold in the vehicle treated mice while the percent change in tumor mass increased approximately 2.4 fold in the Volasertib treated mice over the 4 week period. There was significant difference in percent change in tumor mass between the control and Volasertib treated mice on days 19 ($p=0.035$), 26 ($p= 0.008$) and 33 ($p=0.004$) based on multiple t-test analysis (Figure 14). The percent change in tumor mass at day 33 was significantly different between the control and Volasertib treated mice ($p=0.03$) based on non-parametric Mann-Whitney t-test analysis (Figure 14). The H&E images show that the lungs of the vehicle treated mice have many tumor cells present while the lungs of the Volasertib treated mice have very few tumor cells remaining. This data also supports the hypothesis that mesenchymal NSCLC tumors are sensitive to PLK1 inhibition *in vivo* in an orthotopic, immunocompetent mouse model.

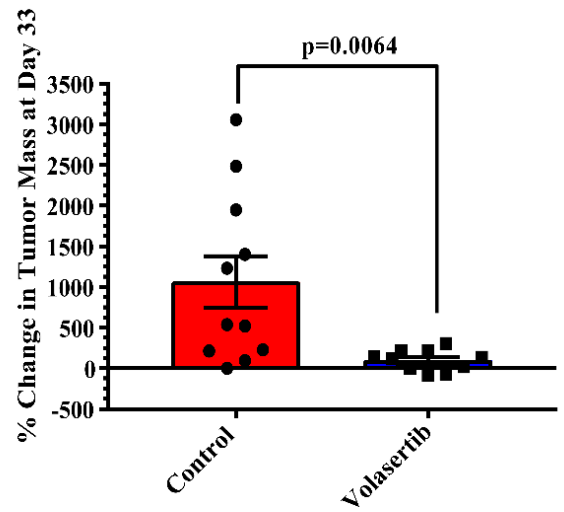
A



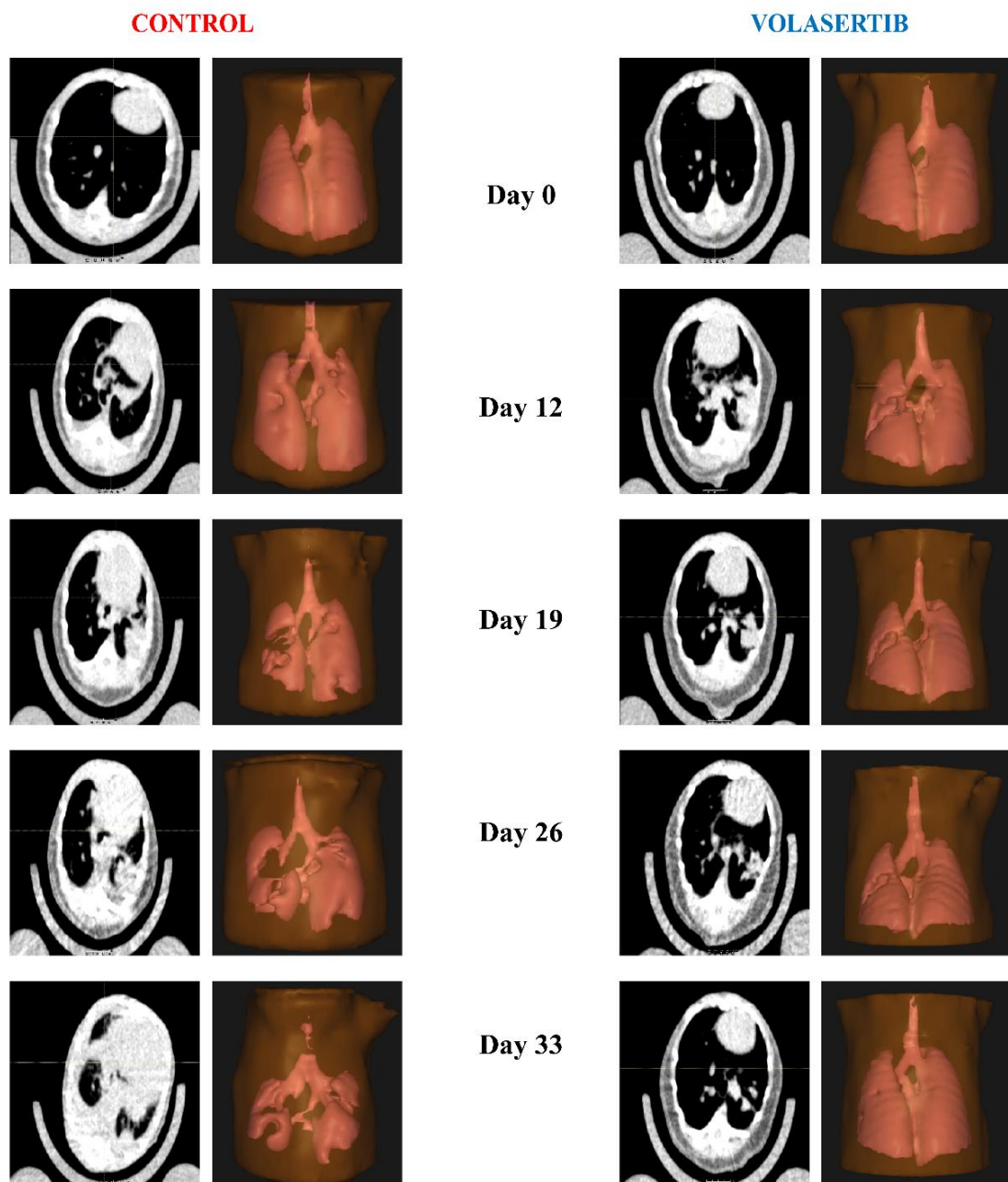
B



C



D

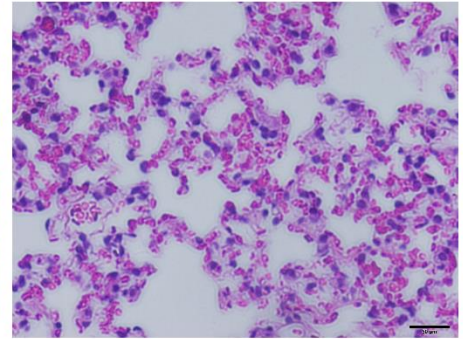
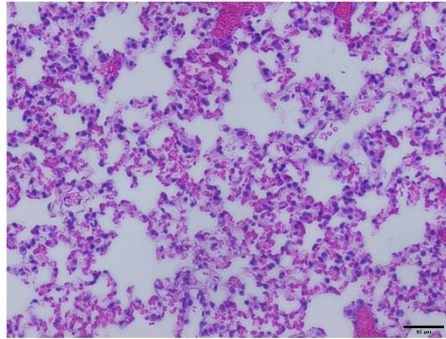


E

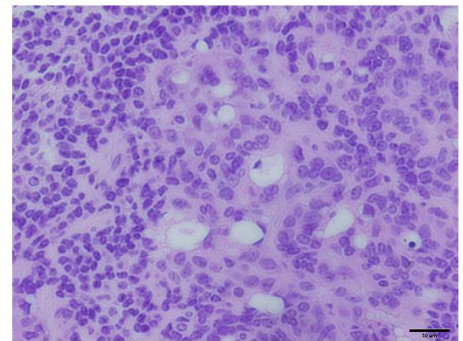
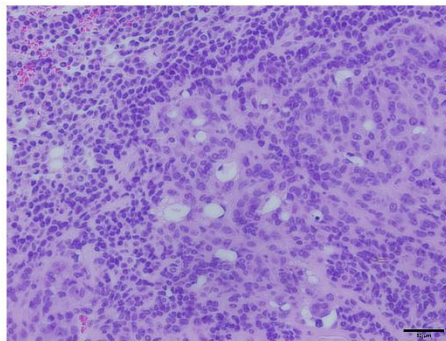
20X

40X

**Negative Control
(No Cancer Cells Injected)**



**344SQ
Vehicle Control**



**344SQ
Volasertib**

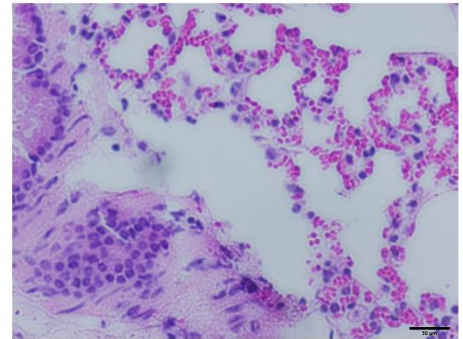
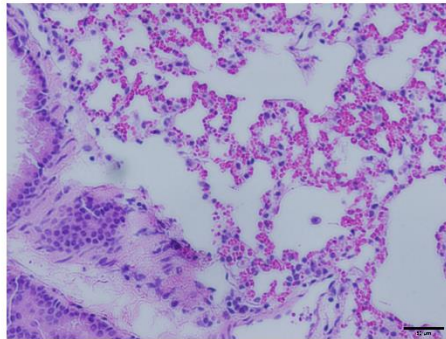


Figure 14: Validation study for MTC method shows that Volasertib treatment reduced tumor mass in a mesenchymal metastatic, orthotopic mouse model

A: The graphs depict the percent change in tumor mass over time from day 12 to day 33.

Volasertib treatment significantly reduced tumor mass in the 344SQ mouse model

B: The waterfall depicts the percent change in tumor mass between the vehicle and Volasertib treated mice at the end of the experiment. Each bar represents mouse.

C: The graph depicts a significant difference in percent change in tumor mass between the control and Volasertib treated mice on day 33.

D: The figure depicts tumor progression in the Control and Volasertib treated mice at baseline and days 12, 19, 26 and 33. The CT images and the 3D representation of MTC is depicted.

E: The figure represents the H&E staining of lungs from negative control, 344SQ mice treated with either vehicle or Volasertib.

9. β -Catenin knock-down (KD) did not reverse resistance to PLK1 inhibition induced apoptosis in epithelial NSCLC cell lines that express high levels of β -Catenin

Because of the striking differential expression of β -Catenin between sensitive and resistant NSCLC cell lines, we hypothesized that β -Catenin might mediate resistance to PLK1 inhibitors (67). In order to elucidate the mechanism for EMT-induced sensitivity to PLK1 inhibition, Dr. Ratnakar Singh compared changes in 303 protein/phosphoprotein expression after PLK1 inhibition using RPPA in 3 epithelial and 3 isogenic pairs (treated with TGF β) and two additional mesenchymal sensitive cell lines (Calu-6 and H1792). In order to identify the molecule or signaling pathway responsible for driving resistance to PLK1 inhibition, we looked for common proteins that were differentially expressed in epithelial and mesenchymal NSCLC cell lines after Volasertib treatment. A decrease in β -Catenin protein expression was observed in mesenchymal but not epithelial NSCLC cell lines after PLK1 inhibition (Figure 15A). β -Catenin mRNA expression was higher in a panel of epithelial NSCLC cell lines in comparison to mesenchymal NSCLC cell lines ($p=0.0106$). (Figure 15B).

We hypothesized that knockdown of β -Catenin in the epithelial NSCLC cell lines would make them more sensitive to PLK1 inhibition induced apoptosis. siRNA was used to silence β -Catenin. 2 mesenchymal (Calu6 and H1792) NSCLC cell lines was treated with 10nM of siRNA targeting β -Catenin (CTNNB1) for 72h. Two epithelial (H1975 and HCC366) NSCLC cell lines were treated with 20nM of siRNA targeting β -Catenin (CTNNB1) for 72h. The control groups of the cell lines were treated with 10nM of non-targeting siRNA. The cells were also treated with 50nM of the PLK1 inhibitor Volasertib or vehicle for 48h. The drug was added 24 hours after the siRNA transfection. Protein lysate was collected from the cells and β -Catenin, PARP, Caspase 3, and phospho-

nucleophosmin (Ser 4), which is a downstream target of PLK1, were measured by western blot analysis (Figure 15C). There was no significant difference in the levels of cleaved PARP or cleaved Caspase 3 after β -Catenin KD and PLK1 inhibition despite achieving good knockdown of the protein (Figure 15C). Likewise, there was no significant difference in the percentage of apoptotic cells measured by Apo BrdU TUNEL assay between the control and β -Catenin KD cells after PLK1 inhibition (Figure 15 D).

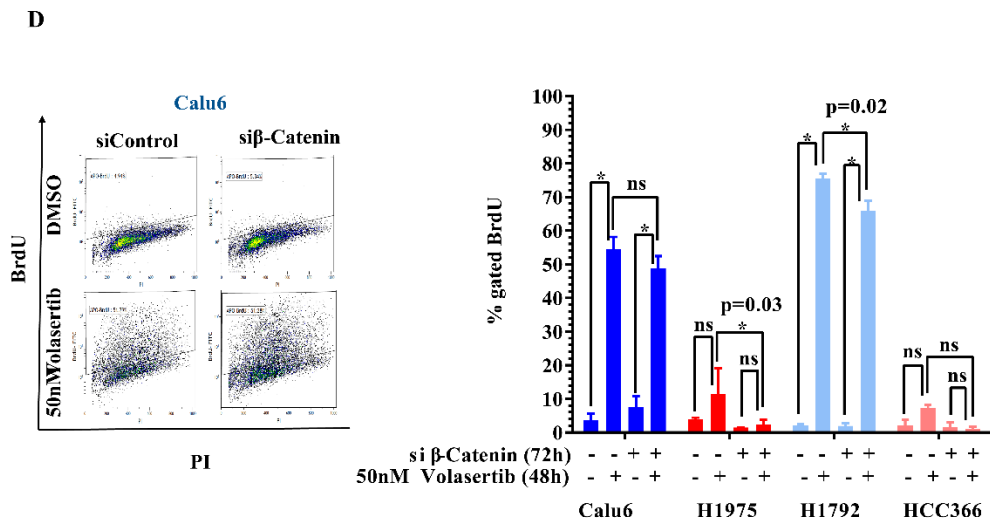
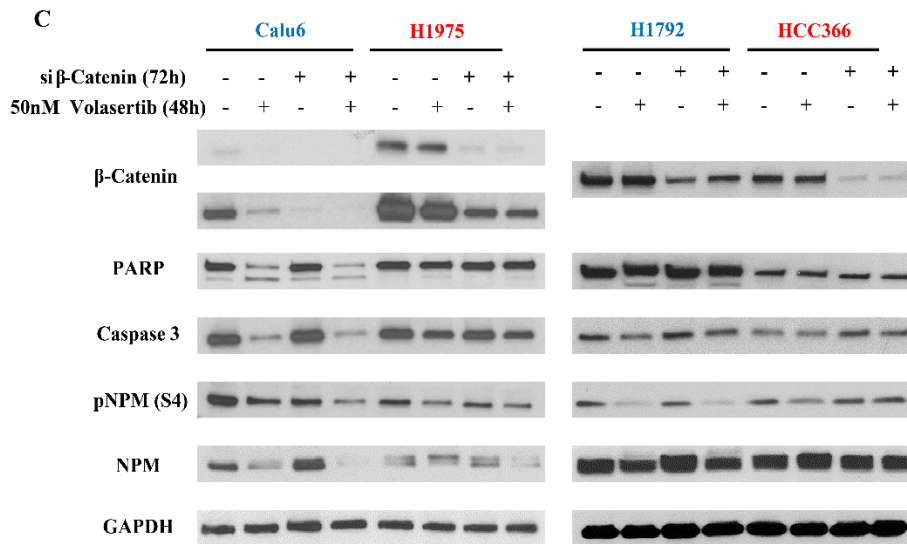
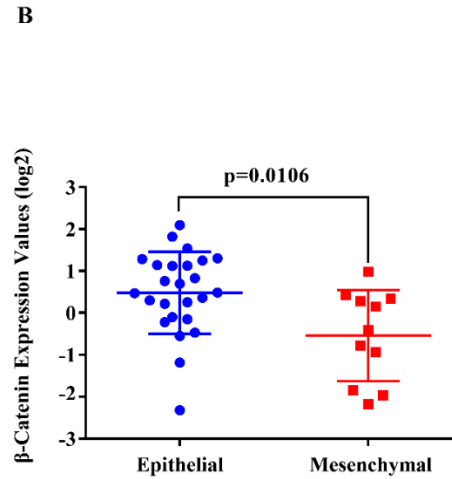
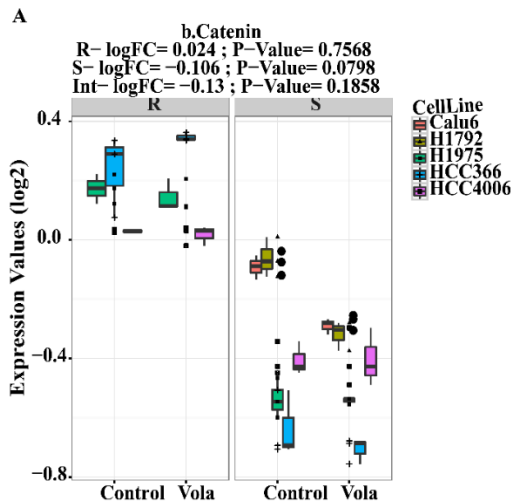


Figure 15: β -Catenin knock-down (KD) did not reverse resistance to PLK1 inhibition induced apoptosis in epithelial NSCLC cell lines that express high levels of β -Catenin

A: RPPA data depicting the changes in β -Catenin protein expression after PLK1 inhibition in epithelial and mesenchymal (as well as isogenic mesenchymal, i.e., epithelial cells treated with TGF β) NSCLC cell lines

B: Differential β -Catenin mRNA expression between epithelial and mesenchymal NSCLC cell lines

C: Western blot showing that there is no significant difference in the levels of cleaved PARP or cleaved Caspase 3 after β -Catenin KD and PLK1 inhibition

D: Apo BrdU TUNEL assay measuring PLK1 inhibition induced apoptosis after β -Catenin KD in NSCLC cell lines. No difference in BrdU positive cells is observed after β -Catenin KD and Volasertib treatment.

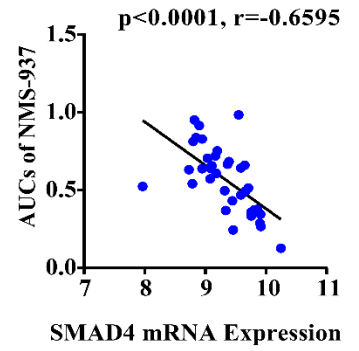
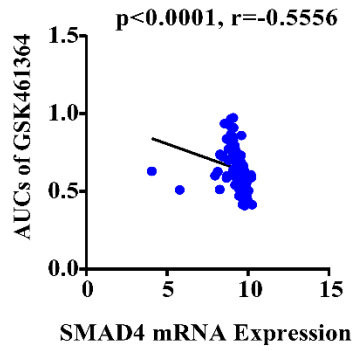
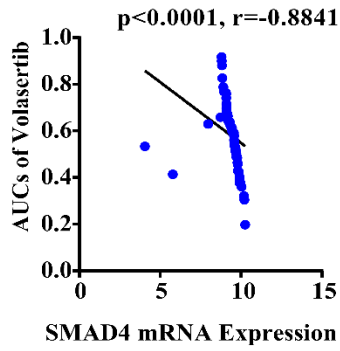
10. SMAD4 knock-down (KD) did not change sensitivity to PLK1 inhibition induced apoptosis in NSCLC cell lines

SMAD4 mutant head and neck squamous cell carcinoma (HNSCC) cell lines were more sensitive to Volasertib than SMAD4 wt HNSCC cell lines (109). The same correlation could not be carried out in NSCLC cell lines due to the small number of SMAD4 mutant cell lines (n=4) but there was a negative correlation between SMAD4 mRNA expression and the AUCs of 3 different PLK1 inhibitors Volasertib ($p < 0.0001$, $r = -0.8841$), GSK461362 ($p < 0.0001$, $r = -0.5556$) and NMS-937 ($p < 0.0001$, $r = -0.6595$), the AUC calculated from an in house drug study in 70 NSCLC cell lines (67) (Figure 16A). There was no difference in SMAD4 mRNA expression in a panel of epithelial and mesenchymal NSCLC cell lines ($p = 0.4827$). (Figure 16B). We treated three pairs of epithelial NSCLC cell lines that had been treated with TGF β and two additional mesenchymal NSCLC cell lines with 50nM Volasertib for 24 hours and then subjected the cells to RPPA. No change in SMAD4 protein expression was observed in NSCLC cell lines after PLK1 inhibition (Figure 16C).

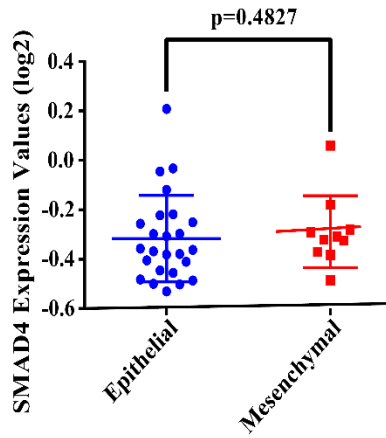
We hypothesized that knockdown of SMAD4 in the mesenchymal NSCLC cell lines would make them more sensitive to PLK1 inhibition induced apoptosis. siRNA was used to silence SMAD4. 2 mesenchymal (Calu6 and H1792) and 2 epithelial (H1975 and HCC366) NSCLC cell lines were treated with 10nM of siRNA targeting SMAD4 for 72h. The control groups of the cell lines were treated with 10nM of non-targeting siRNA. The cells were also treated with 50nM of the PLK1 inhibitor Volasertib or vehicle for 48h. The drug was added 24 hours after the siRNA transfection. Protein lysate was collected from the cells and SMAD4, PARP, Caspase 3, and phospho-nucleophosmin (Ser 4), which is a downstream target of PLK1, were measured by western blot analysis (Figure 16D). There

was no significant difference in the levels of cleaved PARP or cleaved Caspase 3 after SMAD4 KD and PLK1 inhibition despite achieving good knockdown of the protein. (Figure 15D). Likewise, there was no significant difference in the percentage of apoptotic cells measured by Apo BrdU TUNEL assay between the control and SMAD4 KD cells after PLK1 inhibition (Figure 16 E).

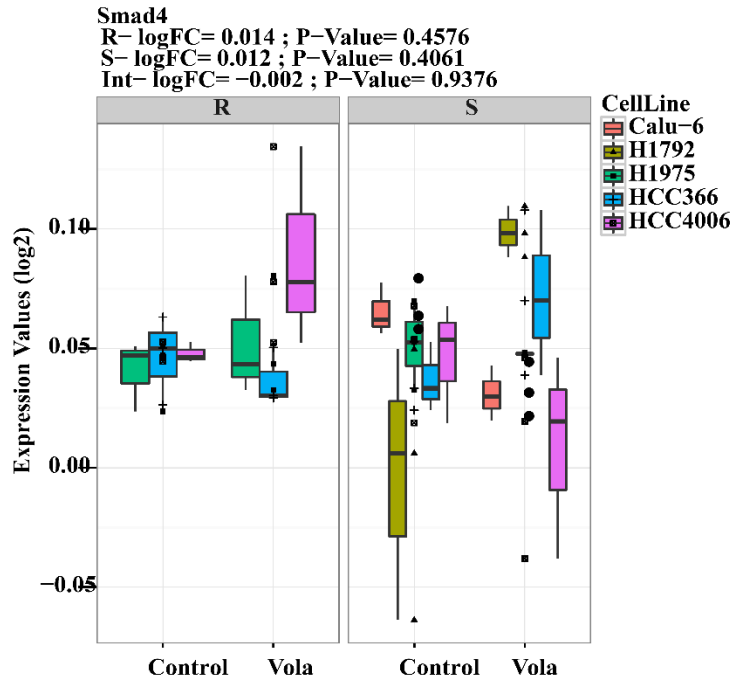
A



B



C



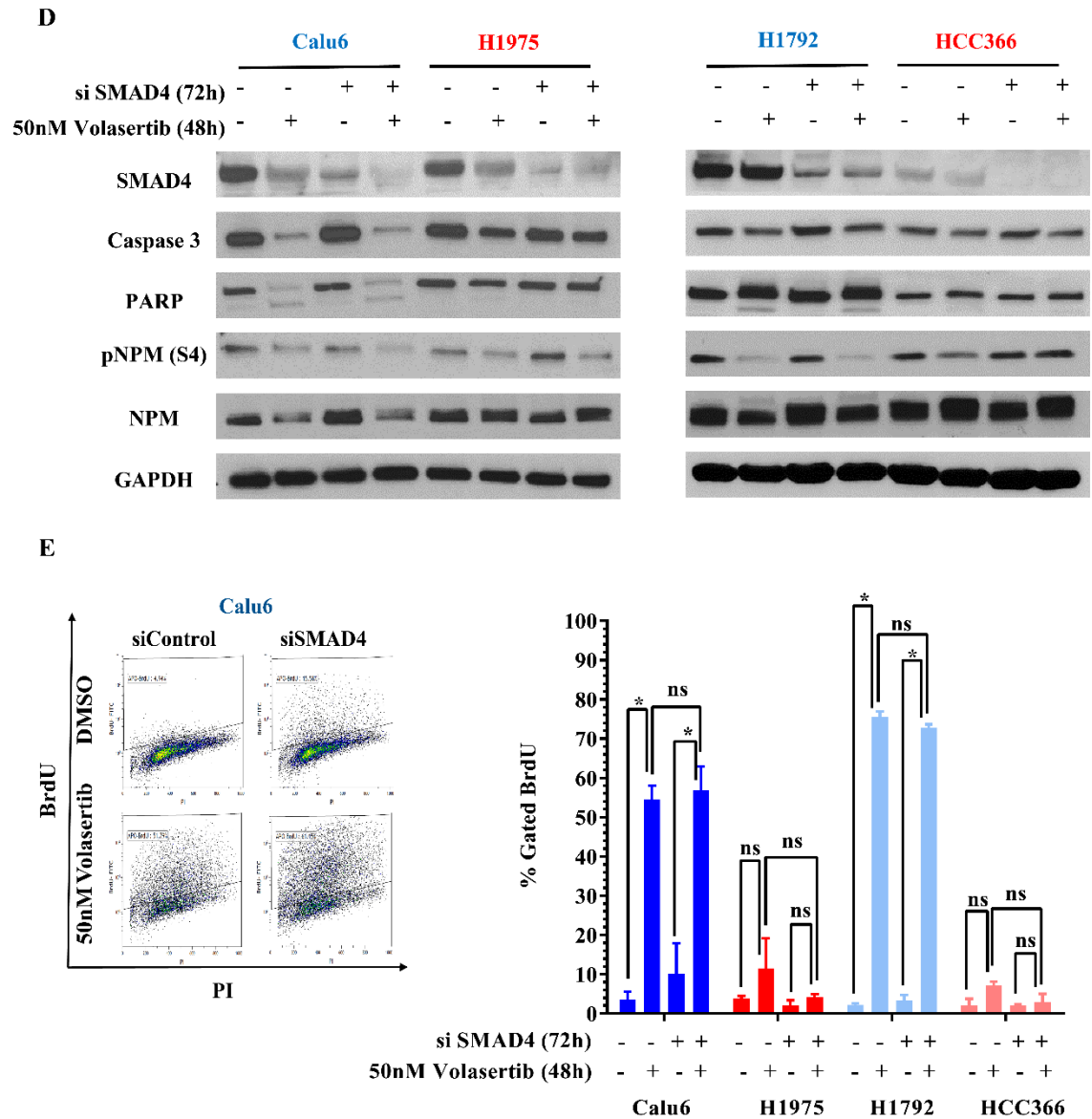


Figure 16: SMAD4 knock-down (KD) did not change sensitivity to PLK1 inhibition induced apoptosis in NSCLC cell lines

A: Correlation of SMAD4 mRNA Expression with AUCs of Volasertib, GSK461364 and NMS-937

B: There is no differential SMAD4 mRNA expression between epithelial and mesenchymal NSCLC cell lines

C: RPPA data depicting the changes in SMAD4 protein expression after PLK1 inhibition in epithelial and mesenchymal (as well as isogenic mesenchymal, i.e., epithelial cells treated with TGF β) NSCLC cell lines

D: Western blot showing that there is no significant difference in the levels of cleaved PARP or cleaved Caspase 3 after β -Catenin KD and PLK1 inhibition

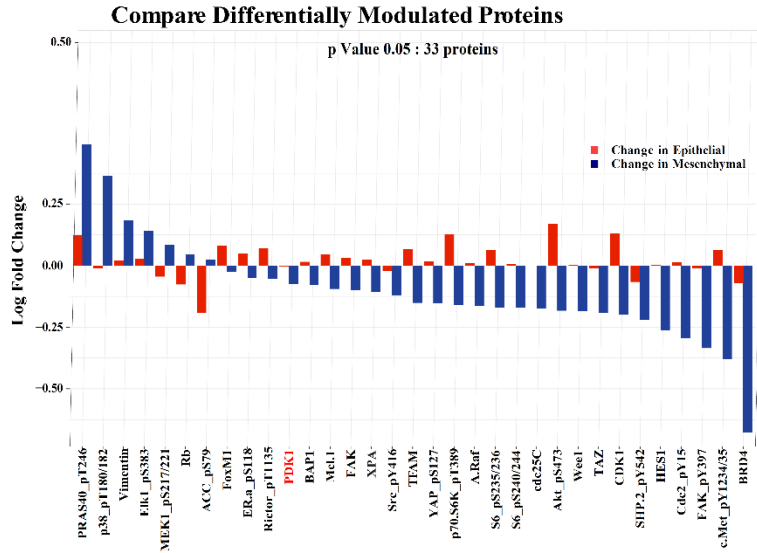
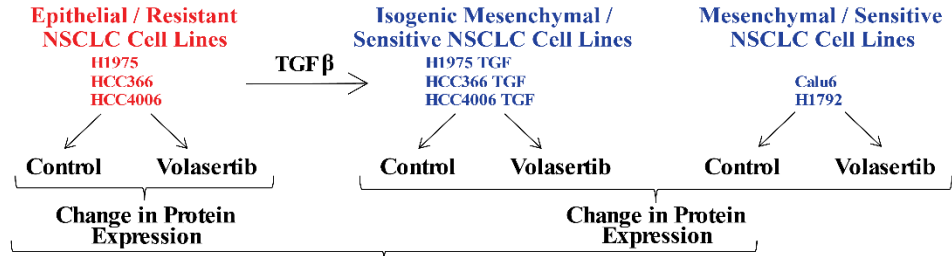
E: Apo BrdU TUNEL assay measuring PLK1 inhibition induced apoptosis after SMAD4 KD in NSCLC cell lines. No difference in BrdU positive cells is observed after SMAD4 KD and Volasertib treatment

11. PDK1 overexpression in a sensitive mesenchymal NSCLC cell line leads to resistance to PLK1 inhibition induced apoptosis

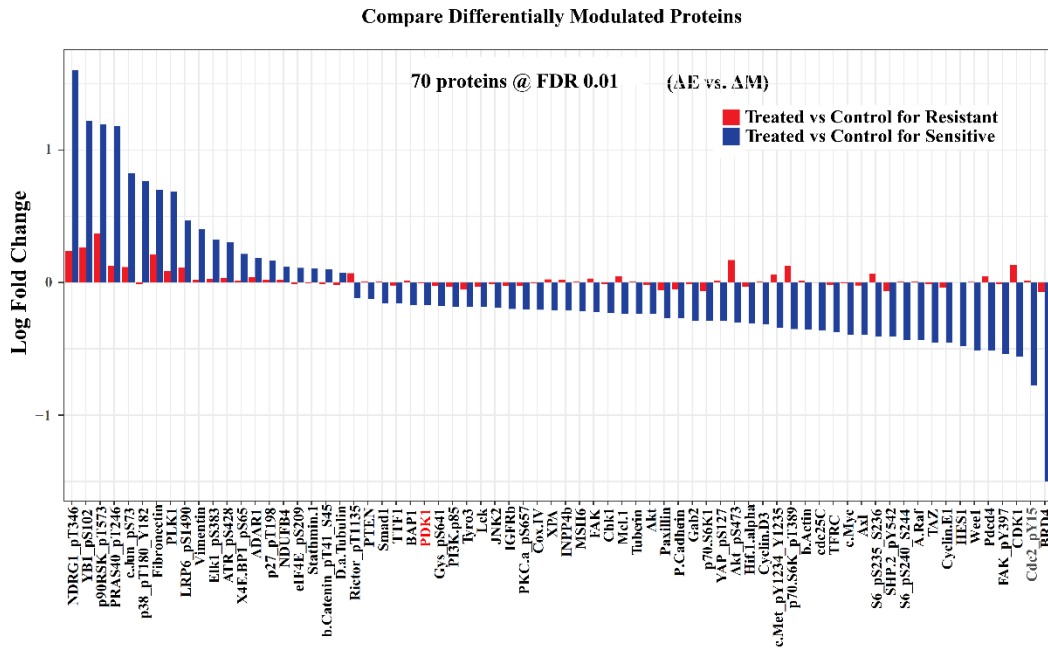
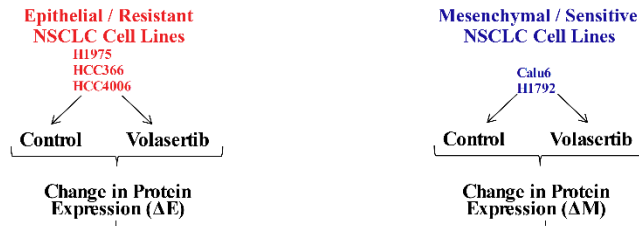
In order to elucidate the mechanism for EMT-induced sensitivity to PLK1 inhibition, we compared changes in 303 protein/phosphoprotein expression after PLK1 inhibition using RPPA using the same set up as mentioned previously. Thirty three proteins/phosphoproteins were differentially regulated at cutoff $p < 0.05$. These data revealed differential effects on both the cMET/FAK/SRC signaling axis (103) (and the PI3K/AKT pathway. Western blot analysis of the members of the PI3K/AKT pathway confirmed a significant decrease in PDK1 and 4E-BP1 phosphorylation and total protein levels in mesenchymal cell lines but not in epithelial cell lines after Volasertib treatment (Figure 17).

In order to test the hypothesis that PDK1 is a driver of resistance to PLK1 inhibition induced apoptosis, we created a stable PDK1 overexpressing mesenchymal NSCLC cell line. The PDK1-EGFP plasmid was kindly provided by Dr. Gordon Mills and was stably transfected into the H1792 mesenchymal NSCLC cell line. Overexpression of PDK1 protein was biologically active in H1792 cell line as evinced by increased downstream S6 (S235/236) phosphorylation (Figure 18A). Overexpression of PDK1 in H1792 cell line increased resistance to PLK1 inhibition compared to parental cell lines as seen by decrease in cleaved PARP ($p=0.007$) and γ H2AX levels ($p=0.003$) (Figure 18A-B). We also observed an increase in percent cell viability in the PDK1 overexpressing cells in comparison to the parental cells as tested by CellTitre Glo assay but it was not statistically significant ($p=0.31$). This result was recapitulated using APO BrdU TUNEL assay where H1792 PDK1 overexpression cells showed less apoptosis in comparison to parental cells after treatment with Volasertib ($p=0.003$) (Figure 18D).

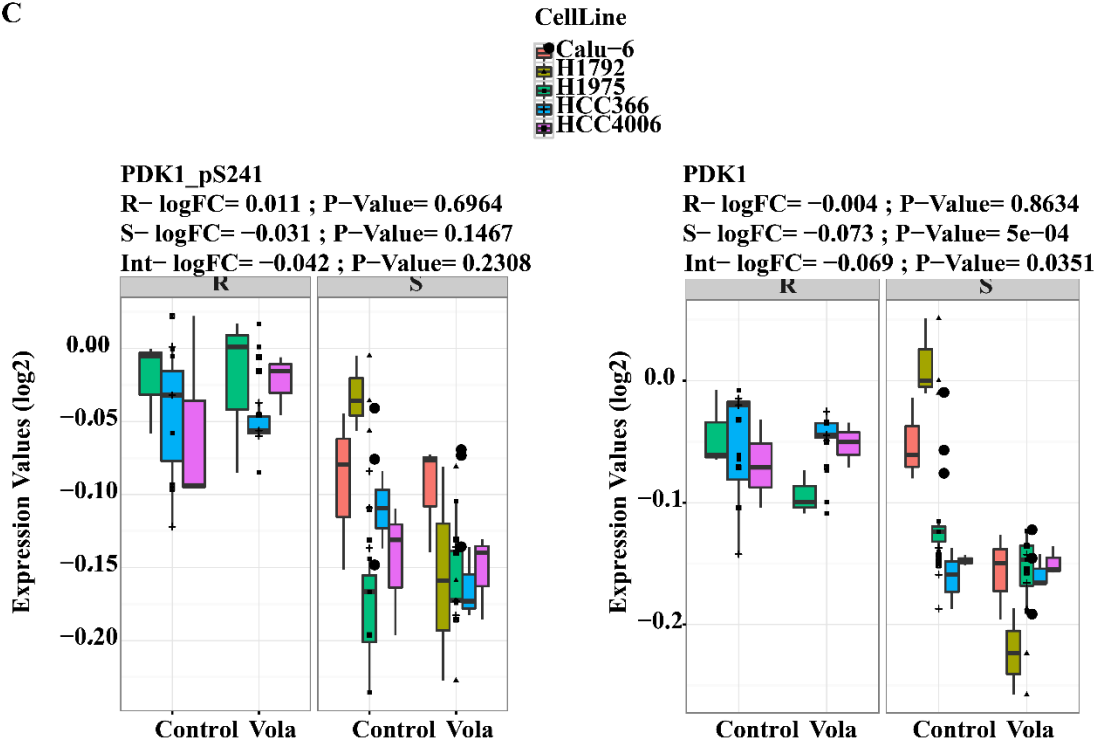
A



B



C



D

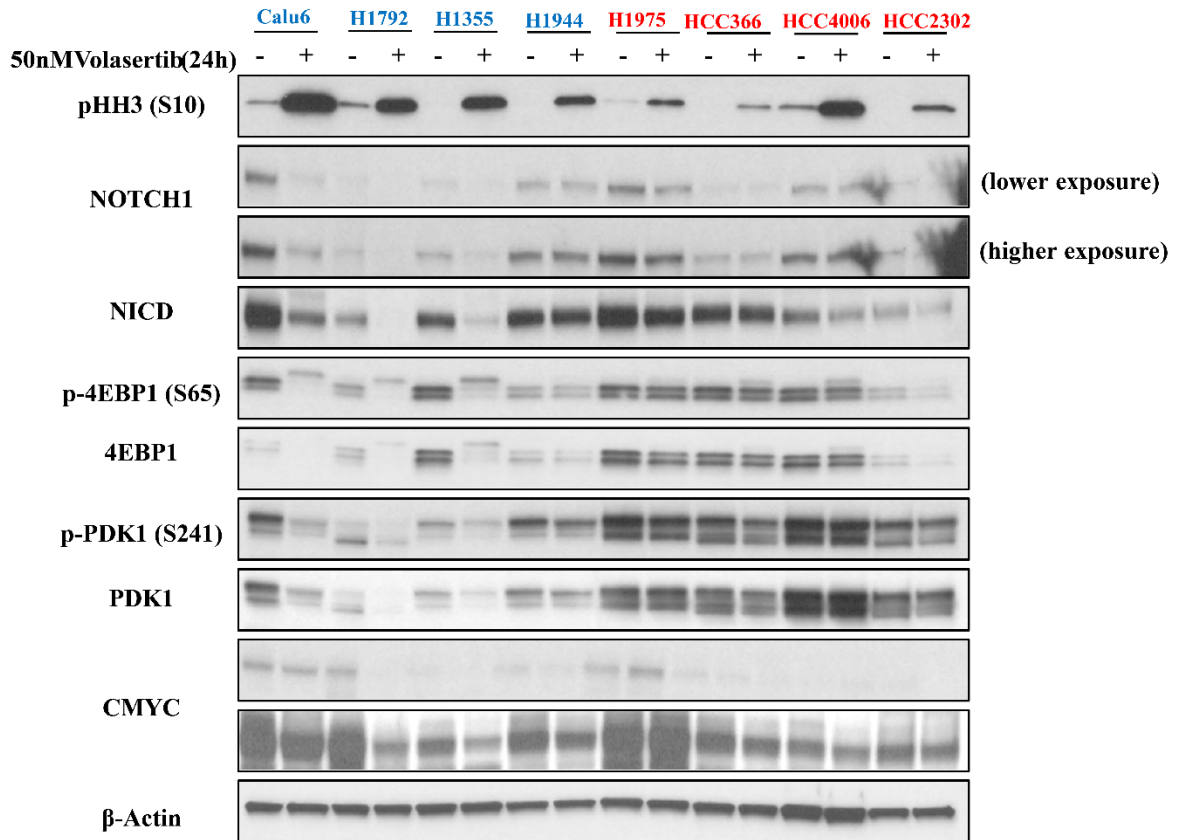


Figure 17: PDK1 protein expression is altered after PLK1 inhibition in mesenchymal but not epithelial NSCLC cell lines

A: 33 proteins are differentially regulated between epithelial and mesenchymal (including isogenic) NSCLC cell lines after Volasertib treatment, one of them being PDK1.

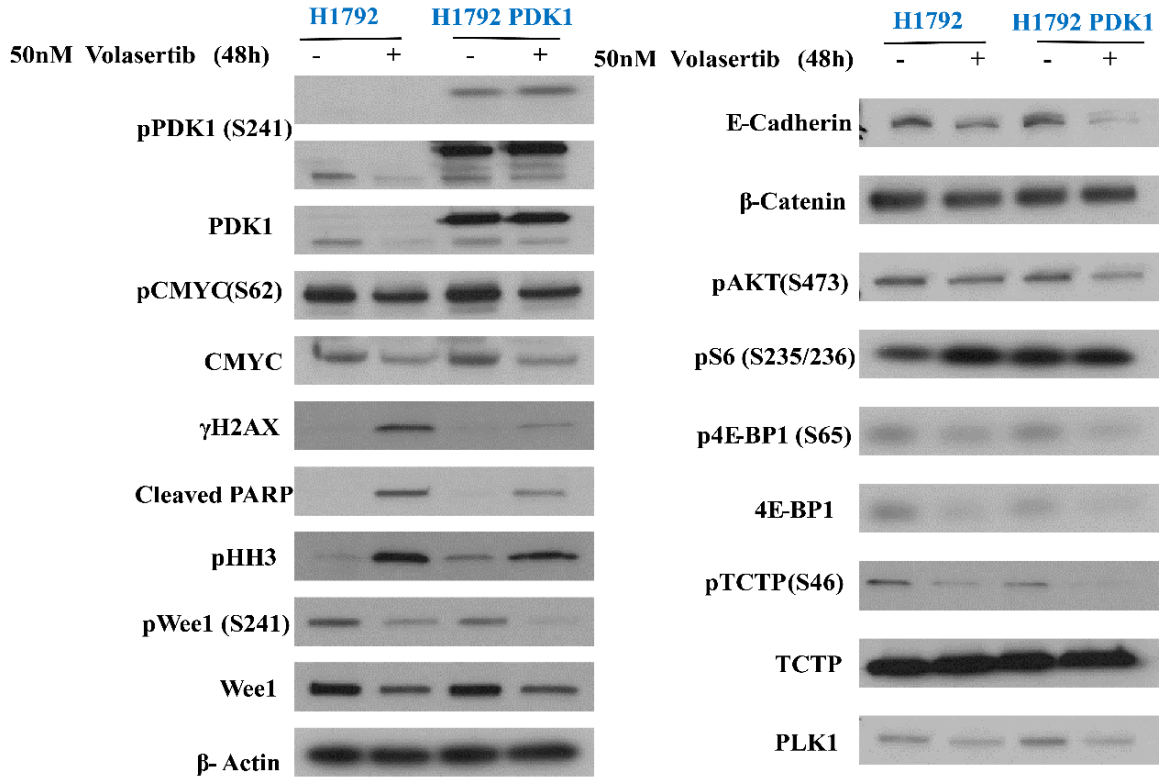
B: 70 proteins are differentially expressed between parental epithelial and mesenchymal NSCLC cell lines after Volasertib treatment, including PDK1.

C: RPPA data shows the changes in pPDK1 (S241) and total PDK1 after Volasertib treatment in epithelial and mesenchymal NSCLC cell lines

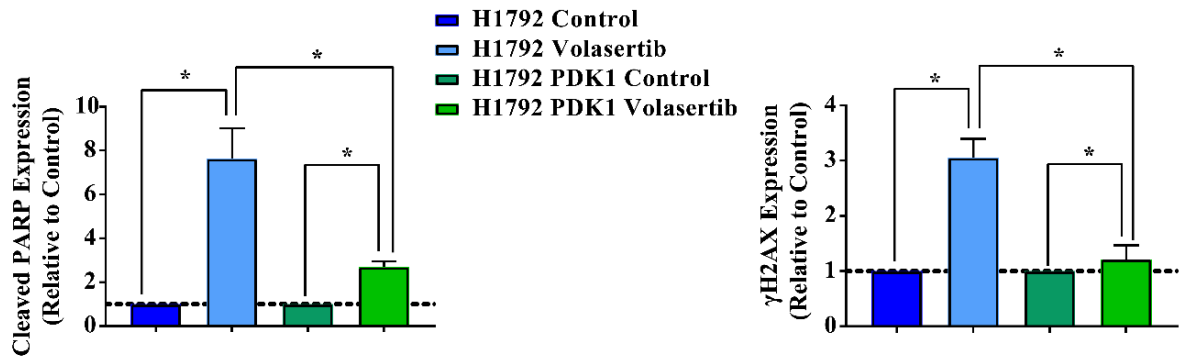
D: Western blot shows differential protein expression in certain PI3K proteins such as PDK1 and 4E-BP1 between epithelial (cell lines depicted in red) and mesenchymal (cell lines depicted in blue) NSCLC cell lines after Volasertib treatment.

NOTE: 17 A-C printed with permission from R.Singh

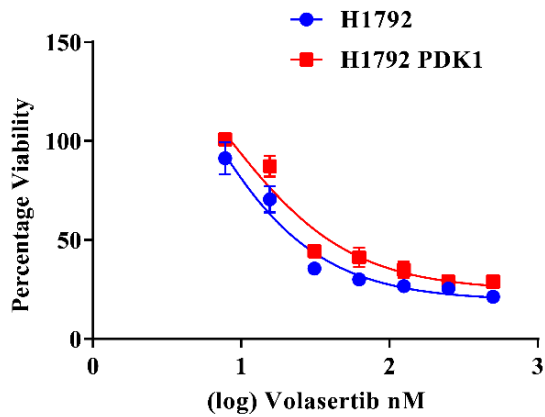
A



B



C



D

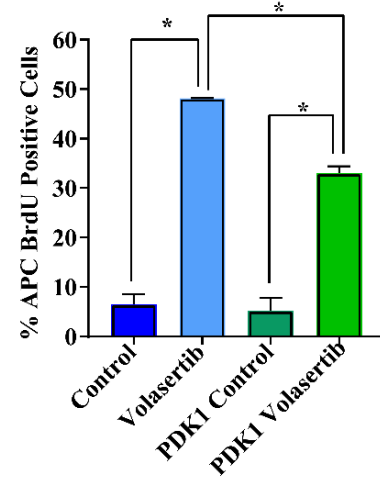


Figure 18: PDK1 overexpression in a sensitive mesenchymal NSCLC cell line leads to resistance to PLK1 inhibition induced apoptosis

A: Western blot of H1792 parental and PDK1 overexpression cell lines treated with 50nM Volasertib for 48h. A decrease in cleaved PARP and γ H2AX levels are observed in H1792 PDK1 cell line compared to parental cell line after Volasertib treatment. The PDK1 is functional as seen by increase in pS6 (S235/236) and PLK1.

B: Quantification of cleaved PARP and γ H2AX protein levels in H1792 PDK1 and parental cell lines after Volasertib treatment. The H1792 PDK1 cells seem to be more resistant to Volasertib treatment in comparison to the parental cells.

C: CellTitre Glo data shows that H1792 PDK1 cells are more resistant to Volasertib in comparison to parental cells.

D: APC BrdU TUNEL assay shows that the H1792 PDK1 cells are resistant to Volasertib in compared to parental cells by around 10%.

Chapter 4: Discussion

Discussion

Accurate preclinical models are an essential component to performing translational cancer research, including discerning molecular pathways of oncogenesis and evaluating therapeutics. One of the main rationales for developing PDX models is based on the expectation that these models will be more predictive of human cancer biology and patient response to treatments. These models are useful for the study of cancer biology, biomarker development, drug screening, and the preclinical evaluation of personalized medicine strategies. PDX models tend to retain the histological characteristics of donor tumors such as tissue structure and gland architecture, mucin production or cyst development. PDX models of NSCLC have similar gene copy number (110), mRNA (22) and protein (111) and retain specific ‘driver’ mutations of the matching primary tumor (26, 112).

Our studies demonstrated surprising heterogeneity in PDX tumors derived from the same, established models. It is now well established that cancer is genetically heterogeneous in an inter- and intra-individual manner and that there is a genetic evolution in cancer as the tumor progresses (113). Thus, a PDX model generated from one individual lesion at a single time point is indeed a snapshot view of a tremendously dynamic process and may not be representative of the full diversity of the disease. The resulting inter-tumoral heterogeneity of PDX models is a double edged sword. It recapitulates the clinical environment, but also adds confounding factors. One such confounding factor is the potential role of mutations, such as TP53 and KRAS, in PLK1 inhibitor sensitivity.

Many studies have shown that generation of a PDX model in a murine host leads to clonal selection which may eventually result in a xenograft that differs from the original patient’s tumor (26, 114, 115). In the case of our study, the EMT status of mice was determined at an earlier passage before the experiment was carried out and clonal

evolution might have played a role in determining tumor response. The sample size for assessing EMT in each individual PDX model (n=4) is too low to make a correlation between EMT and response to PLK1 inhibitors. Another limitation of the PDX studies was that we only completed 4 PDX models and our statistical design dictated that at least 13 models were needed to test our hypothesis. Given the degree of intra-tumoral EMT heterogeneity, more PDX models may indeed be needed than calculated in the original study design.

Although my data support my hypothesis that PLK1 inhibition leads to apoptosis in mesenchymal NSCLC but not in epithelial NSCLC, there are several limitations in the current data that need to be addressed in future studies. A few more PDX models must be used to check for PLK1 inhibition induced apoptosis in order to make a correlation between EMT status and response to PLK1 inhibitors. PDX models are highly heterogeneous and the response to PLK1 inhibitors might be difficult to correlate. The experiments might need to be carried out in early passage PDX models in order to reduce the clonal evolution of PDXs. The EMT status of the PDXs is defined by only two markers in the study, E-Cadherin and vimentin. A panel of markers will be used to determine the EMT phenotype of the PDX models. RNASeq analysis can be carried out in the PDX tumors to calculate the EMT score as well as identify novel biomarkers of response to PLK1 inhibition induced apoptosis in NSCLC.

The 393P Vector cells, though inherently epithelial showed a decrease in tumor mass after PLK1 inhibition but it was not significant. The 393P ZEB1 cells, which are mesenchymal showed tumor regression after PLK1 inhibition. EMT related transcription factor ZEB1 and miR-200 are repressors and activators of E-cadherin expression respectively. The previous studies of our lab showed that manipulation of ZEB1 or

miR200 *in vitro* only slightly reversed sensitivity or resistance while a more robust response was seen with EMT induced by TGF β (67) (103). Another finding from our previous study shows that epithelial NSCLC cells show cell arrest while the mesenchymal NSCLC cells undergo apoptosis after PLK1 inhibition (67) which needs to be confirmed in the PDX models.

GEMMs that are created by introducing oncogenes or altering tumor suppressor genes in the mouse genome are widely used to study cancer biology (116). The KRAS and the KRAS/p53 conditional knock-in mouse models are two GEMMs that recapitulate characteristics of the human lung adenocarcinoma disease (117). The murine cell lines that were used in the study harbored KRAS and p53 mutations and had diverse EMT phenotypes. One limitation in our study was that we used a mouse model with two mutations that may increase sensitivity to PLK1 inhibition. The previous study in our lab showed that there was no correlation between TP53 mutation status and PLK1 inhibitor sensitivity using 63 NSCLC cell lines. Although KRAS mutation did predict sensitivity for 2 of the 3 PLK1 inhibitors tested, the correlation was not robust (67).

Evaluation of lung cancer progression is often based on tumor measurements at the end of treatment. Histopathological analysis of lung tissue is the gold standard for assessment of lung tumorigenesis. Although these *ex vivo* procedures offer many opportunities to perform molecular and cellular analyses, they are limited to only one measurement and do not provide details about the dynamic processes that occur over time *in vivo*. Micro-computed tomography (micro-CT) has been incorporated to study the dynamic changes of tumor progression in preclinical models in a non-invasive manner (118). Although CT is technically challenging due to respiratory movement artifacts, it provides visual and quantitative information about the whole lung in a three-dimensional

manner with high resolution and sensitivity. More importantly, CT allows for longitudinal assessment of therapeutic interventions between different groups and the extent of disease in each individual mouse. CT is safe and there is no radiotoxicity to the lungs in mice with weekly CT imaging up to a period of 12 weeks despite receiving a relatively large radiation dose per micro-CT acquisition (119). For quantification of metastatic tumor burden, the methods that have been previously used relied on a Response Evaluation Criteria in Solid Tumors (RECIST)-like criteria wherein the maximal tumor diameter and the largest perpendicular diameter were measured in the coronal plane to calculate the tumor burden from the sum of cross products (98), tumor nodule segmentation (120), segmentation of aerated lung volume for tumor load quantification with respiratory gating (102), manual segmentation of chest space (121), individual nodule tracking (122), modeling tumors as ellipsoids (107) and volumetric measurement of combined tumor and vasculature from a threshold-based region growing algorithm with manual and semi-automated segmentation (99). The main drawbacks of these methods are that they are labor intensive, require specific skill sets in radiology and do not take all the thoracic metastases into consideration. We developed a micro-CT image analysis method to quantitatively measure tumor mass as a measure of metastatic tumor burden in lung cancer. This method of tumor mass calculation takes into account the metastatic tumors present in the thoracic cavity from the base of the lung to the top of the trachea. As the CT imaging is not respiratory gated, the probability of air escaping into the lungs and variance in the breathing period is high despite breath hold at the time of imaging. Also, tumor tissue and vasculature cannot be distinguished in the non-contrast micro-CT imaging as they have similar X-Ray densities. Thereby, one could expect that the tumor burden is proportional to the changes in the MTC in the adult mice.

Though β -Catenin was highly expressed in the resistant/epithelial NSCLC cell lines in comparison to the mesenchymal NSCLC cell lines, knockdown of β -Catenin was not sufficient to sensitize epithelial cells to PLK1 inhibition. This might be due to the fact that KD of β -Catenin alone does not change the epithelial phenotype. It is possible that β -Catenin may be downstream to the key protein or pathway that mediates resistance to PLK1 inhibitors. Also, though SMAD4 is a member of the TGF β pathway and studies have shown that increased expression of SMAD4 induces EMT or enhances the induction of EMT, KD of did not mediate resistance to PLK1 inhibitors in the mesenchymal NSCLC cell lines. This implies that there may be other factors in the TGF β pathway that govern the mesenchymal phenotype of NSCLC cells. We identified PDK1 to decrease after PLK1 inhibition in mesenchymal NSCLC but not epithelial NSCLC cell lines. PDK1 is a serine/threonine kinase which acts as a master kinase, phosphorylating and activating a subgroup of the cAMP-dependent, cGMP-dependent and protein kinase C (AGC) family of protein kinases such as AKT, p70RSK, p90RSK, SGK1, PAK1 to name a few. PDK1 plays a central role in the transduction of signals from insulin by providing the activating phosphorylation to PKB/AKT1, thus propagating the signal to downstream targets controlling cell proliferation and survival, as well as glucose and amino acid uptake and storage. A stable PDK1 overexpressing mesenchymal NSCLC cell line was established. It was observed that PDK1 overexpression slightly reduced sensitivity to the PLK1 inhibitor Volasertib as observed by reduction in the expression of cleaved PARP and γ H2AX. The limitation of this study is that only one NSCLC cell lines was used to study to the role of PDK1 overexpression in PLK1 inhibition-induced apoptosis. The response observed was minimal and it is possible that PDK1 may not be critical component in mediating resistance to PLK1 inhibitors. This might be due to the possibility that PDK1

is regulated by SRC which is downstream to the CMET-FAK-SRC signaling pathway which has been identified by our lab to mediate PLK1-inhibition induced apoptosis in NSCLC (103).

A study in our lab showed that epithelial NSCLC cell lines are more resistant to PLK1 inhibition in comparison to mesenchymal NSCLC cell lines due to the differential regulation of CMET (103). The study shows that this is because of ligand independent activation of CMET in mesenchymal NSCLC cells in Integrin β 1 due to increase in vimentin expression. Thus CMET activation can be used as a biomarker of response to PLK1 inhibition induced apoptosis (103).

In order to measure PLK1 inhibition induced apoptosis, TUNEL assay is being carried out to measure apoptotic cells in the vehicle and Volasertib treated PDX tumors and the epithelial and mesenchymal lung tumors. Pathological response will be used to correlate with PLK1 inhibitor sensitivity in the *in vivo* studies. Some of the additional studies that can be carried out includes inducing a mesenchymal-to-epithelial transition (MET) in mice by using mesenchymal cells with inducible miR200 expression. Other modalities by which EMT can be manipulated *in vivo* may be used to study PLK1 inhibition induced apoptosis in NSCLC.

In conclusion, preliminary data suggests that mesenchymal NSCLC tumors are more sensitive to PLK1 inhibition in comparison to epithelial NSCLC tumors as seen in the PDX studies, the 344SQ mouse model and the 393P with ZEB1 overexpression mouse models. Though β -Catenin and SMAD4 KD did not reverse resistance or sensitivity to PLK1 inhibitors, it is a possibility that these are downstream to some key elements that drive resistance or sensitivity to PLK1 inhibitors.

Chapter 5: Bibliography

1. Siegel, R. L., K. D. Miller, and A. Jemal. 2018. Cancer statistics, 2018. *CA Cancer J Clin* 68: 7-30.
2. Travis, W. D., E. Brambilla, A. G. Nicholson, Y. Yatabe, J. H. M. Austin, M. B. Beasley, L. R. Chirieac, S. Dacic, E. Duhig, D. B. Flieder, K. Geisinger, F. R. Hirsch, Y. Ishikawa, K. M. Kerr, M. Noguchi, G. Pelosi, C. A. Powell, M. S. Tsao, I. Wistuba, and W. H. O. Panel. 2015. The 2015 World Health Organization Classification of Lung Tumors: Impact of Genetic, Clinical and Radiologic Advances Since the 2004 Classification. *J Thorac Oncol* 10: 1243-1260.
3. Lindeman, N. I., P. T. Cagle, M. B. Beasley, D. A. Chitale, S. Dacic, G. Giaccone, R. B. Jenkins, D. J. Kwiatkowski, J. S. Saldivar, J. Squire, E. Thunnissen, and M. Ladanyi. 2013. Molecular testing guideline for selection of lung cancer patients for EGFR and ALK tyrosine kinase inhibitors: guideline from the College of American Pathologists, International Association for the Study of Lung Cancer, and Association for Molecular Pathology. *Arch Pathol Lab Med* 137: 828-860.
4. Travis, W. D., E. Brambilla, M. Noguchi, A. G. Nicholson, K. R. Geisinger, Y. Yatabe, D. G. Beer, C. A. Powell, G. J. Riely, P. E. Van Schil, K. Garg, J. H. Austin, H. Asamura, V. W. Rusch, F. R. Hirsch, G. Scagliotti, T. Mitsudomi, R. M. Huber, Y. Ishikawa, J. Jett, M. Sanchez-Cespedes, J. P. Sculier, T. Takahashi, M. Tsuboi, J. Vansteenkiste, I. Wistuba, P. C. Yang, D. Aberle, C. Brambilla, D. Flieder, W. Franklin, A. Gazdar, M. Gould, P. Hasleton, D. Henderson, B. Johnson, D. Johnson, K. Kerr, K. Kuriyama, J. S. Lee, V. A. Miller, I. Petersen, V. Roggli, R. Rosell, N. Saijo, E. Thunnissen, M. Tsao, and D. Yankelewitz. 2011. International association for the study of lung cancer/american thoracic society/european respiratory society international multidisciplinary classification of lung adenocarcinoma. *J Thorac Oncol* 6: 244-285.

5. Pao, W., and K. E. Hutchinson. 2012. Chipping away at the lung cancer genome. *Nat Med* 18: 349-351.
6. Tsao, A. S., G. V. Scagliotti, P. A. Bunn, Jr., D. P. Carbone, G. W. Warren, C. Bai, H. J. de Koning, A. U. Yousaf-Khan, A. McWilliams, M. S. Tsao, P. S. Adusumilli, R. Rami-Porta, H. Asamura, P. E. Van Schil, G. E. Darling, S. S. Ramalingam, D. R. Gomez, K. E. Rosenzweig, S. Zimmermann, S. Peters, S. H. Ignatius Ou, T. Reungwetwattana, P. A. Janne, T. S. Mok, H. A. Wakelee, R. Pirker, J. Mazieres, J. R. Brahmer, Y. Zhou, R. S. Herbst, V. A. Papadimitrakopoulou, M. W. Redman, M. W. Wynes, D. R. Gandara, R. J. Kelly, F. R. Hirsch, and H. I. Pass. 2016. Scientific Advances in Lung Cancer 2015. *J Thorac Oncol* 11: 613-638.
7. Li, A. R., D. Chitale, G. J. Riely, W. Pao, V. A. Miller, M. F. Zakowski, V. Rusch, M. G. Kris, and M. Ladanyi. 2008. EGFR mutations in lung adenocarcinomas: clinical testing experience and relationship to EGFR gene copy number and immunohistochemical expression. *J Mol Diagn* 10: 242-248.
8. Weinstein, I. B. 2002. Cancer. Addiction to oncogenes--the Achilles heel of cancer. *Science (New York, N.Y.)* 297: 63-64.
9. Lin, J. J., and A. T. Shaw. 2016. Resisting Resistance: Targeted Therapies in Lung Cancer. *Trends Cancer* 2: 350-364.
10. Ramalingam, S., and C. Belani. 2008. Systemic chemotherapy for advanced non-small cell lung cancer: recent advances and future directions. *Oncologist* 13 Suppl 1: 5-13.
11. Masters, G. A., S. Temin, C. G. Azzoli, G. Giaccone, S. Baker, Jr., J. R. Brahmer, P. M. Ellis, A. Gajra, N. Rackear, J. H. Schiller, T. J. Smith, J. R. Strawn, D. Trent, D. H. Johnson, and P. American Society of Clinical Oncology Clinical. 2015. Systemic Therapy

- for Stage IV Non-Small-Cell Lung Cancer: American Society of Clinical Oncology Clinical Practice Guideline Update. *J Clin Oncol* 33: 3488-3515.
12. Bunn, P. A., Jr., and K. Kelly. 1998. New chemotherapeutic agents prolong survival and improve quality of life in non-small cell lung cancer: a review of the literature and future directions. *Clin Cancer Res* 4: 1087-1100.
 13. Pardoll, D. M. 2012. The blockade of immune checkpoints in cancer immunotherapy. *Nat Rev Cancer* 12: 252-264.
 14. Selby, M. J., J. J. Engelhardt, M. Quigley, K. A. Henning, T. Chen, M. Srinivasan, and A. J. Korman. 2013. Anti-CTLA-4 antibodies of IgG2a isotype enhance antitumor activity through reduction of intratumoral regulatory T cells. *Cancer Immunol Res* 1: 32-42.
 15. Reck, M., D. Rodriguez-Abreu, A. G. Robinson, R. Hui, T. Csoszi, A. Fulop, M. Gottfried, N. Peled, A. Tafreshi, S. Cuffe, M. O'Brien, S. Rao, K. Hotta, M. A. Leiby, G. M. Lubiniecki, Y. Shentu, R. Rangwala, J. R. Brahmer, and K.-. Investigators. 2016. Pembrolizumab versus Chemotherapy for PD-L1-Positive Non-Small-Cell Lung Cancer. *N Engl J Med* 375: 1823-1833.
 16. Kwon, M. C., and A. Berns. 2013. Mouse models for lung cancer. *Mol Oncol* 7: 165-177.
 17. Guerra, C., N. Mijimolle, A. Dhawahir, P. Dubus, M. Barradas, M. Serrano, V. Campuzano, and M. Barbacid. 2003. Tumor induction by an endogenous K-ras oncogene is highly dependent on cellular context. *Cancer Cell* 4: 111-120.
 18. Jackson, E. L., N. Willis, K. Mercer, R. T. Bronson, D. Crowley, R. Montoya, T. Jacks, and D. A. Tuveson. 2001. Analysis of lung tumor initiation and progression using conditional expression of oncogenic K-ras. *Genes & development* 15: 3243-3248.
 19. Winslow, M. M., T. L. Dayton, R. G. Verhaak, C. Kim-Kiselak, E. L. Snyder, D. M. Feldser, D. D. Hubbard, M. J. DuPage, C. A. Whittaker, S. Hoersch, S. Yoon, D. Crowley,

- R. T. Bronson, D. Y. Chiang, M. Meyerson, and T. Jacks. 2011. Suppression of lung adenocarcinoma progression by Nkx2-1. *Nature* 473: 101-104.
20. Moro, M., G. Bertolini, M. Tortoreto, U. Pastorino, G. Sozzi, and L. Roz. 2012. Patient-derived xenografts of non small cell lung cancer: resurgence of an old model for investigation of modern concepts of tailored therapy and cancer stem cells. *J Biomed Biotechnol* 2012: 568567.
21. Daniel, V. C., L. Marchionni, J. S. Hierman, J. T. Rhodes, W. L. Devereux, C. M. Rudin, R. Yung, G. Parmigiani, M. Dorsch, C. D. Peacock, and D. N. Watkins. 2009. A primary xenograft model of small-cell lung cancer reveals irreversible changes in gene expression imposed by culture in vitro. *Cancer Res* 69: 3364-3373.
22. Fichtner, I., J. Rolff, R. Soong, J. Hoffmann, S. Hammer, A. Sommer, M. Becker, and J. Merk. 2008. Establishment of patient-derived non-small cell lung cancer xenografts as models for the identification of predictive biomarkers. *Clin Cancer Res* 14: 6456-6468.
23. Hao, C., L. Wang, S. Peng, M. Cao, H. Li, J. Hu, X. Huang, W. Liu, H. Zhang, S. Wu, A. Pataer, J. V. Heymach, A. K. Eterovic, Q. Zhang, K. R. Shaw, K. Chen, A. Futreal, M. Wang, W. Hofstetter, R. Mehran, D. Rice, J. A. Roth, B. Sepesi, S. G. Swisher, A. Vaporciyan, G. L. Walsh, F. M. Johnson, and B. Fang. 2015. Gene mutations in primary tumors and corresponding patient-derived xenografts derived from non-small cell lung cancer. *Cancer Lett* 357: 179-185.
24. Peng, S., C. J. Creighton, Y. Zhang, B. Sen, T. Mazumdar, J. N. Myers, S. Y. Lai, A. Woolfson, M. V. Lorenzi, D. Bell, M. D. Williams, and F. M. Johnson. 2013. Tumor grafts derived from patients with head and neck squamous carcinoma authentically maintain the molecular and histologic characteristics of human cancers. *J Transl Med* 11: 198.

25. Perez-Soler, R., B. Kemp, Q. P. Wu, L. Mao, J. Gomez, A. Zeleniuch-Jacquotte, H. Yee, J. S. Lee, J. Jagirdar, and Y. H. Ling. 2000. Response and determinants of sensitivity to paclitaxel in human non-small cell lung cancer tumors heterotransplanted in nude mice. *Clin Cancer Res* 6: 4932-4938.
26. Stewart, E. L., C. Mascaux, N. A. Pham, S. Sakashita, J. Sykes, L. Kim, N. Yanagawa, G. Allo, K. Ishizawa, D. Wang, C. Q. Zhu, M. Li, C. Ng, N. Liu, M. Pintilie, P. Martin, T. John, I. Jurisica, N. B. Leighl, B. G. Neel, T. K. Waddell, F. A. Shepherd, G. Liu, and M. S. Tsao. 2015. Clinical Utility of Patient-Derived Xenografts to Determine Biomarkers of Prognosis and Map Resistance Pathways in EGFR-Mutant Lung Adenocarcinoma. *J Clin Oncol* 33: 2472-2480.
27. Reinhardt, H. C., and M. B. Yaffe. 2013. Phospho-Ser/Thr-binding domains: navigating the cell cycle and DNA damage response. *Nat Rev Mol Cell Biol* 14: 563-580.
28. Strebhardt, K., and A. Ullrich. 2006. Targeting polo-like kinase 1 for cancer therapy. *Nat Rev Cancer* 6: 321-330.
29. de Carcer, G., B. Escobar, A. M. Higuero, L. Garcia, A. Anson, G. Perez, M. Mollejo, G. Manning, B. Melendez, J. Abad-Rodriguez, and M. Malumbres. 2011. Plk5, a polo box domain-only protein with specific roles in neuron differentiation and glioblastoma suppression. *Molecular and cellular biology* 31: 1225-1239.
30. Hanisch, A., A. Wehner, E. A. Nigg, and H. H. Sillje. 2006. Different Plk1 functions show distinct dependencies on Polo-Box domain-mediated targeting. *Mol Biol Cell* 17: 448-459.
31. Elia, A. E., L. C. Cantley, and M. B. Yaffe. 2003. Proteomic screen finds pSer/pThr-binding domain localizing Plk1 to mitotic substrates. *Science (New York, N.Y.)* 299: 1228-1231.

32. Park, J. E., N. K. Soung, Y. Johmura, Y. H. Kang, C. Liao, K. H. Lee, C. H. Park, M. C. Nicklaus, and K. S. Lee. 2010. Polo-box domain: a versatile mediator of polo-like kinase function. *Cell Mol Life Sci* 67: 1957-1970.
33. Uchiumi, T., D. L. Longo, and D. K. Ferris. 1997. Cell cycle regulation of the human polo-like kinase (PLK) promoter. *The Journal of biological chemistry* 272: 9166-9174.
34. Archambault, V., and D. M. Glover. 2009. Polo-like kinases: conservation and divergence in their functions and regulation. *Nat Rev Mol Cell Biol* 10: 265-275.
35. Strebhardt, K., and A. Ullrich. 2006. Targeting polo-like kinase 1 for cancer therapy. *Nat Rev Cancer* 6: 321-330.
36. Macurek, L., A. Lindqvist, D. Lim, M. A. Lampson, R. Klompaker, R. Freire, C. Clouin, S. S. Taylor, M. B. Yaffe, and R. H. Medema. 2008. Polo-like kinase-1 is activated by aurora A to promote checkpoint recovery. *Nature* 455: 119-123.
37. Seki, A., J. A. Coppinger, C. Y. Jang, J. R. Yates, and G. Fang. 2008. Bora and the kinase Aurora a cooperatively activate the kinase Plk1 and control mitotic entry. *Science (New York, N.Y.)* 320: 1655-1658.
38. Schmucker, S., and I. Sumara. 2014. Molecular dynamics of PLK1 during mitosis. *Mol Cell Oncol* 1: e954507.
39. Lindon, C., and J. Pines. 2004. Ordered proteolysis in anaphase inactivates Plk1 to contribute to proper mitotic exit in human cells. *J Cell Biol* 164: 233-241.
40. Abrieu, A., T. Brassac, S. Galas, D. Fisher, J. C. Labbe, and M. Doree. 1998. The Polo-like kinase Plx1 is a component of the MPF amplification loop at the G2/M-phase transition of the cell cycle in *Xenopus* eggs. *J Cell Sci* 111 (Pt 12): 1751-1757.

41. Arnaud, L., J. Pines, and E. A. Nigg. 1998. GFP tagging reveals human Polo-like kinase 1 at the kinetochore/centromere region of mitotic chromosomes. *Chromosoma* 107: 424-429.
42. Sumara, I., J. F. Gimenez-Abian, D. Gerlich, T. Hirota, C. Kraft, C. de la Torre, J. Ellenberg, and J. M. Peters. 2004. Roles of polo-like kinase 1 in the assembly of functional mitotic spindles. *Curr Biol* 14: 1712-1722.
43. Lane, H. A., and E. A. Nigg. 1996. Antibody microinjection reveals an essential role for human polo-like kinase 1 (Plk1) in the functional maturation of mitotic centrosomes. *J Cell Biol* 135: 1701-1713.
44. Godinho, S., and A. A. Tavares. 2008. A role for Drosophila Polo protein in chromosome resolution and segregation during mitosis. *Cell Cycle* 7: 2529-2534.
45. Kang, Y. H., J. E. Park, L. R. Yu, N. K. Soung, S. M. Yun, J. K. Bang, Y. S. Seong, H. Yu, S. Garfield, T. D. Veenstra, and K. S. Lee. 2006. Self-regulated Plk1 recruitment to kinetochores by the Plk1-PBIP1 interaction is critical for proper chromosome segregation. *Mol Cell* 24: 409-422.
46. Burkard, M. E., C. L. Randall, S. Laroche, C. Zhang, K. M. Shokat, R. P. Fisher, and P. V. Jallepalli. 2007. Chemical genetics reveals the requirement for Polo-like kinase 1 activity in positioning RhoA and triggering cytokinesis in human cells. *Proceedings of the National Academy of Sciences of the United States of America* 104: 4383-4388.
47. Neef, R., C. Preisinger, J. Sutcliffe, R. Kopajtich, E. A. Nigg, T. U. Mayer, and F. A. Barr. 2003. Phosphorylation of mitotic kinesin-like protein 2 by polo-like kinase 1 is required for cytokinesis. *J Cell Biol* 162: 863-875.
48. Seong, Y. S., K. Kamijo, J. S. Lee, E. Fernandez, R. Kuriyama, T. Miki, and K. S. Lee. 2002. A spindle checkpoint arrest and a cytokinesis failure by the dominant-negative polo-

- box domain of Plk1 in U-2 OS cells. *The Journal of biological chemistry* 277: 32282-32293.
49. Lera, R. F., G. K. Potts, A. Suzuki, J. M. Johnson, E. D. Salmon, J. J. Coon, and M. E. Burkard. 2016. Decoding Polo-like kinase 1 signaling along the kinetochore-centromere axis. *Nat Chem Biol* 12: 411-418.
 50. Roshak, A. K., E. A. Capper, C. Imburgia, J. Fornwald, G. Scott, and L. A. Marshall. 2000. The human polo-like kinase, PLK, regulates cdc2/cyclin B through phosphorylation and activation of the cdc25C phosphatase. *Cell Signal* 12: 405-411.
 51. van Vugt, M. A., A. Bras, and R. H. Medema. 2004. Polo-like kinase-1 controls recovery from a G2 DNA damage-induced arrest in mammalian cells. *Mol Cell* 15: 799-811.
 52. Wasch, R., and D. Engelbert. 2005. Anaphase-promoting complex-dependent proteolysis of cell cycle regulators and genomic instability of cancer cells. *Oncogene* 24: 1-10.
 53. Hyun, S. Y., H. I. Hwang, and Y. J. Jang. 2014. Polo-like kinase-1 in DNA damage response. *BMB Rep* 47: 249-255.
 54. Benada, J., K. Burdova, T. Lidak, P. von Morgen, and L. Macurek. 2015. Polo-like kinase 1 inhibits DNA damage response during mitosis. *Cell Cycle* 14: 219-231.
 55. Alves, I. T., and M. A. van Vugt. 2015. Plk1 Manages DNA break repair during mitosis. *Cell Cycle* 14: 1356-1357.
 56. Holtrich, U., G. Wolf, A. Brauninger, T. Karn, B. Bohme, H. Rubsamen-Waigmann, and K. Strebhardt. 1994. Induction and down-regulation of PLK, a human serine/threonine kinase expressed in proliferating cells and tumors. *Proceedings of the National Academy of Sciences of the United States of America* 91: 1736-1740.
 57. Cholewa, B. D., X. Liu, and N. Ahmad. 2013. The role of polo-like kinase 1 in carcinogenesis: cause or consequence? *Cancer Res* 73: 6848-6855.

58. Benoit, D. S., S. M. Henry, A. D. Shubin, A. S. Hoffman, and P. S. Stayton. 2010. pH-responsive polymeric siRNA carriers sensitize multidrug resistant ovarian cancer cells to doxorubicin via knockdown of polo-like kinase 1. *Mol Pharm* 7: 442-455.
59. Bu, Y., Z. Yang, Q. Li, and F. Song. 2008. Silencing of polo-like kinase (Plk) 1 via siRNA causes inhibition of growth and induction of apoptosis in human esophageal cancer cells. *Oncology* 74: 198-206.
60. Reagan-Shaw, S., and N. Ahmad. 2005. Silencing of polo-like kinase (Plk) 1 via siRNA causes induction of apoptosis and impairment of mitosis machinery in human prostate cancer cells: implications for the treatment of prostate cancer. *FASEB J* 19: 611-613.
61. Liu, Z., Q. Sun, and X. Wang. 2017. PLK1, A Potential Target for Cancer Therapy. *Transl Oncol* 10: 22-32.
62. Luo, J., M. J. Emanuele, D. Li, C. J. Creighton, M. R. Schlabach, T. F. Westbrook, K. K. Wong, and S. J. Elledge. 2009. A genome-wide RNAi screen identifies multiple synthetic lethal interactions with the Ras oncogene. *Cell* 137: 835-848.
63. Sur, S., R. Pagliarini, F. Bunz, C. Rago, L. A. Diaz, Jr., K. W. Kinzler, B. Vogelstein, and N. Papadopoulos. 2009. A panel of isogenic human cancer cells suggests a therapeutic approach for cancers with inactivated p53. *Proceedings of the National Academy of Sciences of the United States of America* 106: 3964-3969.
64. Liu, X. S., B. Song, B. D. Elzey, T. L. Ratliff, S. F. Konieczny, L. Cheng, N. Ahmad, and X. Liu. 2011. Polo-like kinase 1 facilitates loss of Pten tumor suppressor-induced prostate cancer formation. *The Journal of biological chemistry* 286: 35795-35800.
65. Wolf, G., R. Elez, A. Doermer, U. Holtrich, H. Ackermann, H. J. Stutte, H. M. Altmannsberger, H. Rubsamen-Waigmann, and K. Strebhardt. 1997. Prognostic

- significance of polo-like kinase (PLK) expression in non-small cell lung cancer. *Oncogene* 14: 543-549.
66. Riely, G. J., J. Marks, and W. Pao. 2009. KRAS mutations in non-small cell lung cancer. *Proc Am Thorac Soc* 6: 201-205.
67. Ferrarotto, R., R. Goonatilake, S. Y. Yoo, P. Tong, U. Giri, S. Peng, J. Minna, L. Girard, Y. Wang, L. Wang, L. Li, L. Diao, D. H. Peng, D. L. Gibbons, B. S. Glisson, J. V. Heymach, J. Wang, L. A. Byers, and F. M. Johnson. 2016. Epithelial-Mesenchymal Transition Predicts Polo-Like Kinase 1 Inhibitor-Mediated Apoptosis in Non-Small Cell Lung Cancer. *Clin Cancer Res* 22: 1674-1686.
68. Spankuch, B., Y. Matthes, R. Knecht, B. Zimmer, M. Kaufmann, and K. Strebhardt. 2004. Cancer inhibition in nude mice after systemic application of U6 promoter-driven short hairpin RNAs against PLK1. *J Natl Cancer Inst* 96: 862-872.
69. Kawata, E., E. Ashihara, S. Kimura, K. Takenaka, K. Sato, R. Tanaka, A. Yokota, Y. Kamitsuji, M. Takeuchi, J. Kuroda, F. Tanaka, T. Yoshikawa, and T. Maekawa. 2008. Administration of PLK-1 small interfering RNA with atelocollagen prevents the growth of liver metastases of lung cancer. *Mol Cancer Ther* 7: 2904-2912.
70. Byers, L. A., L. Diao, J. Wang, P. Saintigny, L. Girard, M. Peyton, L. Shen, Y. Fan, U. Giri, P. K. Tumula, M. B. Nilsson, J. Gudikote, H. Tran, R. J. Cardnell, D. J. Bearss, S. L. Warner, J. M. Foulks, S. B. Kanner, V. Gandhi, N. Krett, S. T. Rosen, E. S. Kim, R. S. Herbst, G. R. Blumenschein, J. J. Lee, S. M. Lippman, K. K. Ang, G. B. Mills, W. K. Hong, J. N. Weinstein, Wistuba, II, K. R. Coombes, J. D. Minna, and J. V. Heymach. 2013. An epithelial-mesenchymal transition gene signature predicts resistance to EGFR and PI3K inhibitors and identifies Axl as a therapeutic target for overcoming EGFR inhibitor resistance. *Clin Cancer Res* 19: 279-290.

71. Crystal, A. S., A. T. Shaw, L. V. Sequist, L. Friboulet, M. J. Niederst, E. L. Lockerman, R. L. Frias, J. F. Gainor, A. Amzallag, P. Greninger, D. Lee, A. Kalsy, M. Gomez-Caraballo, L. Elamine, E. Howe, W. Hur, E. Lifshits, H. E. Robinson, R. Katayama, A. C. Faber, M. M. Awad, S. Ramaswamy, M. Mino-Kenudson, A. J. Iafrate, C. H. Benes, and J. A. Engelman. 2014. Patient-derived models of acquired resistance can identify effective drug combinations for cancer. *Science (New York, N.Y.)* 346: 1480-1486.
72. Wang, Y., R. Singh, L. Wang, M. Nilsson, R. Goonatilake, P. Tong, L. Li, U. Giri, P. Villalobos, B. Mino, J. Rodriguez-Canales, I. Wistuba, J. Wang, J. V. Heymach, and F. M. Johnson. 2016. Polo-like kinase 1 inhibition diminishes acquired resistance to epidermal growth factor receptor inhibition in non-small cell lung cancer with T790M mutations. *Oncotarget* 7: 47998-48010.
73. Li, S., Y. Zhang, and W. Xu. 2013. Developments of polo-like kinase 1 (Plk1) inhibitors as anti-cancer agents. *Mini Rev Med Chem* 13: 2014-2025.
74. Buschbeck, M. 2006. Strategies to overcome resistance to targeted protein kinase inhibitors in the treatment of cancer. *Drugs R D* 7: 73-86.
75. Gutteridge, R. E., M. A. Ndiaye, X. Liu, and N. Ahmad. 2016. Plk1 Inhibitors in Cancer Therapy: From Laboratory to Clinics. *Mol Cancer Ther* 15: 1427-1435.
76. Archambault, V., and K. Normandin. 2017. Several inhibitors of the Plk1 Polo-Box Domain turn out to be non-specific protein alkylators. *Cell Cycle* 16: 1220-1224.
77. Shin, S. B., S. U. Woo, and H. Yim. 2015. Differential Cellular Effects of Plk1 Inhibitors Targeting the ATP-binding Domain or Polo-box Domain. *J Cell Physiol* 230: 3057-3067.
78. Rudolph, D., M. Steegmaier, M. Hoffmann, M. Grauert, A. Baum, J. Quant, C. Haslinger, P. Garin-Chesa, and G. R. Adolf. 2009. BI 6727, a Polo-like kinase inhibitor with

- improved pharmacokinetic profile and broad antitumor activity. *Clin Cancer Res* 15: 3094-3102.
79. Gjertsen, B. T., and P. Schoffski. 2015. Discovery and development of the Polo-like kinase inhibitor volasertib in cancer therapy. *Leukemia* 29: 11-19.
80. Schoffski, P., A. Awada, H. Dumez, T. Gil, S. Bartholomeus, P. Wolter, M. Taton, H. Fritsch, P. Glomb, and G. Munzert. 2012. A phase I, dose-escalation study of the novel Polo-like kinase inhibitor volasertib (BI 6727) in patients with advanced solid tumours. *Eur J Cancer* 48: 179-186.
81. Lamouille, S., J. Xu, and R. Derynck. 2014. Molecular mechanisms of epithelial-mesenchymal transition. *Nat Rev Mol Cell Biol* 15: 178-196.
82. Kalluri, R., and R. A. Weinberg. 2009. The basics of epithelial-mesenchymal transition. *J Clin Invest* 119: 1420-1428.
83. Moreno-Bueno, G., F. Portillo, and A. Cano. 2008. Transcriptional regulation of cell polarity in EMT and cancer. *Oncogene* 27: 6958-6969.
84. Hugo, H., M. L. Ackland, T. Blick, M. G. Lawrence, J. A. Clements, E. D. Williams, and E. W. Thompson. 2007. Epithelial--mesenchymal and mesenchymal--epithelial transitions in carcinoma progression. *J Cell Physiol* 213: 374-383.
85. Tiwari, N., A. Gheldof, M. Tatari, and G. Christofori. 2012. EMT as the ultimate survival mechanism of cancer cells. *Semin Cancer Biol* 22: 194-207.
86. Comijn, J., G. Berx, P. Vermassen, K. Verschuere, L. van Grunsvan, E. Bruyneel, M. Mareel, D. Huylebroeck, and F. van Roy. 2001. The two-handed E box binding zinc finger protein SIP1 downregulates E-cadherin and induces invasion. *Mol Cell* 7: 1267-1278.
87. Huber, M. A., N. Kraut, and H. Beug. 2005. Molecular requirements for epithelial-mesenchymal transition during tumor progression. *Curr Opin Cell Biol* 17: 548-558.

88. Peinado, H., D. Olmeda, and A. Cano. 2007. Snail, Zeb and bHLH factors in tumour progression: an alliance against the epithelial phenotype? *Nat Rev Cancer* 7: 415-428.
89. Eger, A., K. Aigner, S. Sonderegger, B. Dampier, S. Oehler, M. Schreiber, G. Berx, A. Cano, H. Beug, and R. Foisner. 2005. DeltaEF1 is a transcriptional repressor of E-cadherin and regulates epithelial plasticity in breast cancer cells. *Oncogene* 24: 2375-2385.
90. Ma, L., and R. A. Weinberg. 2008. MicroRNAs in malignant progression. *Cell Cycle* 7: 570-572.
91. Gregory, P. A., C. P. Bracken, A. G. Bert, and G. J. Goodall. 2008. MicroRNAs as regulators of epithelial-mesenchymal transition. *Cell Cycle* 7: 3112-3118.
92. Bracken, C. P., P. A. Gregory, N. Kolesnikoff, A. G. Bert, J. Wang, M. F. Shannon, and G. J. Goodall. 2008. A double-negative feedback loop between ZEB1-SIP1 and the microRNA-200 family regulates epithelial-mesenchymal transition. *Cancer Res* 68: 7846-7854.
93. Gregory, P. A., A. G. Bert, E. L. Paterson, S. C. Barry, A. Tsykin, G. Farshid, M. A. Vadas, Y. Khew-Goodall, and G. J. Goodall. 2008. The miR-200 family and miR-205 regulate epithelial to mesenchymal transition by targeting ZEB1 and SIP1. *Nat Cell Biol* 10: 593-601.
94. Korpala, M., E. S. Lee, G. Hu, and Y. Kang. 2008. The miR-200 family inhibits epithelial-mesenchymal transition and cancer cell migration by direct targeting of E-cadherin transcriptional repressors ZEB1 and ZEB2. *The Journal of biological chemistry* 283: 14910-14914.
95. Park, S. M., A. B. Gaur, E. Lengyel, and M. E. Peter. 2008. The miR-200 family determines the epithelial phenotype of cancer cells by targeting the E-cadherin repressors ZEB1 and ZEB2. *Genes & development* 22: 894-907.

96. Wu, J., A. I. Ivanov, P. B. Fisher, and Z. Fu. 2016. Polo-like kinase 1 induces epithelial-to-mesenchymal transition and promotes epithelial cell motility by activating CRAF/ERK signaling. *Elife* 5.
97. Rivera, B., M. J. Bushman, R. G. Beaver, D. D. Cody, and R. E. Price. 2006. Breath-hold device for laboratory rodents undergoing imaging procedures. *J Am Assoc Lab Anim Sci* 45: 54-59.
98. Singh, M., A. Lima, R. Molina, P. Hamilton, A. C. Clermont, V. Devasthali, J. D. Thompson, J. H. Cheng, H. Bou Reslan, C. C. Ho, T. C. Cao, C. V. Lee, M. A. Nannini, G. Fuh, R. A. Carano, H. Koeppen, R. X. Yu, W. F. Forrest, G. D. Plowman, and L. Johnson. 2010. Assessing therapeutic responses in Kras mutant cancers using genetically engineered mouse models. *Nat Biotechnol* 28: 585-593.
99. Haines, B. B., K. A. Bettano, M. Chenard, R. S. Sevilla, C. Ware, M. H. Angagaw, C. T. Winkelmann, C. Tong, J. F. Reilly, C. Sur, and W. Zhang. 2009. A quantitative volumetric micro-computed tomography method to analyze lung tumors in genetically engineered mouse models. *Neoplasia* 11: 39-47.
100. Dachman, A. H., P. M. MacEneaney, A. Adedipe, M. Carlin, and L. P. Schumm. 2001. Tumor size on computed tomography scans: is one measurement enough? *Cancer* 91: 555-560.
101. Sapi, J., L. Kovacs, D. A. Drexler, P. Kocsis, D. Gajari, and Z. Sapi. 2015. Tumor Volume Estimation and Quasi-Continuous Administration for Most Effective Bevacizumab Therapy. *PLoS One* 10: e0142190.
102. Rodt, T., C. von Falck, S. Dettmer, K. Hueper, R. Halter, L. Hoy, M. Luepke, J. Borlak, and F. Wacker. 2012. Lung tumour growth kinetics in SPC-c-Raf-1-BB transgenic mice assessed by longitudinal in-vivo micro-CT quantification. *J Exp Clin Cancer Res* 31: 15.

103. Ratnakar Singh, P. V., Shaohua Peng, Vaishnavi Sambandham, Li Shen, Lerong Li, Bingliang Fang, Jing Wang, Faye M. Johnson. 2018. Non canonical cMet activation mediates de novo and acquired resistance to polo-like kinase 1 inhibitor-induced apoptosis in non-small cell lung cancer. In *AACR Annual Meeting 2018*. AACR, Chicago.
104. Li, J., W. Zhao, R. Akbani, W. Liu, Z. Ju, S. Ling, C. P. Vellano, P. Roebuck, Q. Yu, A. K. Eterovic, L. A. Byers, M. A. Davies, W. Deng, Y. N. Gopal, G. Chen, E. M. von Euw, D. Slamon, D. Conklin, J. V. Heymach, A. F. Gazdar, J. D. Minna, J. N. Myers, Y. Lu, G. B. Mills, and H. Liang. 2017. Characterization of Human Cancer Cell Lines by Reverse-phase Protein Arrays. *Cancer Cell* 31: 225-239.
105. Prudkin, L., D. D. Liu, N. C. Ozburn, M. Sun, C. Behrens, X. Tang, K. C. Brown, B. N. Bekele, C. Moran, and Wistuba, II. 2009. Epithelial-to-mesenchymal transition in the development and progression of adenocarcinoma and squamous cell carcinoma of the lung. *Mod Pathol* 22: 668-678.
106. Ungewiss, C., Z. H. Rizvi, J. D. Roybal, D. H. Peng, K. A. Gold, D. H. Shin, C. J. Creighton, and D. L. Gibbons. 2016. The microRNA-200/Zeb1 axis regulates ECM-dependent beta1-integrin/FAK signaling, cancer cell invasion and metastasis through CRKL. *Sci Rep* 6: 18652.
107. Li, X. F., P. Zanzonico, C. C. Ling, and J. O'Donoghue. 2006. Visualization of experimental lung and bone metastases in live nude mice by X-ray micro-computed tomography. *Technol Cancer Res Treat* 5: 147-155.
108. Eisenhauer, E. A., P. Therasse, J. Bogaerts, L. H. Schwartz, D. Sargent, R. Ford, J. Dancey, S. Arbuck, S. Gwyther, M. Mooney, L. Rubinstein, L. Shankar, L. Dodd, R. Kaplan, D. Lacombe, and J. Verweij. 2009. New response evaluation criteria in solid tumours: revised RECIST guideline (version 1.1). *Eur J Cancer* 45: 228-247.

109. Zhang, M., R. Singh, S. Peng, T. Mazumdar, V. Sambandam, L. Shen, P. Tong, L. Li, N. N. Kalu, C. R. Pickering, M. Frederick, J. N. Myers, J. Wang, and F. M. Johnson. 2017. Mutations of the LIM protein AJUBA mediate sensitivity of head and neck squamous cell carcinoma to treatment with cell-cycle inhibitors. *Cancer Lett* 392: 71-82.
110. Ilie, M., M. Nunes, L. Blot, V. Hofman, E. Long-Mira, C. Butori, E. Selva, A. Merino-Trigo, N. Venissac, J. Mouroux, P. Vrignaud, and P. Hofman. 2015. Setting up a wide panel of patient-derived tumor xenografts of non-small cell lung cancer by improving the preanalytical steps. *Cancer Med* 4: 201-211.
111. Li, L., Y. Wei, C. To, C. Q. Zhu, J. Tong, N. A. Pham, P. Taylor, V. Ignatchenko, A. Ignatchenko, W. Zhang, D. Wang, N. Yanagawa, M. Li, M. Pintilie, G. Liu, L. Muthuswamy, F. A. Shepherd, M. S. Tsao, T. Kislinger, and M. F. Moran. 2014. Integrated omic analysis of lung cancer reveals metabolism proteome signatures with prognostic impact. *Nat Commun* 5: 5469.
112. John, T., D. Kohler, M. Pintilie, N. Yanagawa, N. A. Pham, M. Li, D. Panchal, F. Hui, F. Meng, F. A. Shepherd, and M. S. Tsao. 2011. The ability to form primary tumor xenografts is predictive of increased risk of disease recurrence in early-stage non-small cell lung cancer. *Clin Cancer Res* 17: 134-141.
113. Gerlinger, M., A. J. Rowan, S. Horswell, M. Math, J. Larkin, D. Endesfelder, E. Gronroos, P. Martinez, N. Matthews, A. Stewart, P. Tarpey, I. Varela, B. Phillimore, S. Begum, N. Q. McDonald, A. Butler, D. Jones, K. Raine, C. Latimer, C. R. Santos, M. Nohadani, A. C. Eklund, B. Spencer-Dene, G. Clark, L. Pickering, G. Stamp, M. Gore, Z. Szallasi, J. Downward, P. A. Futreal, and C. Swanton. 2012. Intratumor heterogeneity and branched evolution revealed by multiregion sequencing. *N Engl J Med* 366: 883-892.

114. Aparicio, S., M. Hidalgo, and A. L. Kung. 2015. Examining the utility of patient-derived xenograft mouse models. *Nat Rev Cancer* 15: 311-316.
115. Cassidy, J. W., C. Caldas, and A. Bruna. 2015. Maintaining Tumor Heterogeneity in Patient-Derived Tumor Xenografts. *Cancer Res* 75: 2963-2968.
116. Olive, K. P., and D. A. Tuveson. 2006. The use of targeted mouse models for preclinical testing of novel cancer therapeutics. *Clin Cancer Res* 12: 5277-5287.
117. Jackson, E. L., K. P. Olive, D. A. Tuveson, R. Bronson, D. Crowley, M. Brown, and T. Jacks. 2005. The differential effects of mutant p53 alleles on advanced murine lung cancer. *Cancer Res* 65: 10280-10288.
118. Gammon, S. T., N. Foje, E. M. Brewer, E. Owers, C. A. Downs, M. D. Budde, W. M. Leevy, and M. N. Helms. 2014. Preclinical anatomical, molecular, and functional imaging of the lung with multiple modalities. *Am J Physiol Lung Cell Mol Physiol* 306: L897-914.
119. Vande Velde, G., E. De Langhe, J. Poelmans, P. Bruyndonckx, E. d'Agostino, E. Verbeken, R. Bogaerts, R. Lories, and U. Himmelreich. 2015. Longitudinal in vivo microcomputed tomography of mouse lungs: No evidence for radiotoxicity. *Am J Physiol Lung Cell Mol Physiol* 309: L271-279.
120. Namati, E., J. Thiesse, J. C. Sieren, A. Ross, E. A. Hoffman, and G. McLennan. 2010. Longitudinal assessment of lung cancer progression in the mouse using in vivo micro-CT imaging. *Med Phys* 37: 4793-4805.
121. Fushiki, H., T. Kanoh-Azuma, M. Katoh, K. Kawabata, J. Jiang, N. Tsuchiya, A. Satow, Y. Tamai, and Y. Hayakawa. 2009. Quantification of mouse pulmonary cancer models by microcomputed tomography imaging. *Cancer Sci* 100: 1544-1549.

122. Rudyanto, R. D., G. Bastarrika, G. de Biurrun, J. Agorreta, L. M. Montuenga, C. Ortiz-de-Solorzano, and A. Munoz-Barrutia. 2013. Individual nodule tracking in micro-CT images of a longitudinal lung cancer mouse model. *Med Image Anal* 17: 1095-1105.

Vita

Pavitra Viswanath was born in Hyderabad, India. She is the daughter of S. Viswanathan and Uma Viswanathan. She received her Bachelor of Engineering degree in Biotechnology from BMS College of Engineering in Bangalore, India in June 2016. In August of 2016, she entered The University of Texas MD Anderson Cancer Center UTHealth Graduate School of Biomedical Sciences, aspiring to attain the degree of Master of Science in Biomedical Sciences.

Permanent address:
Renaissance Park-2
207, 2nd Floor
Malleswaram West
Bangalore-560055
Karnataka, India.